

ANCO

CR-184098

SBIR- 09.02-5050
release date 6/11/91✓

REPORT

1311.16, Contract No. NAS8-37336
August 1989

SBIR Phase II

TETHER DEPLOYMENT MONITORING SYSTEM

Prepared for

GEORGE C. MARSHALL SPACE FLIGHT CENTER
NATIONAL AERONAUTICS AND SPACE FLIGHT ADMINISTRATION
Marshall Space Flight Center, Alabama

**ANCO
ENGINEERS,
INC.**

9937 Jefferson Boulevard
Culver City
California 90230-3591
(213) 204-5050
Telex: 182378
Cable: ANCOENG

(NASA-CR-184098) TETHER DEPLOYMENT
MONITORING SYSTEM, PHASE II Final
Report (Anco Engineers) 180 p

N93-13425

Unclass

63/13 01/11/92

Final Report

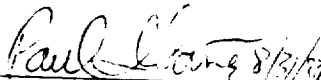

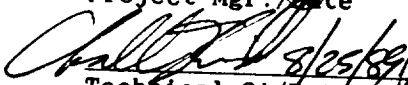
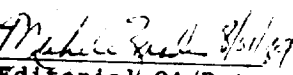

TETHER DEPLOYMENT MONITORING SYSTEM

Phase II SBIR

Prepared for

GEORGE C. MARSHALL SPACE FLIGHT CENTER
National Aeronautics and Space Flight Administration
Under Contract No. NAS8-37336
Marshall Space Flight Center, Alabama

Approval Signatures

	
Project Mgr./Date	Cog. Prin./Date
	
Technical QA/Date	Editorial QA/Date
	8/31/89
Chief Engineer/Date	

Prepared by

The Technical Staff
ANCO ENGINEERS, INC.
9937 Jefferson Boulevard
Culver City, California 90232-3591
(213) 204-5050

August 1989

ACKNOWLEDGMENTS

ANCO Engineers, Inc., was afforded valuable help by Mr. James Harrison and Mr. Chris Rupp of Marshall Space Flight Center, both of whom provided assistance and direction during both the Phase I and Phase II of this NASA-funded SBIR project. NASA's support is gratefully acknowledged.

At ANCO, Paul Ibanez, John Gray, and Alex Levi had primary responsibility for the project. They were assisted by other members of the ANCO's technical staff where appropriate.

TABLE OF CONTENTS

	<u>Page</u>
1.0 PROJECT SUMMARY.....	1-1
2.0 INTRODUCTION.....	2-1
3.0 CONTRACT REQUIREMENTS.....	3-1
3.1 Technical Objective.....	3-1
3.2 Scope.....	3-1
3.3 Contract Deliverables.....	3-3
4.0 EQUIPMENT DESCRIPTION.....	4-1
4.1 Module Launchers.....	4-1
4.2 Modules.....	4-4
4.3 Tracking System.....	4-9
4.4 Recording System.....	4-10
4.5 Positioning Gimbal.....	4-14
4.6 Control System.....	4-18
4.7 Tether Attitude and Tension Detection System.....	4-20
4.8 Housing Assembly.....	4-26
5.0 TETHER INTERACTION STUDY/DATA.....	5-1
6.0 TESTING.....	6-1
6.1 General.....	6-1
6.2 Laboratory Tests.....	6-1
6.3 Field Trials.....	6-3
7.0 POTENTIAL USES/CONCLUSIONS.....	7-1
APPENDIX A: LAUNCH SPRING CALCULATIONS.....	A-1
APPENDIX B: DRAWINGS.....	B-1
APPENDIX C: CALCULATIONS.....	C-1
APPENDIX D: ANALYSIS OF DEPLOYMENT OF THE EXPENDABLE TETHERED SYSTEM.....	D-1

ILLUSTRATIONS

<u>Figure</u>		<u>Page</u>
4.1	Clamshell Launch Tube and Positioning Gimbal.....	4-3
4.2	Origami Launcher.....	4-5
4.3	Clamshell Module.....	4-7
4.4	Origami Modules.....	4-8
4.5a	KA 126 Antenna.....	4-11
4.5b	KI 244 Indicator.....	4-11
4.6	Timing Diagram for Radar Scanning.....	4-12
4.7a	Index Unit and Positioning Gimbal.....	4-13
4.7b	Index Unit and Radar Antenna.....	4-13
4.8	Attitude Detector/Positioning Gimbal Interface.....	4-15
4.9	Positioning Gimbal.....	4-16
4.10	Simplified Schematic Diagram of Control System.....	4-19
4.11	Attitude and Tension Detector.....	4-21
4.12	Attitude Measurement Diagram.....	4-23
4.13	Gimbal Alignment Diagram.....	4-24
4.14	View on Plane Y.....	4-25
4.15	Housings for Control System Modules.....	4-27
6.1	Laboratory Test Fixture.....	6-4

1.0 PROJECT SUMMARY

ANCO Engineers, Inc., conducted a Phase I research effort to investigate the feasibility of monitoring the position of a tether during orbital deployment. Based upon the encouraging results of this study, a Phase II contract was awarded to ANCO by the NASA/Marshall Space Flight Center. This contract required the construction of an operational Tether Deployment Monitoring System (TEDEMS) that would demonstrate system functionality in a terrestrial environment.

The principle function of the TEDEMS system is the launching and attachment of reflective targets onto the tether during its deployment. These targets could be tracked either visually, with a video system, or with a radar unit that was pointed towards the targets by a positioning system. The system requirements include: 1) a method for tether attitude and tension detection, and 2) a launching device to attach small instrumentation platforms onto the tether during deployment.

This is the Final Report of the Phase II work. It describes the approach taken to develop the system configuration and the equipment which was developed to perform the functional tasks.

After a tradeoff analysis between visible light and radar, the latter was selected for module tracking. Serious concerns regarding visible light intensity impacting NASA flight personnel, both inside and outside the vehicle, was a major factor in this choice.

The Radar unit is aligned with the tether by a Positioning Gimbal which is driven by stepping motors. The position commands are provided by a tether Attitude Detector which provides a continuous indication of the angular relationship of the tether to the axes of the vehicle.

Three types of radar targets ("Origami" modules) were developed. All types were corner cubes; the difference being in their profile (square, round and triangular).

A spring powered launcher (Origami Launcher), which would accommodate all three types of targets, was designed and fabricated. As each of these targets were attached to the tether by a flexible lanyard, dynamic

positioning of the launching axis of this device was not necessary (although they could be oriented with their axes in line with the planned tether attitude at time of launch).

An instrumentation platform (Clamshell) and launcher (Tube Launcher) were also developed. These devices will allow a variety of instrumentation packages to be placed on the tether in future projects.

Clamshell Modules are relatively heavy and will influence tether deployment scenarios, unless they are released with a velocity and trajectory closely matching that of the tether. Consequently, the Tube Launcher was also aligned with the tether axis with a Positioning Gimbal similar to the unit used for aligning the Radar antenna.

Owing to the tracking range limitations encountered during field trials of the Radar system, final TEDEMS system integration was not completed. Successful tests of other subsystems indicate that the proposed system is a feasible approach to tether position monitoring, although additional work will be necessary to complete the system and fully verify its capabilities.

2.0 INTRODUCTION

Several National Aeronautics and Space Administration (NASA) and International programs are now in effect to make use of tethers in space. Tethers offer the possibility of fuel economy for payload launching, unique measurement systems in the upper atmosphere and space, and hitherto impractical orbital maneuvers.

Under a Phase I contract, ANCO Engineers, Inc., (ANCO) investigated the feasibility of monitoring the position of a tether during orbital deployment. These investigations explored techniques for attaching reflectors to the tether at periodic intervals during the deployment process, determining its attitude with respect to the axes of the launching vehicle, and directing a visible light source and video camera or radar antenna at the reflectors so that the deployment profile of the tether could be tracked.

The benefits that would accrue from an operational Tether Deployment Monitoring System (TEDEMS) system include: 1) warning of possible tether failures, 2) location of severed tethers, and 3) validation of mathematical models of tether deployment scenarios.

This is the Final Report of a Phase II contract issued by NASA to ANCO to design, build, and test a functioning TEDEMS system. The report details the technical objectives of the project, describes the system and equipment designed and developed for tether tracking, and the results of tests performed to verify operational functionality.

3.0 CONTRACT REQUIREMENTS

3.1 Technical Objective

The technical objective of the Phase II program was the design, development, and testing of an operational TEDEMS system that would function in a one-g environment.

3.2 Scope

The scope of the Phase II program was the implementation of the recommendations of the Phase I study.

Task 1: Development and Testing of Both Launcher Configurations

Both configurations of launchers (for Clamshell and Origami modules) are to be developed and tested. Tether velocity, at the time of launch, is on the order of 2-10 m/sec. The Clamshell launcher is to be capable of launching from 3-5 modules consecutively without reloading. Typical module weight is to be between 100-1,000 grams.

The Clamshell launcher is to be interfaced with a gimbal unit that will permit the aligning of the launcher axis with the tether. In addition to the launcher development, GTOSS analysis of the dynamic impact of module attachment on tether wave dynamics will also be performed.

Task 2: Development of a Prototype Clamshell Module

A prototype Clamshell module is to be developed. Enhancements for optical tracking (such as reflective materials) are to be investigated, as will methods of enhancing radar visibility (by addition of reflectors or variations in module geometry). Analysis to optimize the payload capacity for diagnostic and other instrumentation will be conducted. This will involve consultations with NASA investigators, in particular, personnel from Marshall Space Flight Center and Goddard Space Flight Center.

Task 3: Development of a Prototype Origami Module (Ku-Band Radar Target)

Small, lightweight radar reflectors are to be developed for indicating location of points on the tether's profile to the Orbiter's Ku-Band

rendezvous radar. ANCO will consult with engineers from Hughes Aircraft Company (Radar Systems) and Lockheed Aircraft Corporation (Shuttle Operations) to determine suitable operational procedures for utilizing the Orbiter's Ku-Band rendezvous radar for this purpose. Cognizant of the problems that have been encountered in the past with the ability of the Ku-Band radar to track multiple targets, consideration will be given to the use of a separate radar system for the TEDEMS system.

Task 5: Development and Prototyping of the Tether Attitude/Tension Detector and Tracking Gimbal

A Tether Attitude Detector (as outlined in Appendix B of the Phase I Final Report) is to be constructed and tested. It will be interfaced with the Positioning Gimbal. The Positioning Gimbal is to be utilized both for the Clamshell launcher (to aim the launcher tube) and with the Tracking System (to point the transmitting/receiving equipment). The detector will also provide a continuous measurement of tether tension.

Task 6: Development of the Passive Optical Module Tracking System

A Passive Module Tracking System consists of an optical source (either a large 25-50 kilojoule strobe or a large defocused YAG-type laser). Camera system, data recording system, power supply, and control electronics and actuators are to be developed and tested to track the Cluster module. For this system, aiming and pointing is to be accomplished by utilizing the Tether Attitude Detector and Tracking Gimbal arrangement outlined above.

The scope of the task was revised in Modification No. 2. Wherein, the Tracking System was specified to be a radar-based system. The other requirements of the task remain as applicable to a radar-based system.

Task 7: Get Away Special (GAS) Canister Integration

It is anticipated that during actual use in Phase III, the TEDEMS system will be stored and activated from within a pair of GAS canister pallets. During Phase II, full-size GAS canister mockups are to be constructed and used to resolve integration issues.

Task 8: Tether Deployment Simulation Test

A full Tether Deployment Simulation Test of the complete system is to be conducted either at Ames Research Center/Edwards AFB, Kirtland AFB, or

the National Balloon Center in Palestine, Texas. It will involve all components of the TEDEMS, with the exception of the use of the Orbiter's Ku-Band radar, and will serve as a ground-based proof-of-concept mission.

During this test, a balloon will be used to provide a lifting force for tether deployment. A tether length of two kilometers will be used, that being a practical upper limit in length for ground testing. During the deployment, the various modules built during this phase will be attached utilizing both the Clamshell and Origami launchers. The modules are to be tracked using the Tracking System which, in turn, shall be positioned by the gimbal and controlled by the Tether Attitude/Tension Detector. The deployment will be recorded with the system video camera and recorder.

The Phase II work scope also required that the respective merits of visible and radar tracking be analyzed and that the most meritorious system be selected. This activity was to be executed early in the schedule as many design decisions were contingent upon the choice made. After weighing the various factors, a radar-based system was selected. This led to Contract Modification No. 2, which revised the original work scope and contract deliverables.

3.3 Contract Deliverables

The contract deliverables, as revised by Modification No. 2, are listed in Table 3.1. The TEDEMS equipment was grouped into five major subsystems.

TABLE 3.1: CONTRACT DELIVERABLES

<u>Quantity</u>	<u>Description</u>
1	Axial Launch Tube Assembly - including lab and field checkout. [Tube Launcher]
1	Lanyard Clip Launch Module Assembly - including lab and field checkout. [Origami Launcher]
4	Clamshell modules [Instrumentation Platform]
9	Origami modules (radar reflectors, 3 each of square, circle, and triangular type).
1	Radar Tracking System to include: <ul style="list-style-type: none"> - Radar Emitter/Receiver [Radar Unit] - Camera System [Recording System] - Video Recorder System [Recording System] - Power Supply [Recording System] - Power And Signal cables [Recording System] - Tracking Gimbals and Actuator [Positioning Gimbal] - Control Electronics [Control System] - Tether Attitude and Tension Detection System - including lab tests [Attitude Detector] - TEDEMS Housing Assembly - Tether Interaction Study/Data

4.0 EQUIPMENT DESCRIPTION

4.1 Module Launchers

Two different types of module launchers were designed and fabricated; one for the Clamshell and one for the Origami modules. Both were spring powered and designed to accelerate the module to a velocity matching that of the tether at the moment of launch.

Data, from the mission scenarios developed for the Small Expendable Deployer System [SEDS], were used to establish some basic design parameters for the TEDEMS launcher.

Values of payout velocity and tether angle were selected from graphs developed for the SEDS program for appropriate increments of deployment length. Launch spring parameters were calculated to achieve matching module velocities and launch angles under a 1-g environment.

The derivation of formulas to calculate spring values is included in this report as part of Appendix A. These formulas were used to develop a software program (LAUNCHMD) which calculates module exit velocity for different springs, given a certain set of input parameters, such as module weight, travel distance, etc.

As the Clamshell modules are relatively heavy with respect to the tether, it is necessary to align the module launch trajectory with the longitudinal axis of the tether at the time of release in order to prevent the attachment process from influencing the planned tether deployment scenario. An open-loop, two-axis positioning system was developed to accomplish this. It points the launcher tube directly in line with the tether axis during the launch operation.

The Origami modules are lightweight and are attached to the tether with flexible lanyards. Consequently, dynamic positioning of these launchers were not necessary, although during assembly their axes could be aligned with the tether's anticipated attitude at the time of launch.

4.1.1 Tube Launcher

The Tube Launcher accommodates three Clamshell modules. They are stacked in a specially designed tube which permits them to be released individually at different preset velocities. The two hinged halves of the module are held partially open (30° including angle) in the tube and remain in this attitude as they accelerate down the tube after being released by their respective retaining solenoids. As they exit the tube, the two halves close together around the tether under spring pressure.

A tracking system is used to dynamically position the launching tube so that the correct relationship between module and tether is achieved. The tube has a vee notch which allows it to be positioned so that the axis of the module coincides with the longitudinal axis of the tether during launching.

The Tube Launcher is mounted on a Positioning Gimbal that receives its positioning signals from the Attitude Detector. A similar gimbal is used for aligning the radar antenna with the longitudinal axis of the tether. Assembly and detail drawings of the Tube Launcher are included in Appendix B of this report (Drawing No. 131116-115).

Figure 4.1 is a simplified illustration of the device showing an outline of the launching tube and Positioning Gimbal assembly loaded with three Clamshell modules together with a photograph showing the unit during construction.

4.1.2 Origami Launcher

These launchers consist of a box canister with a pair of hinged lids. Within the box, which is large enough to enclose the biggest Origami module, is a frame that supports the module at four locations. This frame can move vertically on four guide rods which are mounted at the base of the box.

Concentrically positioned on these rods are compression springs which are located between the box base plate and the threaded compression adjusters which are screwed into the frame.

When the frame is in its cocked position, these springs are held compressed by a solenoid which engages with a tab at the base of the frame.

Two hinged links provide a connection between the frame and the hinged lids. In the cocked position, these links keep the lids closed. Upon release, the upward motion of the frame causes the links to open the lids so that the module can be ejected.

The canister is mounted with an adjustable fitting that allows it to be swiveled and tilted. This permits the vertical axis to be aligned with the anticipated direction of the tether's longitudinal axis at the time of launch. The assembly and detail drawings of the Origami Launcher are included in Appendix B of this report (Drawing No. 131116-109). Figure 4.2 is a photograph of the unit (shown with lids open).

4.2 Modules

4.2.1 General

During the Phase I feasibility study, two types of modules were designed and prototypes fabricated. They were the Clamshell Modules, a relatively heavy axially-mounted instrumentation platforms; and the Origami Modules, a lightweight lanyard-attached, corner-cube targets.

4.2.2 Clamshell Modules

The Clamshell Modules are primarily instrumentation platforms, which can also act as radar targets with the addition of a reflector. (As these devices are oriented axially on the tether, a simple corner cube mounted in the rear of the module would provide this facility at the expense of some payload room.)

Prior to designing this module, ANCO consulted with various NASA investigators (e.g., MSFC, GSFC) on the nature of instrument packages that might be borne by the module to ensure that the configuration developed would be adaptable to potential payloads.

The dimensions selected for the module were 8 in. in diameter and 12-in. long. It provides a payload volume of 0.35 cubic foot. The empty module weighs 350-400 grams.

A module is comprised of two half cylinders hinged along one 12-in. edge. When in the launch position, the two portions are held apart at an

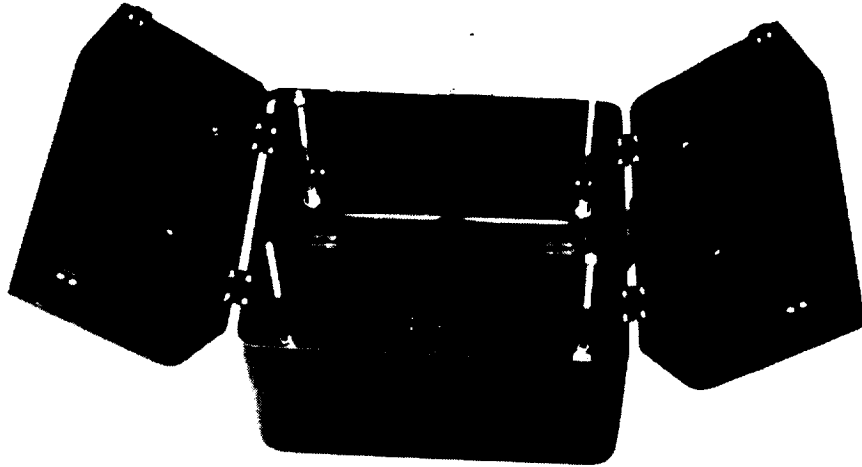


Figure 4.2: Origami Launcher

angle of 30° by guides in the launching tube. During launching, they are accelerated in this open configuration with the tether positioned in the vee formed between them. As they exit the launcher, they close under spring pressure, thereby clamping themselves axially on the tether. Drawings showing details of their construction are included in Appendix B (Drawing No. 131116-121).

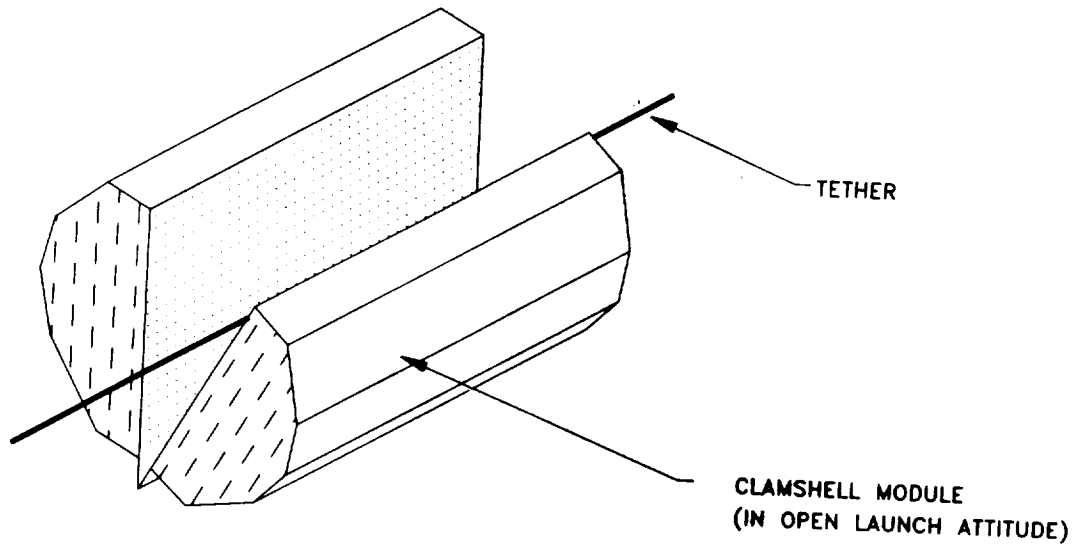
They consist of a lightweight aluminum frame covered with 1/8-in. thick Fomecor (a lightweight polystyrene foam filled board faced with paper laminate manufactured by Monsanto). Prior to assembly, the Fomecor sections were metallized with aluminum to provide a radar beam reflecting surface. An illustration of a Clamshell module in its open launching attitude is shown in Figure 4.3a; and a photograph of the module in Figure 4.3b.

4.2.3 Origami Modules

The Origami Modules are tether position indicating devices consisting of large-low mass (25-cm major axis, 100 gram) retro-reflectors which can be attached to the tether by means of a spring clip and an elastic lanyard. They were intended to be detectable at distances up to 20 Km, by the radar system chosen for tracking. For Phase II, three variants of these omnidirectional retro-reflecting modules were designed each with different profiles (square, triangular and circular). Each give a different response to the impinging beam from the radar unit. The most powerful but also most directional signal is returned from the square (23° lobe) and the least powerful but more dispersed signal from the triangular with a 40° lobe. The circular module generates a 32° lobe and, consequently, provides the best combination response.

The module is attached to the tether by a short flexible lanyard and spring clip. It is a passive system, and is designed to be relatively benign on the overall dynamics of the tether. To minimize the dynamic effects of attaching these devices to the tether, their weight was restricted. The target weight of each was a maximum of 100 grams. Drawings showing details of their construction are included in Appendix B of this report (Drawing No. 131116-110).

Figure 4.4 is an illustration of all three types.



(a)



(b)

Figure 4.3: Clamshell Module

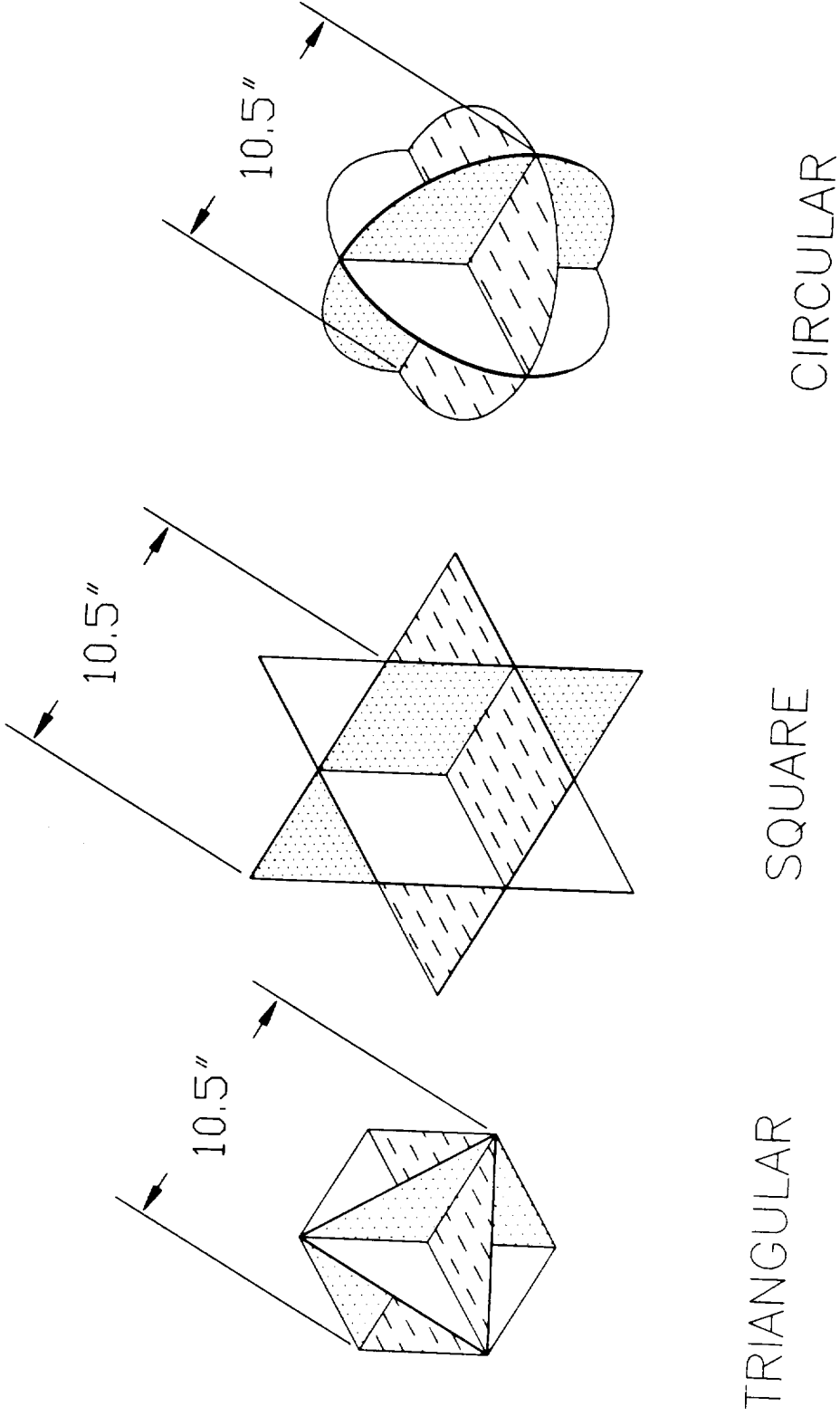


Figure 4.4: Origami Modules

4.3 Tracking System

4.3.1 General

Two different approaches to tracking were suggested in the Phase I Final Report and an early task performed in Phase II was an analysis of their advantages and disadvantages so that the optimum technique could be selected.

The choices were visible light and Radar. After analysis of the tradeoffs, Radar was selected. A major consideration in this choice was that calculations indicated that a strobe pulse of 25,000 joules would be necessary to achieve visibility at the 20 Kilometer range desired. A visible light pulse of such intensity posed serious concerns regarding its impact on NASA flight personnel, both inside and outside the vehicle.

Should radar be chosen, one of the options proposed in Phase I was the use of the Shuttle's Ku-band Radar system for tether tracking (even though it was mandated that the TEDEMS system should not be dependent on any existing Space Shuttle system unless absolutely necessary). However, consultation with experts indicated that the Ku-band Radar is not suitable for tracking multiple targets and, consequently, was not appropriate for the TEDEMS tracking task. Therefore, it was decided that a stand-alone X-Band Radar tracking system would be developed for this project.

4.3.2 Radar Unit

A survey of readily available radar systems, that were appropriate for this application, was performed.

Calculations indicated that an Origami module with an edge length of 13.5 cm would be detectable at 25 kilometers (a range 20% greater than that necessary to meet the project requirements) with a Narco Avionics KWX-56 Radar System. Targets of this size were acceptable from the standpoint of other system modules; and therefore, the Narco KWX-56 system was selected. It generates a peak output of 7.5 kilowatts at 9,375 MHz, and has a range of approximately 60 kilometers. It is comprised of two modules: 1) a KA 126 Antenna/Receiver/Transmitter and 2) a KI 244 Indicator.

4.3.3 KA 126 Antenna/Receiver/Transmitter

This device is illustrated in Figure 4.5a. It is a compact 10-in., flat-plate phased array antenna that scans a 9° wideband over a 90° sector at 13 sweeps per minute. The band elevation is continuously adjustable over an angle of 12° upwards and downwards from its mid position. By arranging to tilt the band in 4° increments every 4-5 seconds and simultaneously indexing it from the horizontal to the vertical once every 2 minutes, a 90° cone can be progressively scanned. A sequence diagram showing the timing for one complete cycle is shown in Figure 4.6.

The alignment of the 90° cone and the indexing of the antenna from horizontal to vertical and back again is accomplished by two different mechanisms. Alignment is achieved with a similar gimbal to that used to point the Tube Launcher both gimbals being directed by tether position data generated by the Attitude Detector (see Section 4.7).

The indexing mechanism uses a bell crank lever rotated by a linear actuator. The actuator is extended and retracted alternately by the TFCU controller which also controls several other system functions (see Section 4.6.3). Details of the Indexing mechanism are included in Appendix B, Drawing No. 131116-118. Figure 4.7a illustrates the mechanism installed on a Gimbal Positioner and Figure 4.7b is a photograph of the unit with the radar antenna attached mounted on the Gimbal Positioner.

4.3.4 KI 244 Indicator

This device is illustrated in Figure 4.5b. It utilizes a 5-in. diagonal black matrix raster CRT with HEA anti-reflective glass to provide a clear and undistorted view of the 3 color display. The manual controls for adjusting Range, Tilt, Brightness, and Gain are provided on the front bezel. For this application, the manual tilt control was deactivated and a remote signal was provided from the TFCU controller to tilt the antenna in accordance with the sequence shown on Figure 4.6.

4.4 Recording System

The radar system detects the signals reflected by the modules and displays them as colored light blips on the CRT display. A video camera,



KA 126 or 128 Receiver/Transmitter/Antenna

Figure 4.5a: KA 126 Antenna

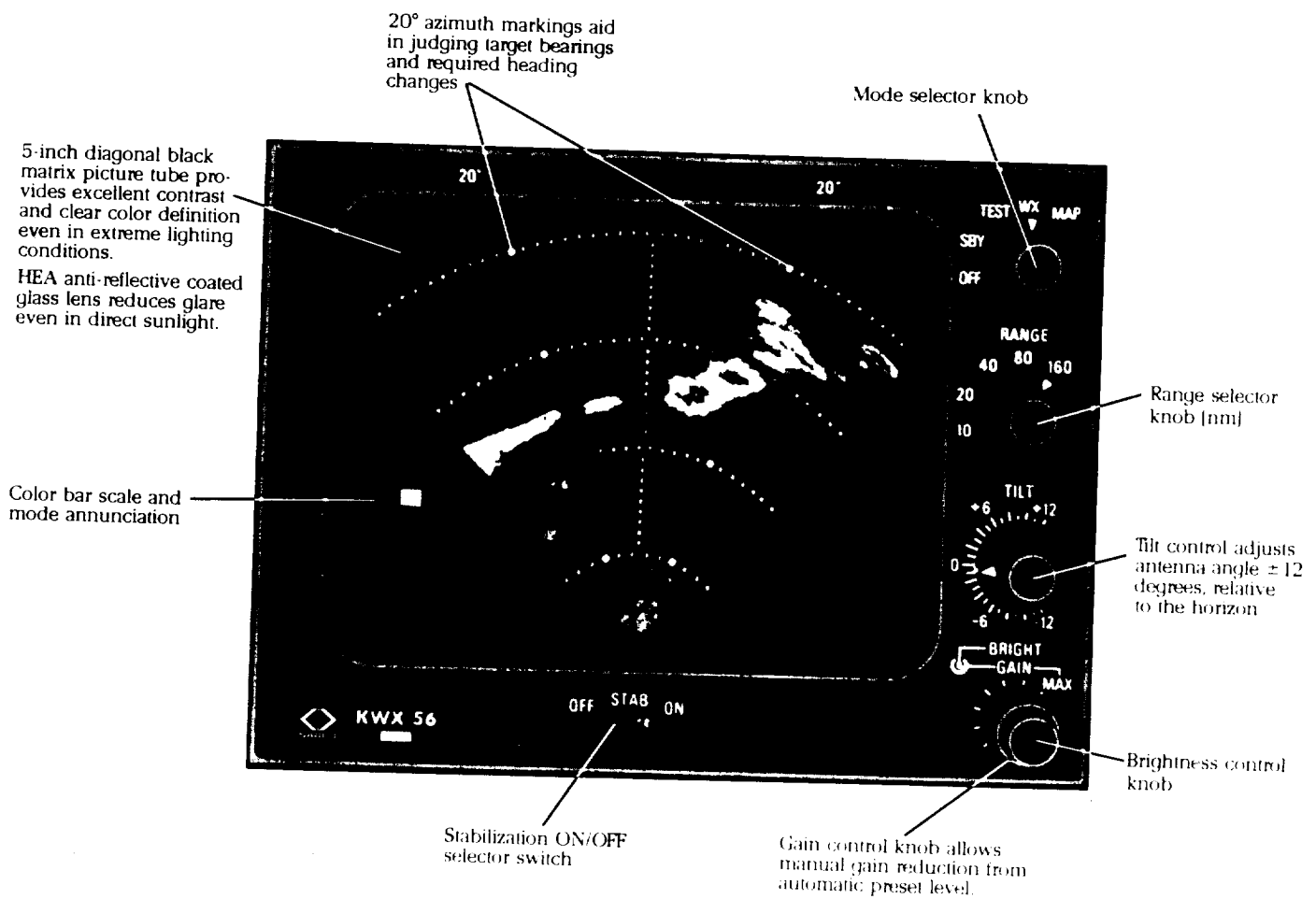


Figure 4.5b: KI 244 Indicator

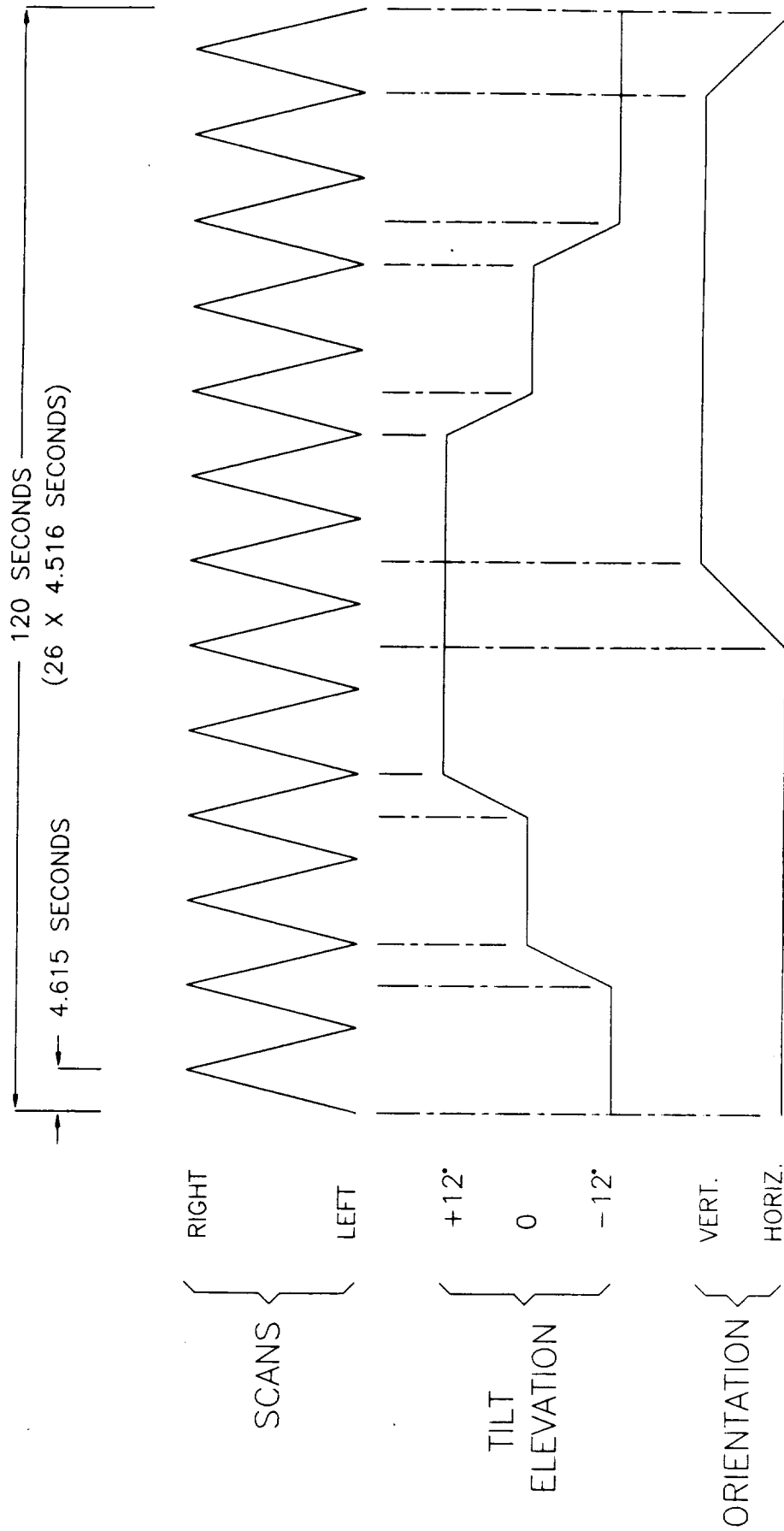


Figure 4.6: Timing Diagram for Radar Scanning

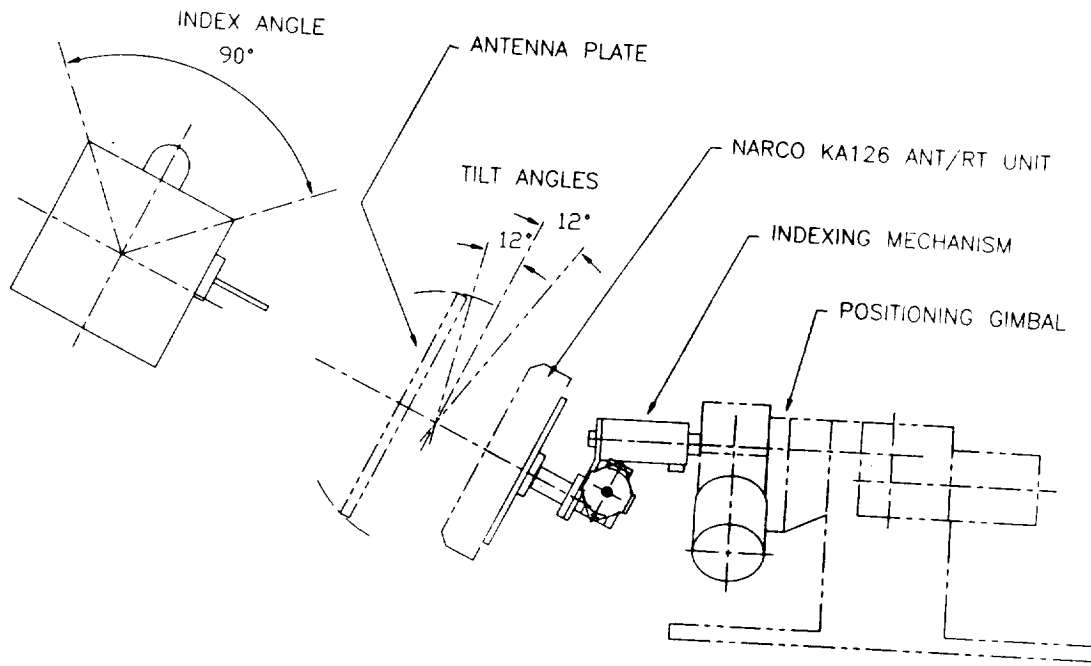


Figure 4.7a: Index Unit and Positioning Gimbal



Figure 4.7b: Index Unit and Radar Antenna

focused on the display, monitors the relative positions of the modules and simultaneously the rotational orientation and elevation of the antenna. By correlating these, an indication of tether profile can be obtained. Within the field of view, of the CCTV camera, is an alphanumeric display connected to the SCC computer system (see Section 4.6.2). This displays time-of-day and tether tension, as measured by the Attitude Detector, in engineering units.

All data can be displayed in real time on a video monitor and recorded by a VCR recorder for later analysis.

4.5 Positioning Gimbal

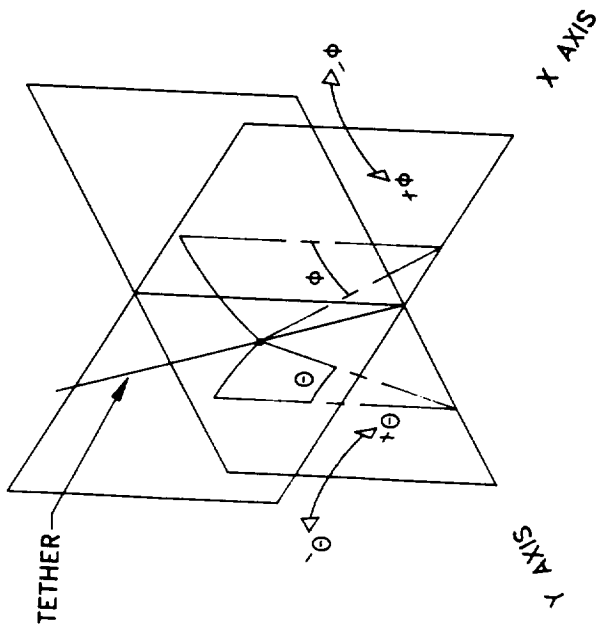
In the TEDEMS system, two positioning devices are required. One to align the radar antenna and the other, the Tube Launcher, along the axis of the tether. Each positioning system consists of a two-axis gimbal driven by an open loop servo system powered by a pair of stepping motors. The motors receive their positioning commands from the Attitude Detector via the System Control Computer [SCC]. A block diagram showing the inter-relationship of these modules is shown in Figure 4.8.

The angle of the tether is measured in two planes by the Attitude Detector. This data is converted into pitch and roll angular values by the SCC which then issues commands to the Indexing Modules which power the Positioning Motors (see Section 4.7.3).

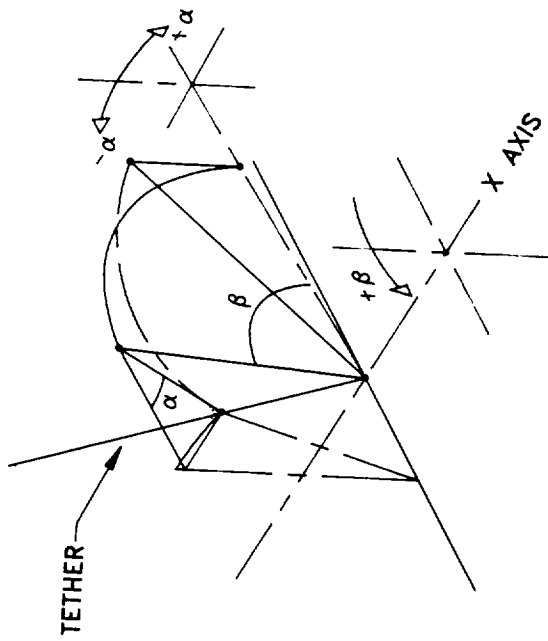
The gimbal is designed to point to any location within a 120° circular cone centered on its vertical axis.

It consists of a base unit with two vertical pillars. These support a U-shaped bracket between the output shaft of the Pitch gearbox on one side and a stub shaft and a sleeve bearing on the other. The bracket, which is capable of 360° rotation in the horizontal plane, supports the Roll gearbox (the output shaft of which is designed to accept either the Tube Launcher or the Indexing Mechanism). This shaft can also rotate 360°, although the angular rotation of both shafts is restricted by limit switches. Figure 4.9 is a photograph of the positioning gimbal.

The positioning velocity is low, taking approximately 40 seconds to traverse across the 120° cone angle. However, this speed is more than



ϕ = ANGULAR DEFLECTION FROM X PLANE
 θ = ANGULAR DEFLECTION FROM Y PLANE



α = ROLL ANGLE
 β = PITCH ANGLE

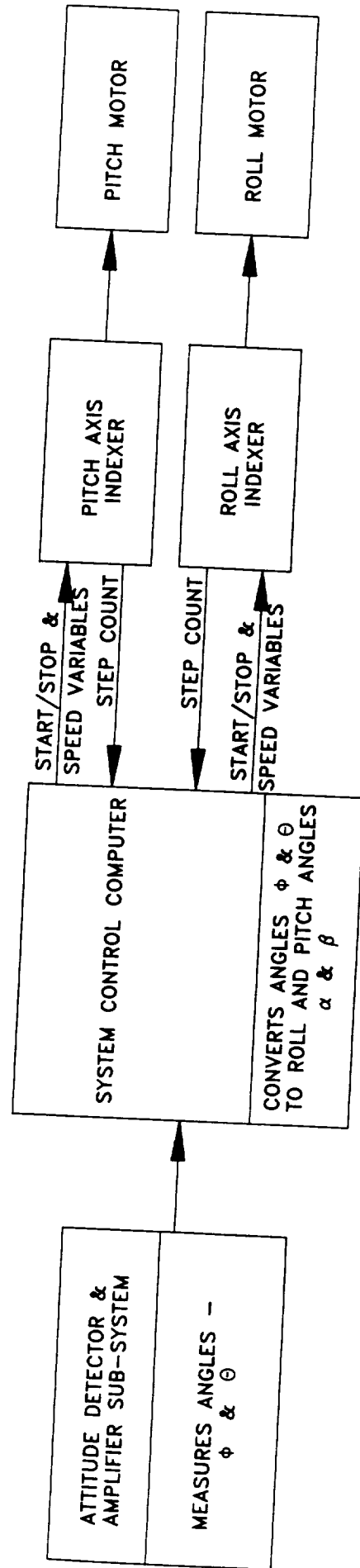


Figure 4.8: Attitude Detector/Positioning Gimbal Interface

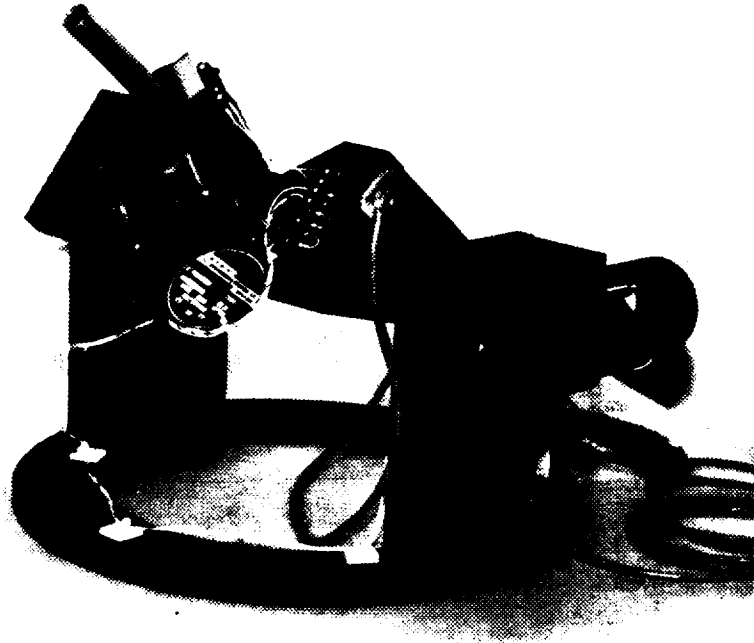


Figure 4.9: Positioning Gimbal

adequate for the application, as the tether angular rate of change is small during the period which modules are to be attached. Low-speed traversing has the advantage of allowing a high-gear reduction ratio in the drive system, permitting smaller motors to be employed. Both the Pitch and Roll axes have motors with 20:1 reduction ratios driving worm and wheel gearboxes which provided a further 20:1 reduction, giving an overall reduction of 400:1.

The gimbal operates differently for each of the two applications. The radar antenna will be active continuously and, consequently, so will its positioning system.

The Tube Launcher will be retracted below 120° cone angle (so that it will not interfere with the normal excursions of tether) during the majority of the deployment period.

When the time to attach a module approaches, the system will be activated and the tube will move to acquire the tether. (It has an open vee notch along its length that is designed to envelope the tether when they are both aligned.)

When the tube is in position it will move in concert with the tether as its attitude varies, as measured by the Attitude Detector. At the appropriate time, the module will be released and then the tube will return to its retracted position.

Drawings showing details of the construction of the gimbal frame and drive gearboxes are included in Appendix B (Gimbal Frame - Drawing No. 131116-116) and Gearbox - Drawing No. 131116-117).

Control of the stepping motors is achieved by initiating motion with a start command and then counting the number of steps taken and issuing a stop command when they total a desired value.

The motors are each powered by a Superior Electric Co. Type 430-PI Programmable Preset Indexer Module. This device can be interfaced to a microprocessor via a RS 232 link. It also has a number of discrete inputs and outputs that can be used for a variety of control activities.

The normal approach to motor positioning, when this device is interfaced to a host computer, is that destination (step count) acceleration

and velocity parameters followed by a start command are downloaded from the host over the RS 232 link. This arrangement is not appropriate for the TEDEMS system; because once issued, the destination step count cannot be altered until traversing is completed.

In the TEDEMS system, the tether location can alter in the interim period, so a different approach was adopted.

Acceleration and velocity parameters are calculated by the host and downloaded together with a start command. The microprocessor monitors the number of steps taken (via one of the discrete outputs) and, at the appropriate time, issues a stop command to allow for deceleration. This allows the destination to be updated while traversing is occurring and also permits rapid retraction should an emergency be detected (tether slewing at a rate greater than a predetermined value).

4.6 Control System

4.6.1 General

Two major control subsystems provide the control intelligence for the TEDEMS system. They are System Control Computer [SCC] and the Tilt and Flip Control Unit [TFCU].

Figure 4.10 is a simplified schematic diagram showing the interrelationship of the major system modules. A detailed diagram is included in Appendix B, Drawing No. 131116-114.

4.6.2 System Control Computer

The main task of the SCC is the interpretation of attitude and tension signals received from the Attitude Detector, and conversion of this data into positioning commands for the Positioning Gimbals and alphanumerics for the LCD display. This procedure is automatic and continuous once it has been initiated by system turn on.

4.6.3 Tilt and Flip Control Unit

A programmable controller provides the logic sequences for the TFCU unit. The various activities under its control are initiated manually. Some then continue until stopped. It controls:

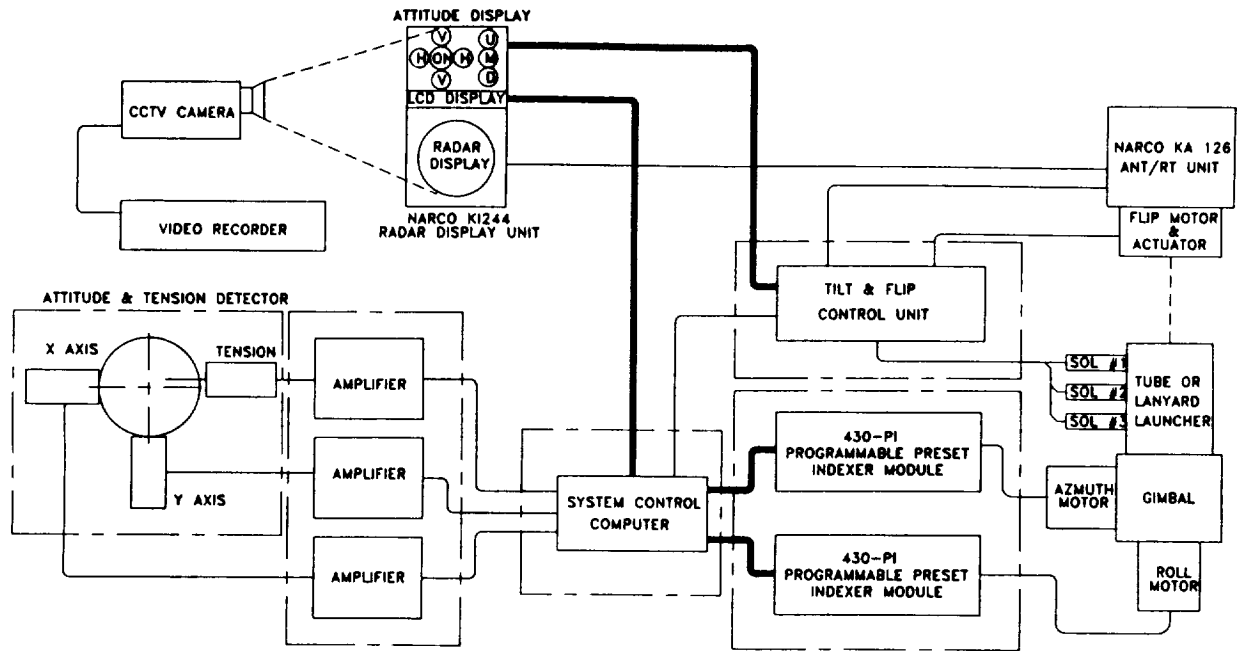


Figure 4.10: Simplified Schematic Diagram of Control System

- Radar Antenna scanning (tilting and horizontal/vertical rotation)
- Module launching

This subsystem controls the radar scan path and provides a real-time indication of its orientation with a matrix of indicator lights which are displayed adjacent to the radar CRT screen and alphanumeric display so that all can be captured with a video camera and recorded on the VCR. An electrical schematic diagram of the TFCU subsystem is included in Appendix B, Drawing No. 131116-119.

4.7 Tether Attitude and Tension Detection System

4.7.1 General

In order to align the Positioning Gimbals with the deployed tether, it is necessary to measure its attitude with respect to a known reference. In addition, the sensing of tether tension during deployment will permit the comparison with predicted values so that safety of the process can be continuously monitored.

In Phase I, ANCO developed a concept for a device that would accomplish both these tasks without affecting the dynamics of the tether. This device was designed and built in Phase II.

4.7.2 Attitude and Tension Detector

This device consists of three semi-circular hoops mounted on a circular base. All three hoops rotate on precision instrument bearings and require minimal force for movement. The two larger hoops are arranged at right angles to each other and can rotate freely through an angle of 60° on either side of the vertical centerline. The axis of the smaller hoop is coaxial with one of the larger hoops to which it is coupled with a torsion leaf spring. An illustration of the Attitude and Tension detector [Attitude Detector] is shown in Figure 4.11. Detailed component and assembly drawings are included in Appendix B (Drawing No. 131116-112).

In operation, the tether, which is dispensed from a storage container under the base plate, issues through a bush in the center of the circular base and then passes through a nozzle located at the intersection of the two larger hoops. This nozzle is supported in position by two flanged instrument

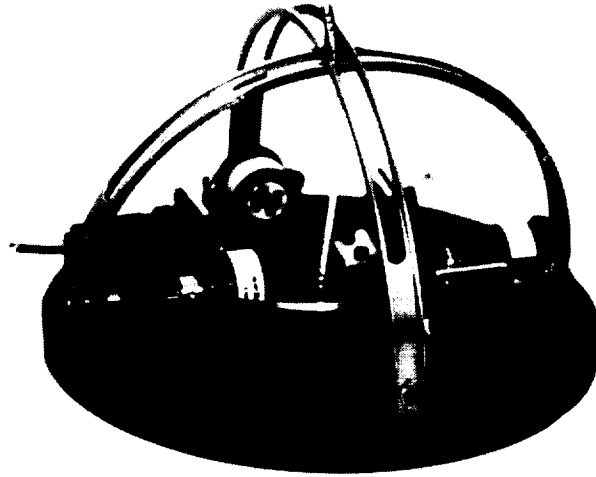


Figure 4.11: Attitude and Tension Detector

bearings, one being engaged with the outer hoop and the other with the inner hoop. The hoops move in unison with changes of tether position. A combination of their angles providing a measurement of tether attitude with respect to the vertical axis. Angular deflection is provided by measuring devices attached to the hoops which generate an output voltage proportional to position.

The smaller hoop is offset at a 10° angle to the inner hoop to which it is axially coupled with a torsion leaf spring. The tether continuously contacts the smaller hoop and, as tension increases, applies a force that tends to reduce the 10° angle against the resistance of the leaf spring. This smaller hoop also has an angular measuring device so by comparison of signals from it and the device on its associated larger hoop, tether tension can be determined.

Model R30A Rotary Variable Differential Transformers [RVDT], manufactured by Schaevitz Engineering, were used for all angular measurements. These devices produce a voltage whose magnitude varies linearly with the angular position of their shaft. The shaft is mounted on miniature precision ball bearings, consequently, only electromagnetic coupling exists between the stationary windings and rotor frictional torque is insignificant (0.015 inch-ounces). Their sensitivity is 2.3 mV/V/° .

The signals from the RVDT modules were amplified by a Schaevitz Engineering Series LMP-210 LVDT Signal Conditioner. This amplifier generated a $\pm 10 \text{ VDC}$, 5 ma full range output signal.

4.7.3 Attitude Detector/Positioning Gimbal Interface

The angles measured by the Attitude Detector and the Roll and Pitch angles used to align the Positioning Gimbal are different. In the case of the Attitude Detector, both X and Y axes are independent and the angles measured $\pm \phi$ and $\pm \theta$ are with respect to a fixed common reference. With the Positioning Gimbal, the Roll axis is physically located on the Pitch axis and, consequently, movement of the latter affects the angle of the former.

The SCC performs the task of converting the signals generated by the Attitude Detector into commands for the Positioning Gimbals and data (in engineering units) for the alphanumeric display. To enable the SCC system

to perform this function, a mathematical expression was derived to convert the Attitude Detector angles to alignment angles for the Positioning Gimbal. This was used as the basis to develop a software algorithm that would perform the desired function in real time.

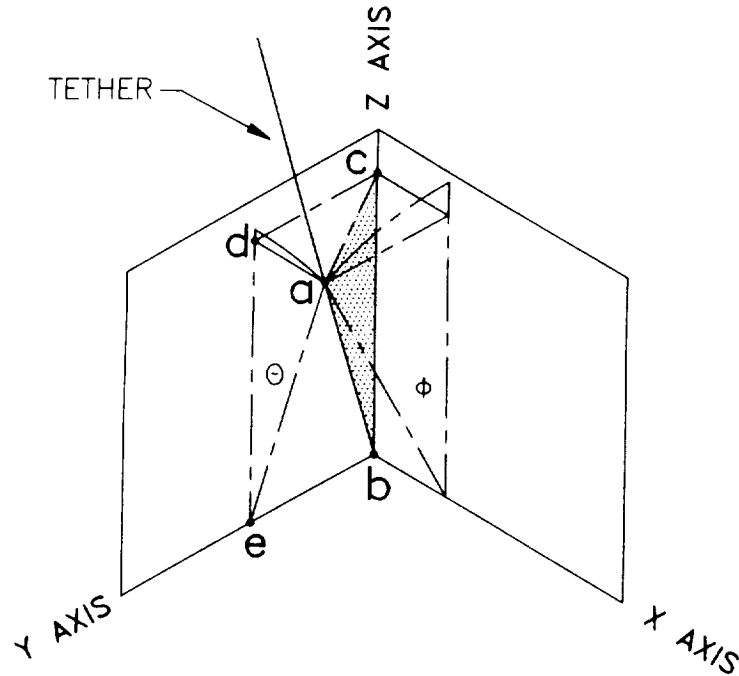


Figure 4.12: Attitude Measurement Diagram

In Figure 4.12, the tether originates at (b) (the intersection of Axes X, Y and Z) and subtends any pair of angles (within the limits 0°-60°) ϕ and θ to planes X and Y, respectively. By calculation, it can be shown that:

$$de = \frac{4}{(\tan^2\theta + \tan^2\phi + 1)^{1/2}}$$

Note: the derivation of this equation and those that establish the Pitch and Roll angles are included in Appendix C.

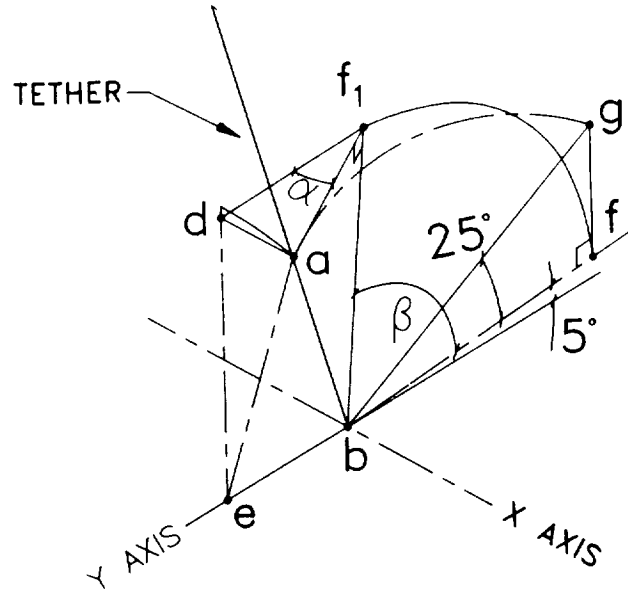


Figure 4.13: Gimbal Alignment Diagram

In Figure 4.13, the tether position is unchanged (as is its intersection point (a) with the inner and outer hoops. Point (a) is now also located by a right angled link (bfg) which represents the mechanical structure of the Gimbal Positioner. To reach Point (a), the link has moved through Angle (α) with respect to Plane Y (Roll Angle) and Angle (β) in Plane Y (Pitch Angle) from its original position.

$$\text{Angle } af_1d = \text{Roll Angle} = \alpha$$

$$\alpha = \text{Sin}^{-1} \frac{4 \text{Tan} \theta}{1.6905 (\text{Tan}^2 \theta + \text{Tan}^2 \phi + 1)^{1/2}}$$

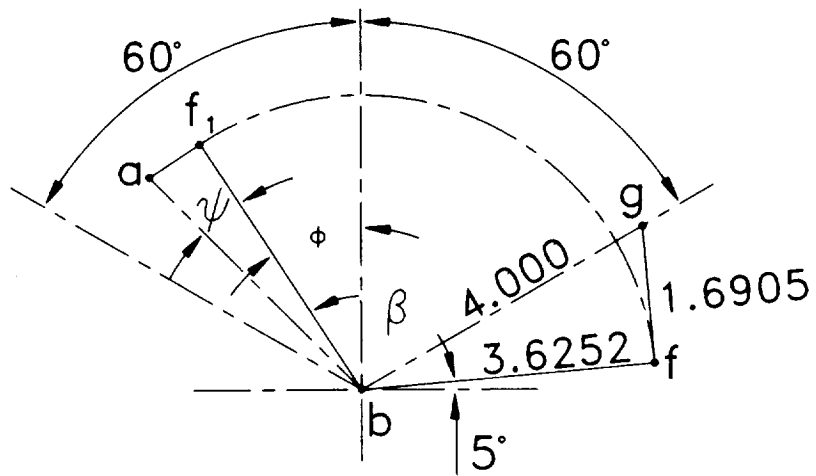


Figure 4.14: View on Plane Y

Angle fbf_1 = Pitch angle = β

$$\beta = 85^\circ + \phi - \psi$$

Note: $\psi = \text{Tan}^{-1} \frac{(1.6905 \text{ Cos}\alpha)}{(3.6252)}$

4.8 Housing Assembly

Because of the need to conduct field trials, all TEDEMS equipment was designed to be modular and portable.

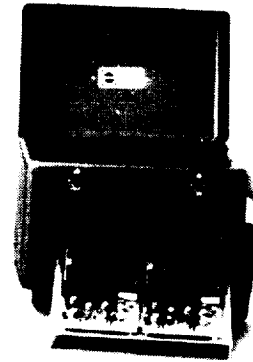
The control system was divided into logical units and each were housed in individual enclosures with provision for interconnection by plug and receptacle.

These units are illustrated in Figure 4.15. They are:

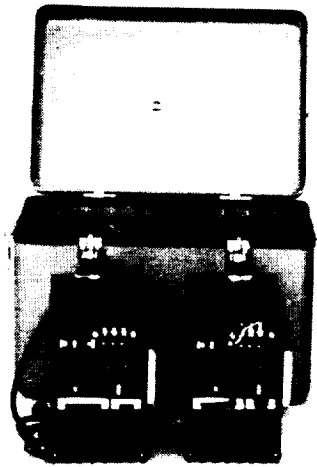
- a - System Control Computer
- b - TFCU Module
- c - Attitude Detector amplifiers
- d - Positioning indexers



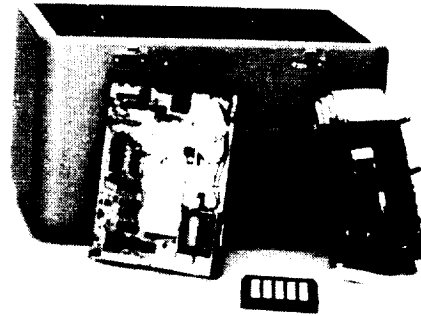
TFCU Module



Attitude Detector Amplifiers



Positioning Indexers



System Control Computer

Figure 4.15: Housings for Control System Modules

5.0 TETHER INTERACTION STUDY/DATA

A study of the dynamic affects that attachment of three Origami modules, each weighing approximately 100 grams, would have on a SEDS configuration tether was conducted by Dr. Enrico Lorenzini of Smithsonian Astrophysical Observatory.

Dr. Lorenzini determined that Origami attachment would not significantly affect tether control variables, such as tether tension, length, and payout velocity, and would not appreciably impact the longitudinal dynamics of the system.

The major affect of emplacement of the Origami modules would lie in the in-plane shape of the tether (the impact being predicted to be less than a 10% departure of tether shape from the baseline). This suggests that the utilization of Origami modules to determine tether shape during deployment is a viable option.

A copy of this study is included in this report as Appendix D.

6.0 TESTING

6.1 General

In order to simplify system integration, an incremental approach to testing was adopted. Each module was to be individually tested, then integrated subsystems of tested modules were to be tested; and finally after complete system integration, a tether deployment simulation exercise was to be conducted in the field. This step-by-step approach allows problems to be quickly identified and corrected.

Inherently, this approach requires that testing first be conducted in a laboratory environment prior to attempting field trials.

6.2 Laboratory Tests

6.2.1 Module Testing

The various modules were to be tested throughout their assembly stages to ensure that they met all performance criteria established during their design. These tests were functional. The equipment was operated over its intended ranges to ensure that mechanical and electrical limits and outputs were correct. Module tests were performed on the:

- Attitude and Tension Detector
- Positioning Gimbal
- Indexing Mechanism
- Origami Launcher
- Radar System

6.2.1.1 Module Test Results

Attitude and Tension Detector

This unit was bench tested in conjunction with the signal conditioning amplifiers. Testing involved a series 10° angular displacements of the positioning hoops and the measurement of the voltage output generated by the amplifier. The results obtained indicated a linear response over the $\pm 60^\circ$ range of the device. The tether tension measuring facility was not tested.

Positioning Gimbal

This unit was bench tested using an Indexing Programmer (borrowed from the drive vendor). This device permitted the motors and associated servo-amplifiers to be commanded to drive in both clockwise and counterclockwise directions at selectable velocities. The gimbal performed satisfactorily with respect to speed and mechanical construction.

Indexing Mechanism

The indexing mechanism was bench tested using an AC supply. It rotated both clockwise and counterclockwise through a 90° arc in approximately six seconds as intended.

Origami Launcher

This device failed the initial bench test. The solenoid release mechanism had insufficient power to overcome the spring tension on the tab at the base of the frame. After modification of the release mechanism (adding a second solenoid so that both operated in tandem), this problem was overcome and module launching was accomplished. (It is recommended that prior to using this device on any future program, further work on the release mechanism be performed to simplify the existing arrangement.)

Radar System

This system consists of the KA 126 Antenna/Receiver/Transmitter and the KI 244 Indicator modules manufactured by Narco Avionics connected together with a multi-conductor cable manufactured by ANCO. This subsystem was tested by interconnecting the modules together and observing the display on the KI 244. The various controls for range, tilt, brightness, gain, etc., were adjusted and their functionality verified. This test was performed on the roof of ANCO's facility in Culver City, California.

6.2.2 Subsystem Testing

A fixture for dynamic evaluation of the performance of an integrated subsystem, comprising the Attitude Detector and the two types of module launchers, was designed and built. It was installed in a laboratory at ANCO's Culver City facility where the headroom was sufficient to allow 18 ft

of simulated tether (1/8 dia. steel cable) to be deployed vertically. It is illustrated in Figure 6.1.

The fixture consisted of a variable speed powered winch, which simultaneously deployed one end of a cable while it retrieved the other. After leaving the winch drum, the cable passes over a pair of overhead pulleys mounted on a frame attached to the roof trusses. These pulleys were arranged so that the inclined leg of the cable could be positioned at any angle within a 120° x 30° elliptical cone.

The lower end of the cable emanates vertically through a hole in the top plate of the frame that houses the winch assembly. At this point, it passes through the Attitude Detector. This top plate also provided an anchoring surface for the two types of launcher.

The fixture can simulate a tether under different tensions traveling up to the maximum speeds envisioned in the SEDS project. The cable is reversible and can be decelerated to a full stop in one meter. It was planned to test both types of launchers and the tether Attitude Detector with this unit.

As system integration was suspended prior to the time that subsystem testing was practical, this equipment has yet to be utilized. However, if it is put to use in the future the following should be noted.

Owing to limited headroom, it would be necessary to launch modules one at a time to allow removal of the previous unit from the tether.

Proper positioning of the Positioning Gimbal, during tether attitude changes, would be demonstrated by utilizing this equipment. The performance of the launchers and the modules would be monitored by a video camera.

As this is a ground-based test (in a one g vertical field), the Origami modules would be equipped with stronger clips than those envisioned for an orbital application.

6.3 Field Trials

The only equipment tested in the field was the radar system. Several trials were performed at a variety of locations:

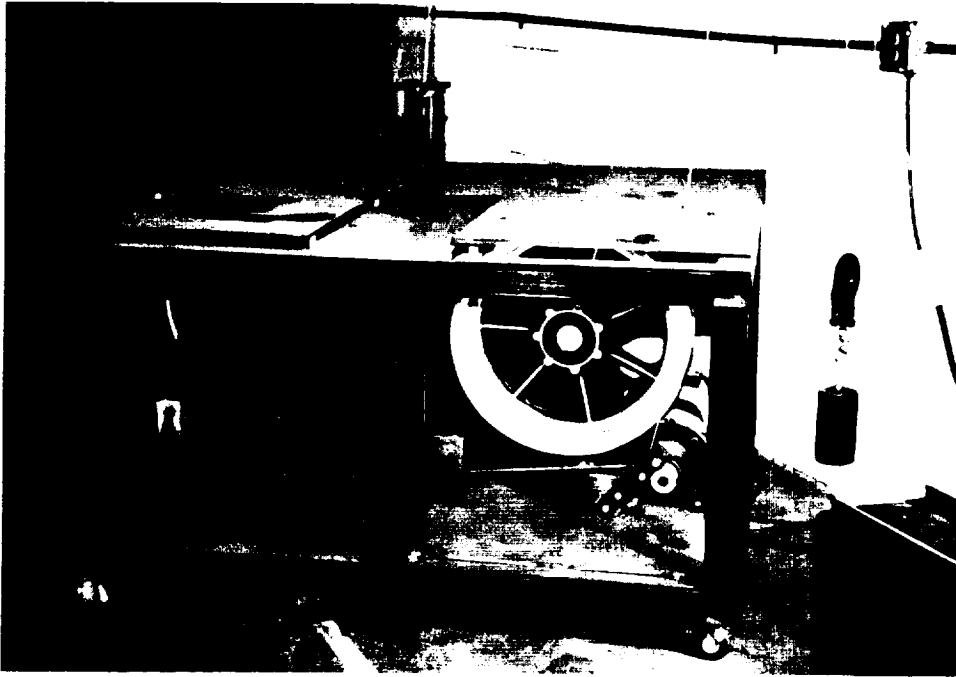


Figure 6.1: Laboratory Test Fixture

- Edward's Airforce Base (dry lake bed),
- Culver City (LA basin),
- Marina Del Rey (Santa Monica Bay), and
- Hemet (Lake Elsinore Valley and airspace).

Problems with transmission power limited detection of the Origami modules to approximately 8-10 kilometers (a distance approximately 1/3 of the 25 kilometer predicted range).

Initially, the system was checked out on topographical features around the Los Angeles basin. These tests were performed on roofs, hills, hotel balconies, and similar high locations with the targets being elevated with balloon and kites over both land and water.

Ground clutter and strong aerodynamic oscillations (during balloon and kite lifts) inhibited module detection in these tests. However, a test at Edwards AFB was more successful and the target was detected at a distance of 7-8 kilometers.

Encouraged by success, an additional test was conducted at Hemet (a rural area approximately 100 miles east of Los Angeles). A wooden glider was used as the vehicle to carry the Origami module aloft (it having a minimal radar profile). Again, we were unsuccessful in detecting the module.

7.0 POTENTIAL USES/CONCLUSIONS

Radar tests were performed at a variety of locations but the only test where encouraging results were obtained was at Edward's Airforce Base, where the Origami Module was detected at a distance of 7-8 kilometers. Initially, this test was conducted using a much larger radar target to establish exact target location, and then the Origami module was substituted and the response observed. It was found that the signal faded as the range increased between 7-8 kilometers. This testing was conducted under close to ideal conditions with the target being held stationary and oriented towards the receiver. Owing to this range limitation in tracking, further system integration work was suspended.

The major item not completed was the system control computer. Its hardware was only partially integrated and the software for converting tether attitude angles into Gimbal Positioning commands was not developed. The lack of this device prevented any subsystem testing or field trials to be conducted. (Other items only partially complete were the Clamshell launcher and modules and the Origami launcher.)

Prior to work suspension, design, construction, and module testing of several other subsystems had been conducted. These included the Attitude Detector and its associated amplifiers; the Positioning Gimbal with its axis drive motors and servo-amplifiers; the Indexing Mechanism; and the Origami Launcher.

The work completed and the tests performed suggest that the proposed system continues to be a feasible approach to tether monitoring, although additional effort is still necessary to increase the range at which modules can be detected.

The results obtained during the radar testing indicate that a radar system with approximately 30 times the power of the Narco system would suffice. Such aircraft systems are available "off-the-shelf" but their cost and the cost of retesting were beyond the budget of this project.

This report describes the system concept, the hardware design, and the testing approach planned for the TEDEMS project. As the SCC system was not completed, only limited testing was performed and, consequently, performance

of the hardware when integrated together is unknown. The equipment completed and tested, to the extent stated, is available to NASA for use on any future program that requires tether tracking capability.

It should be noted that the developed system was for concept verification in a terrestrial environment and, consequently, space qualification of the hardware was not a factor in the design.

ANCO

APPENDIX A
LAUNCH SPRING CALCULATIONS

LPW

9/23/87

CCK

8/25/89

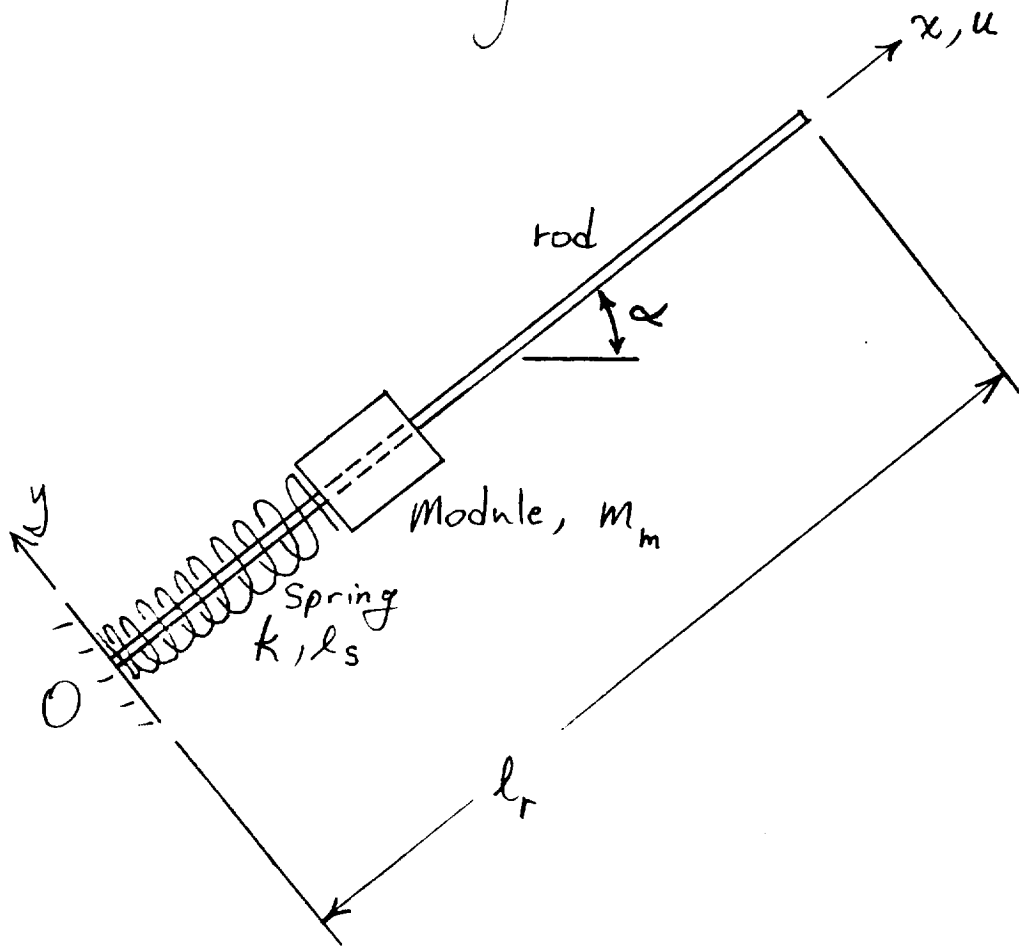
B11.16

1

21

Exit Velocity of Spring

Do A 1st Order Estimation of Exit Velocity of Module Spring From Launching Device



MADE BY

WJW

DATE

9/23/87

CHECKED BY

CCK

DATE

8/25/89

JOB NUMBER

B1116

PAGE

2

OF

21

DESCRIPTION

Exit velocity of Spring

The problem is broken up into four parts. They are 1) the velocity of the module as it loses contact with the spring, 2) the velocity of the center of gravity of the spring as the module loses contact with it, 3) the velocity of the module as it leaves the end of the rod, and 4) the velocity of the center of gravity of the spring as it leaves the end of the rod.

- 1) The two ends of the spring are not attached to anything. The spring is compressed by moving the module towards the origin of the x, y coordinate system. The module is then held in place until it is time to release it.

WSW

9/23/07

CCK

8/25/09

1311.16

3

21

Exit Velocity of Spring

Assume for now that the spring is massless. Also, assume that the end of it at the origin is fixed in space. Upon release of the module, it would travel with increasing velocity until the spring is in a state of zero strain energy (approximate statement). At that time the module would lose contact with the spring. This is because of the massless state of the spring —

$$\sum F_x = \left(\frac{m_s}{2}\right) \ddot{u}_{s2} = -F_s = -k u_{s2} \quad (1)$$

$$\text{But } m_s = 0 \Rightarrow \underline{\underline{u_{s2} = 0}}$$

However, the spring is not fixed at 0. So it will leave the base at 0. The module will still lose contact with the

WJW

9/24/87

CCK

8/25/89

1311.6

4

21

Exc + Velocity of Spring

Spring as will be shown shortly.

The motion of the module while it is in contact with the spring is given by

$$u_m = \frac{u_{m0} e^{-\beta \omega_0 t}}{(1-\beta^2)^{1/2}} \cos(\omega' t - \phi) \quad (2)$$

where u_m = motion of module while it is in contact with the spring
 u_{m0} = initial displacement of the module
 β = fraction of critical damping
 ω_0 = "undamped" natural frequency of the spring/module system

t = time

$$\omega' = \omega_0 (1-\beta^2)^{1/2}$$

$$\phi = \tan^{-1}(\beta / (1-\beta^2)^{1/2})$$

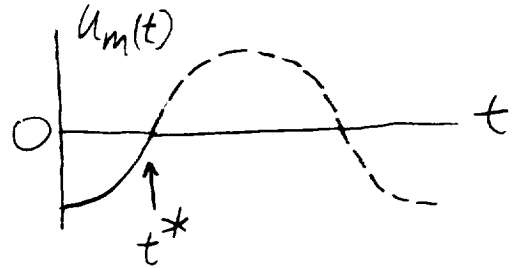
For this approximate analysis take $\beta=0$.

Then,

$$u_m \Big|_{\beta=0} = u_{m0} \cos(\omega_0 t) \quad (3)$$

The spring will be compressed initially, so $u_{m0} < 0$. The module will lift off of the spring after $1/4$ cycle of response.

$$t^* = \frac{2\pi}{4} \frac{1}{\omega_0}$$



$$\dot{u}_m = -u_{m0} \omega_0 \sin(\omega_0 t)$$

$$\dot{u}_m(t^*) = -u_{m0} \omega_0 \sin\left(\omega_0 \cdot \frac{2\pi}{4} \frac{1}{\omega_0}\right)$$

$$= -u_{m0} \omega_0$$

$$= v_0 \text{ (no gravity)}$$

(4)

The influence of gravity must be included. This will be done by superimposing the solution (response of the module in contact with the spring) for 1) gravity loading and 2) initial displacement force.

NSW

9/25/87

CCK

8/25/89

1311.16

6

21

Exit Velocity of Spring

The two solutions will now be superimposed. To do this the following is looked at:

$$m\ddot{u} + c\dot{u} + ku = f(t) \quad (5)$$

or $(mp^2 + cp + k)u = f(t)$

Define $mp^2 + cp + k$ to be represented by \mathcal{L} - a differential linear operator.

$$\mathcal{L}u = f(t) \quad (6)$$

Apply forces f_1 and f_2 separately

$$\mathcal{L}u_1(t) = f_1(t)$$

$$\mathcal{L}u_2(t) = f_2(t)$$

WBJ

9/25/87

CCK

8/25/89

1311.16

7

21

Ex + Velocity of Spring

Add to obtain the following:

$$\mathcal{L}u_1 + \mathcal{L}u_2 = f_1 + f_2$$

$$\mathcal{L}(u_1 + u_2) = f_1 + f_2 \quad (7)$$

Thus, for forcing f_1 and f_2 acting together, the solution of the problem is $u_1 + u_2$.

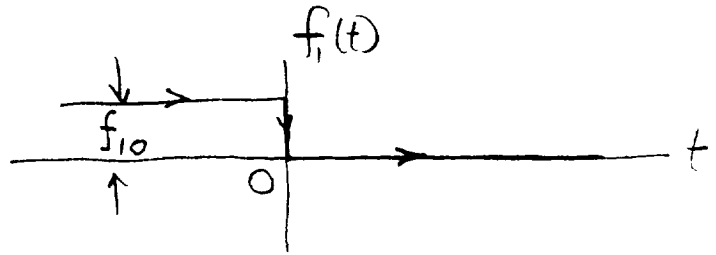
The loading f_1 and f_2 and their corresponding solutions will now be obtained using the previously obtained solution. The forces f_1 and f_2 are taken to correspond to the applied load excluding gravity and the gravity force, respectively. The equation of motion of the module is

$$m_m \ddot{u}_m + c_s \dot{u}_m + k u_m = f(t) \quad (8)$$

Force f_1

$$f_{10} = K u_{m10}$$

The equation for $t > 0$ is



$$m_m \ddot{u}_{m1} + C_s \dot{u}_{m1} + K u_{m1} = 0$$

The initial conditions are found from

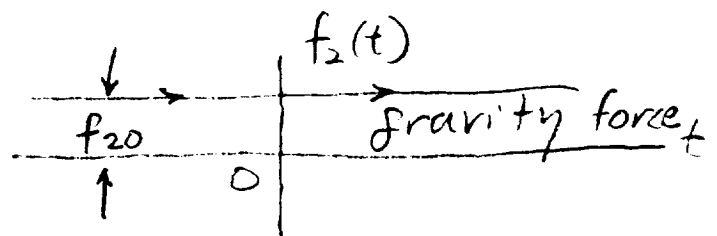
$$m_m \ddot{u}_{m1}(0_+) + C_s \dot{u}_{m1}(0_+) + K u_{m1}(0_+) = 0$$

$$\dot{u}_{m1}(0_+) = 0, \quad u_{m1}(0_+) = u_{m10}$$

The solution to this problem (forcing f_1 only) is given by Equation 3 ($\beta = 0$) with u_{m0} replaced with u_{m10} , so

$$u_{m1}(t) = u_{m10} \cos(\omega_0 t) \quad (9)$$

Force f_2



$f_{20} = k u_{m20}$
 This is a static problem!

$$u_{m2}(t) = u_{m20} \quad (10)$$

Determine u_{m10} & u_{m20} —

$$u_{m0} = u_{m10} + u_{m20} \quad (\text{superposition of static solutions})$$

$$f_{20} = -m_m g \sin(\alpha) = k u_{m20}$$

$$u_{m20} = -\frac{m_m g \sin(\alpha)}{k} = -\frac{m_m g \sin(\alpha)}{\omega_0^2 m_m} \quad *$$

$$= -\frac{g \sin(\alpha)}{\omega_0^2}$$

* $\omega_0^2 \approx k/m_m$

Determine $u_m(t)$ —

$$u_m(t) = u_{m1}(t) + u_{m2}(t) \quad (11)$$

$$= u_{m10} \cos(\omega_0 t) + u_{m20}$$

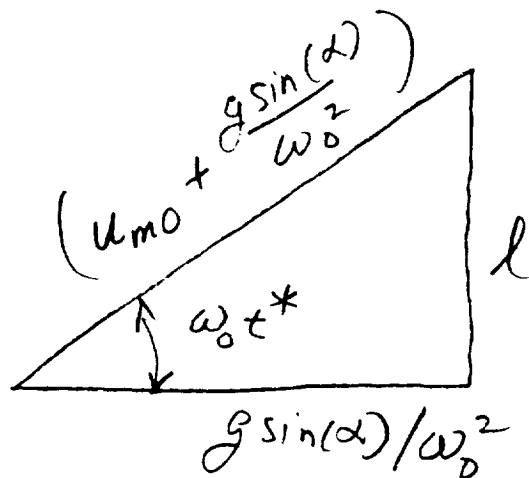
$$= (u_{m10} - u_{m20}) \cos(\omega_0 t) + u_{m20}$$

$$u_m(t) = \left(u_{m10} + \frac{g \sin(\alpha)}{\omega_0^2} \right) \cos(\omega_0 t) - \frac{g \sin(\alpha)}{\omega_0^2}$$

← (12)

Now, find the time, t^* , at which the spring is undeformed, $u_m = 0$.

$$u_m(t^*) = 0 = \left(u_{m10} + \frac{g \sin(\alpha)}{\omega_0^2} \right) \cos(\omega_0 t^*) - \frac{g \sin(\alpha)}{\omega_0^2}$$



$$l^2 + \frac{g^2 \sin^2(\alpha)}{\omega_0^4} = \left(u_{m0} + \frac{g \sin(\alpha)}{\omega_0^2} \right)^2$$

$$= u_{m0}^2 + \frac{g^2 \sin^2(\alpha)}{\omega_0^4} +$$

$$2 u_{m0} g \sin(\alpha) / \omega_0^2$$

$$l^2 = u_{m0}^2 + 2 u_{m0} g \sin(\alpha) / \omega_0^2$$

$$l = \pm \left(u_{m0}^2 + 2 u_{m0} g \sin(\alpha) / \omega_0^2 \right)^{1/2} \quad (\text{use negative root})$$

$$\dot{u}_m(t) = \left(u_{m0} + \frac{g \sin(\alpha)}{\omega_0^2} \right) (-\sin(\omega_0 t) \omega_0)$$

WRW

9/25/87

CCC

9/25/87

1311.16

12

21

Exit Velocity of Spring

$$\dot{u}_m(t^*) = -\left(u_{m0} + \frac{g \sin(\alpha)}{\omega_0^2}\right) \omega_0 \sin(\omega_0 t^*)$$

$$= -\left(u_{m0} + \frac{g \sin(\alpha)}{\omega_0^2}\right) \omega_0 \frac{\left(u_{m0}^2 + 2u_{m0}g \sin(\alpha)/\omega_0^2\right)^{1/2}}{\left(u_{m0} + g \sin(\alpha)/\omega_0^2\right)}$$

$$\dot{u}_m(t^*) = \omega_0 \left(u_{m0}^2 + (2u_{m0}g \sin(\alpha)/\omega_0^2)\right)^{1/2}$$

(13)

Note that when $g=0$, Equation 13 reduces to Equation 4, except for a sign. Equation 13 is the result that is desired!!

WON

9/28/87

CCK

8/25/89

1311.16

13

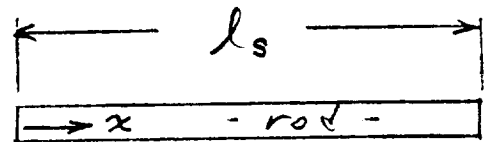
21

Ex. + Velocity of Spring

2) Now the velocity of the c.g. of the spring, as the module loses contact with it, must be found. The spring is looked at as a continuous elastic rod. The motion of the c.g. is found by determining the motion ^{involving} the rigid body mode, $U_0(x)$.*

$$U_0(x) = \sqrt{m l_s}$$

$$\omega_0 = 0$$



m, EA are constants

$m \equiv \text{mass per unit length}$

Generalized coordinate $\eta_0(t)$ is given by

$$\eta_0(t) = \frac{1}{\omega_0} \int_0^t N_0(\tau) \sin \omega_0(t-\tau) d\tau + \eta_0(0) \cos \omega_0 t + \dot{\eta}_0(0) \sin(\omega_0 t) / \omega_0 \quad (14)$$

* Ref. - Analytical Methods In Vibrations by Leonard Meirovitch, Macmillan, 1967, p. 284.

The generalized force $N_0 = 0$. Take $t=0$ for this part only, 2), as corresponding to t^* in the previous part, 1).

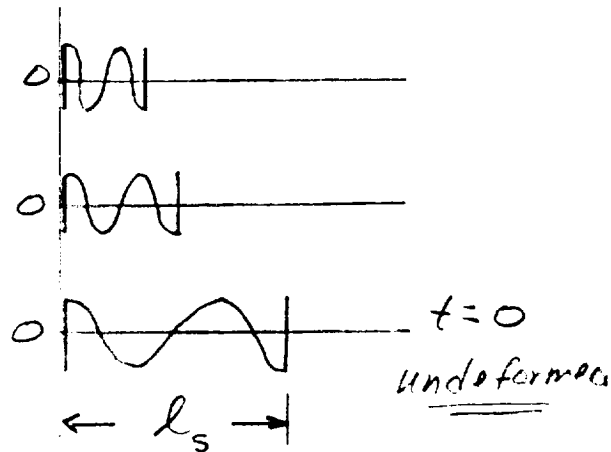
$$\eta_0(0) = 0 \quad (u(x, 0) = 0)$$

$$\dot{\eta}_0(0) = \int_0^{l_s} m(x) U_0(x) \dot{u}(x, 0) dx$$

Look at the spring during its compression stage only —

$$u(x, t) = \int_0^x \frac{P dx}{AE} = \frac{P}{AE} x \Big|_0^x$$

$$= Px/AE \quad (\text{static})$$



$\dot{u}(x, t)$ must be found from this expression

$$u(l_s, t) = Pl_s/AE$$

$$u(x, t) = u(l_s, t) (x/l_s), \quad t \leq 0 \quad (15)$$

NBN

9/28/87

CCK

8/25/89

13/1.16

15

21

Exist Velocity of Spring

$$\dot{u}(x,t) = \dot{u}(l_s, t) (x/l_s), \quad t \leq 0 \quad (16)$$

$$\dot{\eta}_0(0) = \int_0^{l_s} m \frac{1}{(ml_s)^{1/2}} \dot{u}(l_s, 0) (x/l_s) dx$$

$$= \left(\frac{m}{l_s}\right)^{1/2} \frac{\dot{u}(l_s, 0)}{l_s} \int_0^{l_s} x dx$$

$$= \left(\frac{m}{l_s}\right)^{1/2} \frac{\dot{u}(l_s, 0)}{l_s} \frac{x^2}{2} \Big|_0^{l_s} = \left(\frac{m}{l_s}\right)^{1/2} \frac{\dot{u}(l_s, 0)}{l_s} \frac{l_s^2}{2}$$

$$= \frac{1}{2} l_s \left(\frac{m}{l_s}\right)^{1/2} \dot{u}(l_s, 0)$$

$$\eta_0(t) = \dot{\eta}_0(0) \sin(\omega_0 t) / \omega_0$$

$$\lim_{\omega_0 \rightarrow 0} \sin(\omega_0 t) / \omega_0 = \lim_{\omega_0 \rightarrow 0} \cos(\omega_0 t) \cdot t \cdot 1/1$$

$$= t$$

$$\eta_0(t) = \dot{\eta}_0(0) t$$

$$u(x,t) = \sum_r U_r(x) \eta_r(t) = \sum_r u_r(x,t)$$

$$u_0(x,t) = U_0(x) \eta_0(t)$$

$$= \frac{1}{(m l_s)^{1/2}} \cdot \dot{\eta}_0^{(0)} t = \frac{1}{(m l_s)^{1/2}} \cdot \frac{1}{2} l_s \left(\frac{m}{l_s}\right)^{1/2} \dot{u}(l_s, 0) t$$

$$= \frac{1}{2} \dot{u}(l_s, 0) t$$

$$\dot{u}_0(x,t) = \frac{1}{2} \dot{u}(l_s, 0) \quad (\text{during compression stage})$$

However, at $t=0$ (or $t=t^*$ in part 1)

$$\dot{u}(l_s, 0) = \dot{u}_m(t^*) \quad (17)$$

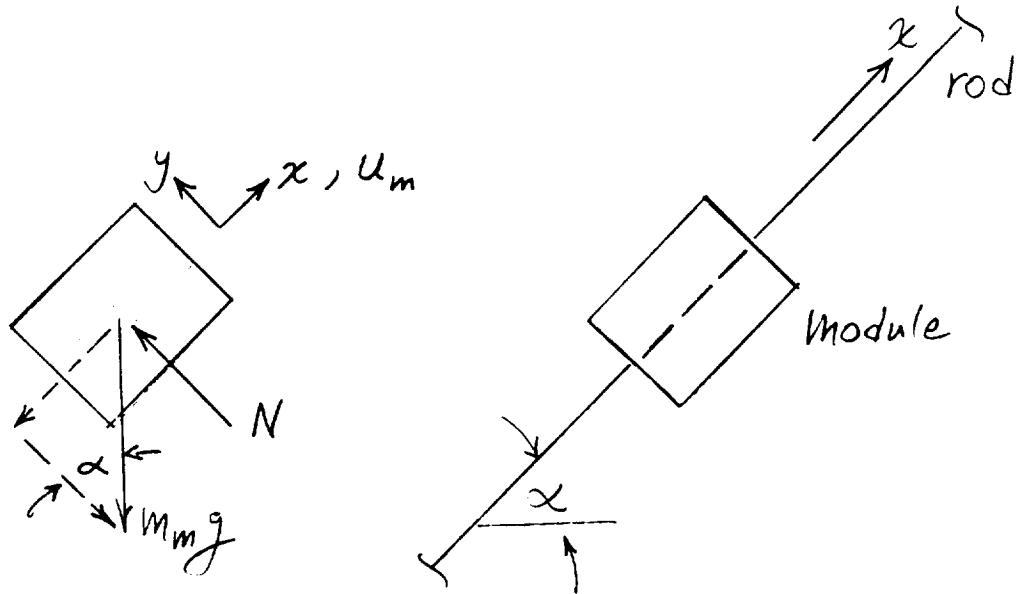
Thus,

$$\dot{u}_{SCG}(t^*) = \frac{1}{2} \dot{u}_m(t^*)$$

(shifted to time frame for part 1)

← (18)

3) Velocity of module as it leaves the end of the rod - calc. it.



$$\Sigma F_x = m_m \ddot{u}_m = -m_m g \sin(\alpha) \quad (19)$$

$$\ddot{u}_m = -g \sin(\alpha)$$

$$\frac{d}{dt}(\dot{u}_m) = -g \sin \alpha$$

$$\int d(\dot{u}_m) = -g \sin \alpha \int dt + C_1$$

$$\dot{u}_m = -g \sin(\alpha) t + C_1 \quad (20)$$

$$\frac{du_m}{dt} = -g \sin(\alpha) t + c_1$$

$$\int du_m = \int (-g \sin(\alpha) t + c_1) dt + c_2$$

$$u_m(t) = -g \sin(\alpha) \frac{t^2}{2} + c_1 t + c_2 \quad (21)$$

Using the value of $\dot{u}_m(t^*)$ from 1) and $u_m(t^*) = 0$, the following is found:

$$u_m(t^*) = -g \sin(\alpha) \frac{(t^*)^2}{2} + c_1 t^* + c_2 = 0$$

$$\dot{u}_m(t^*) = -g \sin(\alpha) t^* + c_1$$

$$c_1 = \dot{u}_m(t^*) + g \sin(\alpha) t^* \quad (22)$$

$$c_2 = g \sin(\alpha) \frac{(t^*)^2}{2} - c_1 t^* \quad (23)$$

MADE BY

WBN

DATE

9/28/87

CHECKED BY

CCK

DATE

8/25/89

JOB NUMBER

1311.16

PAGE

19

OF

21

DESCRIPTION

Ext. + Velocity of Spring

$$u_m(t_e) = l_r - l_s = -g \sin(\alpha) \frac{t_e^2}{2} + C_1 t_e + C_2$$

$$-g \frac{\sin(\alpha)}{2} t_e^2 + C_1 t_e + C_2 - (l_r - l_s) = 0$$

$$t_{e,2} = \frac{-C_1 \pm \left(C_1^2 - 4 \left(-\frac{g \sin(\alpha)}{2} \right) (C_2 - (l_r - l_s)) \right)^{\frac{1}{2}}}{2 \left(-\frac{g \sin(\alpha)}{2} \right)}$$

$$t_{e,2} = \frac{C_1 \mp \left(C_1^2 + 2 g \sin(\alpha) (C_2 - (l_r - l_s)) \right)^{\frac{1}{2}}}{g \sin(\alpha)}$$

(24)

$$\dot{u}_m(t_e) = -g \sin(\alpha) t_e + C_1$$

(25)

4) Velocity of spring as it leaves the end of the rod - calc. it. The calculation is essentially the same as that for 3). Instead of using the modulo, use the spring. The displacement of the spring is $u_s(t)$. Equations 19 - 21 can be used to easily obtain the corresponding equations for the spring as follows:

$$\sum F_x = m_s \ddot{u}_s = -m_s g \sin(\alpha) \quad (26)$$

$$\dot{u}_s = -g \sin(\alpha) t + C'_1 \quad (27)$$

$$u_s(t) = -g \sin(\alpha) \frac{t^2}{2} + C'_1 t + C'_2 \quad (28)$$

Using the value of $\dot{u}_{SCG}(t^*)$ from Eq. 18 and $u_s(t^*) = 0$, the following is found:

$$C'_1 = \dot{u}_{SCG}(t^*) + g \sin(\alpha) t^* \quad (29)$$

$$C'_2 = g \sin(\alpha) \frac{(t^*)^2}{2} - C'_1 t^* \quad (30)$$

$$\dot{u}_{SCG}(t^*) = \frac{1}{2} \dot{u}_m(t^*)$$

$$u_s(t'_e) = l_r = -g \sin(\alpha) \frac{(t'_e)^2}{2} + C'_1 t'_e + C'_2$$

The solution to this equation can be found from Equation 24 —

$$t'_{e,1,2} = \frac{C'_1 \mp (C'_1^2 + 2g \sin(\alpha)(C'_2 - l_r))^{1/2}}{g \sin(\alpha)} \quad (31)$$

$$\dot{u}_s(t'_e) = -g \sin(\alpha) t'_e + C'_1 \quad (32)$$

Tube Launcher Spring Requirements

Data from the SEDS-STD Case Condition Assumptions

From Figure 8:

<u>Module</u>	<u>Launch Point</u>	<u>Launch Speed</u>	<u>Launch Angle (to vertical)</u>
1	1/4 (2000 sec)	0.5 m/s	75° (α)
2	1/2 (4000 sec)	2.0 m/s	85° (α)
3	3/4 (6000 sec)	4.3 m/s	85° (α)

Note: TEDEMS hardware would require a 45° tilt if it was used in the Shuttle. SEDS total arc of travel is approximately 90° well within the range of the TEDEMS equipment but its angles range from 0°-90° from vertical, whereas TEDEMS is designed for $\pm 60^\circ$ from vertical.

For test purposes, a 45° spacer will be added to the TEDEMS hardware.

Module 1 parameters for LAUNCHMD:

$$\alpha = 30^\circ$$

$$\text{weight} = 350 \text{ grams}$$

$$\text{Rod Travel (}lr_1\text{)} = 14 \text{ in.} + \text{Spring Compression}$$

$$\text{Desired velocity} = 0.5 \text{ m/s}$$

Module 2 parameters for LAUNCHMD:

$$\alpha = 40^\circ$$

$$\text{weight} = 350 \text{ grams}$$

$$\text{Rod Travel (}lr_2\text{)} = lr_1 + 12 \text{ in.} + \text{Spring Compression}$$

$$\text{Desired velocity} = 2.0 \text{ m/s}$$

Module 3 parameters for LAUNCHMD:

$$\alpha = 40^\circ$$

$$\text{weight} = 350 \text{ grams}$$

$$\text{Rod Travel (}lr_3\text{)} = lr_2 + 12 \text{ in.} + \text{Spring Compression}$$

$$\text{Desired velocity} = 4.5 \text{ m/s}$$

Calculation Sheets 1 through 21 show the derivation of the formulae used to calculate spring tension.

Program LAUNCHMD is Fortran listing of program used to size springs.

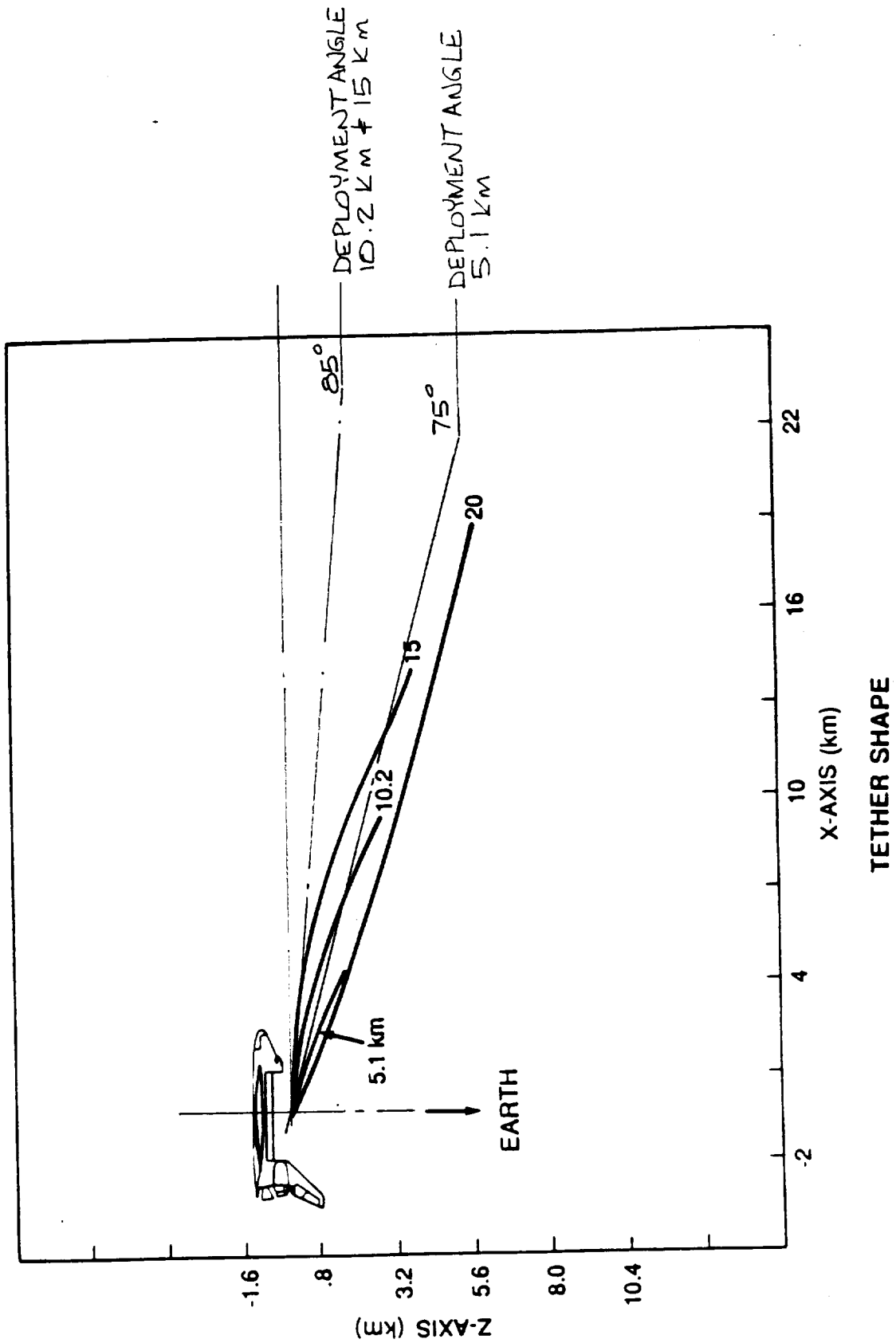


FIGURE 3

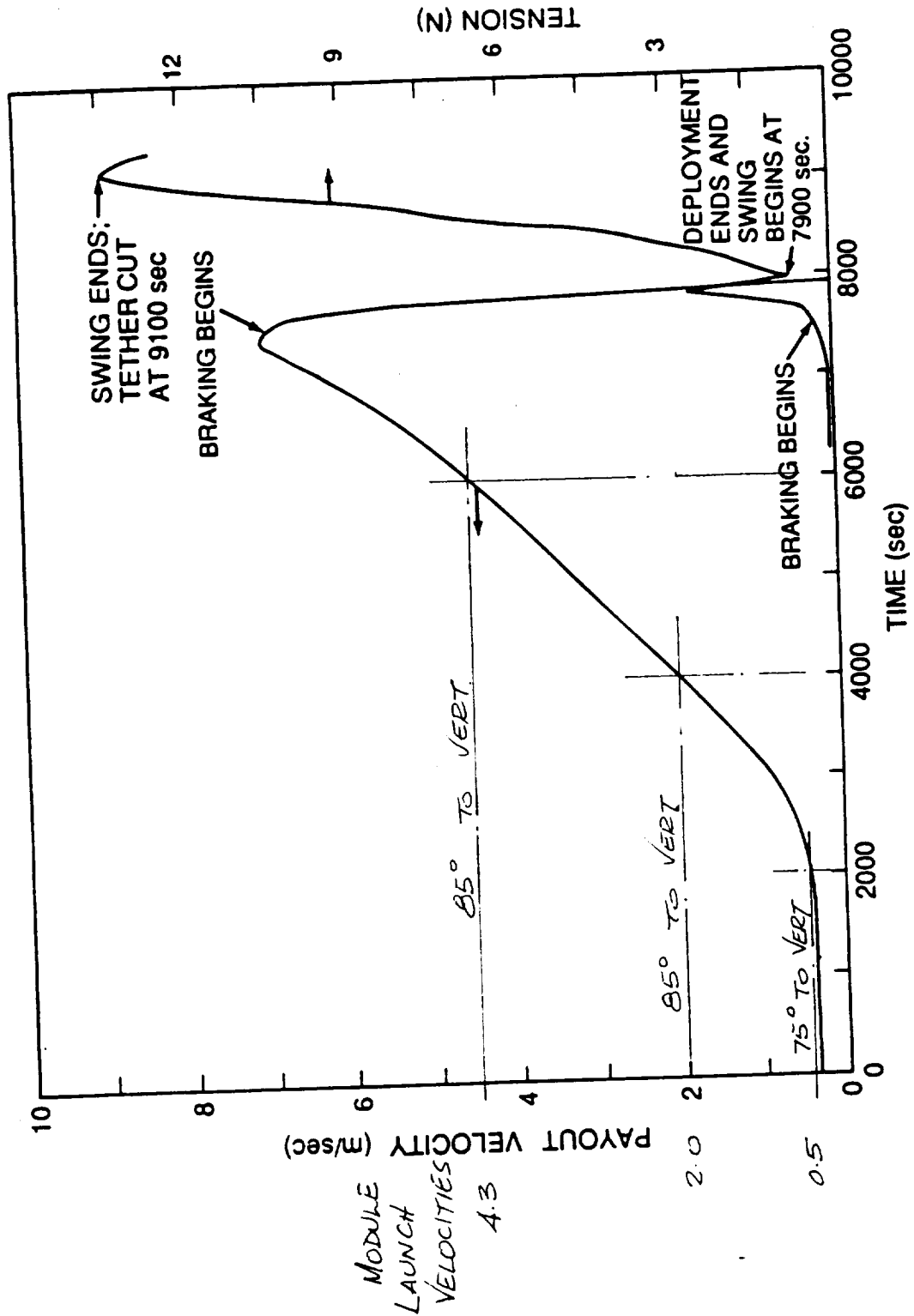


FIGURE 8

PROGRAM LAUNCHMD

```

*****
C *****
C THIS PROGRAM CALCULATES THE VELOCITY OF A TETHER MODULE JUST AS
C IT LEAVES THE END OF THE LAUNCH ROD. THE EQUATIONS USED ARE
C TAKEN FROM "EXIT VELOCITY OF SPRING" BY WBW, 9/23/87.
C *****
CHARACTER*16 IRESP
REAL K,MM,LR,LS
51 CONTINUE
C CALL VCLEAR
C CALL VCURXY(0,0)
PRINT *, 'PROGRAM LAUNCHMD -- CALCULATE EXIT VELOCITY OF '
PRINT *, ' TETHER MODULE '
PRINT *, ' '
PRINT *, ' '
PRINT *, ' '
C BEGIN ENTERING THE DATA
PRINT *, ' ENTER PARAMETER VALUES '
PRINT *, ' '
PRINT *, ' ENTER SPRING CONSTANT, K '
11 READ (*,11) K
FORMAT (F10.3)
PRINT *, ' ENTER MODULE MASS, MM '
READ (*,11) MM
PRINT *, ' ENTER INITIAL SPRING DISPLACEMENT, UMO '
READ (*,11) UMO
PRINT *, ' ENTER ACCELERATION OF GRAVITY, G '
READ (*,11) G
PRINT *, ' ENTER ANGLE OF ROD FROM HORIZONTAL, ALPHA(DEG) '
READ (*,11) ALPHA
PRINT *, ' ENTER ROD LENGTH, LR '
READ (*,11) LR
PRINT *, ' ENTER UNDEFORMED SPRING LENGTH, LS '
READ (*,11) LS
C END OF ENTERING THE DATA
C
C BEGIN THE CALCULATIONS
DUMY1 = K/MM
OMEGA0 = SQRT(DUMY1)
DUMY2 = ALPHA*3.1416/180.0
DUMY3 = SIN(DUMY2)
DUMY4 = G*DUMY3/OMEGA0**2
DUMY5 = DUMY4/(UMO + DUMY4)
TSTAR = ACOS(DUMY5)/OMEGA0
DUMY6 = UMO**2 + 2.0*UMO*DUMY4
DUMY7 = SQRT(DUMY6)
UMDOTTS = OMEGA0*DUMY7
C1 = UMDOTTS + G*DUMY3*TSTAR
C2 = G*DUMY3*TSTAR**2/2 - C1*TSTAR
DUMY8 = C1**2 + 2.0*G*DUMY3*(C2-(LR-LS))
DUMY9 = SQRT(DUMY8)
TE1 = (C1 - DUMY9)/G*DUMY3
UMDOTTE = -G*DUMY3*TE1 + C1
C END OF THE CALCULATIONS
C
C BEGIN WRITING OUT THE SOLUTION TO THE SCREEN
PRINT *, ' '
PRINT *, ' '
PRINT *, ' THE INPUT PARAMATER VALUES ARE GIVEN BELOW '
WRITE (*,25) K,MM,UMO,G,ALPHA,LR,LS
25 FORMAT (' K = ',F10.3,' MM = ',F10.3,' UMO = ',F10.3,/,
* ' G = ',F10.3,' ALPHA = ',F10.3,' LR = ',F10.3,/,
* ' LS = ',F10.3)
PRINT *, ' '
PRINT *, ' THE SOLUTION OBTAINED IS GIVEN BELOW '

```

```
PRINT *, ' '
WRITE (*,21) TSTAR
21 FORMAT (' TIME OF SEPERATION FROM SPRING, TSTAR ',F10.3)
PRINT *, ' '
WRITE (*,22) UMDOTTS
22 FORMAT (' VELOCITY AT TSTAR, UMDOTTS ',F10.3)
PRINT *, ' '
WRITE (*,23) TE1
23 FORMAT (' EXIT TIME FROM ROD END, TE1 ',F10.3)
PRINT *, ' '
WRITE (*,24) UMDOTTE
24 FORMAT (' VELOCITY AT EXIT FROM ROD, UMDOTTE ',F10.3)
END WRITING OUT THE SOLUTION

C
C
C
DETERMINE IF ANOTHER SOLUTION IS DESIRED
PRINT *, 'IS ANOTHER SOLUTION DESIRED? '
READ (*,31) IRESP
31 FORMAT (A16)
IRESP = IRESP(1:2)
IF(IRESP.EQ.'Y') GO TO 51
STOP
END
```

ANCO

APPENDIX B

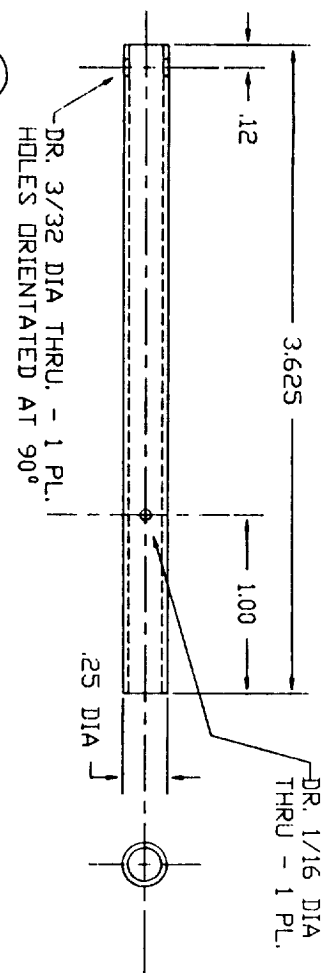
DRAWINGS

DRAWING NUMBER	No. OF SHEETS	DESCRIPTION
131116-109	5	ORIGAMI LAUNCHER
131116-110	3	ORIGAMI MODULES
131116-112	4	ATTITUDE DETECTOR
131116-113	1	CLAMSHELL MODULE ASSEMBLY
131116-114	1	CONTROL DIAGRAM
131116-115	3	TUBE LAUNCHER
131116-116	3	GIMBAL
131116-117		GEARBOX
131116-118	2	INDEXING MECHANISM
131116-119	1	ELECTRICAL SCHEMATIC TFCU SUBSYSTEM
131116-120		CLAMSHELL MODULE COVER ASSEMBLY
131116-121		CLAMSHELL MODULE BASE ASSEMBLY

0.0094
0.0094

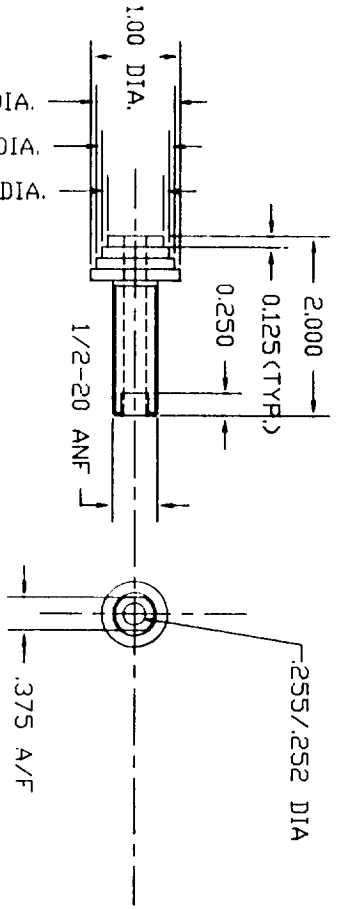
1

SCREW (MODD)
MATL. : 1/4-28 UNF X 1 1/4 LG RH BRASS SCREW.
FINISH : NONE
H.T. : NONE
QTY. : 2 PER ASSY



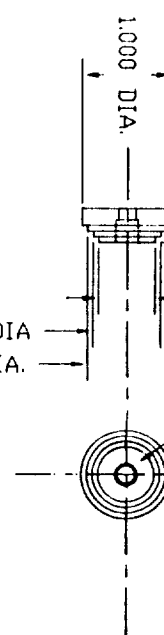
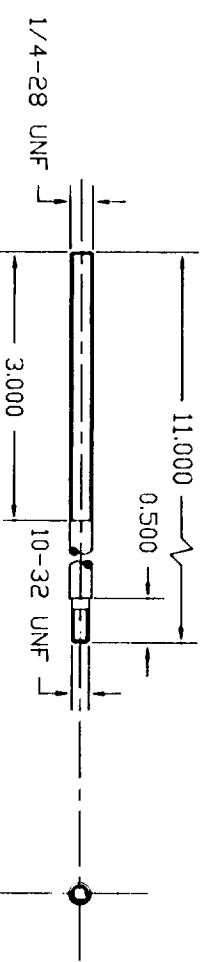
5

SPRING TUBE
MATL. : 1/4 DIA X .028 WALL 2024T AL. TUBE
FINISH : BLACK ANODIZE
H.T. : NONE
QTY. : 2 PER ASSY



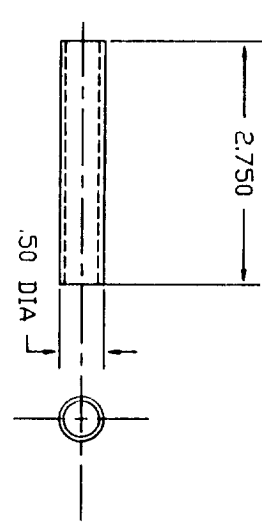
8

SPRING FORCE ADJUSTER
MATL. : 1 DIA X 2 1/2 LG. BRASS ROD
FINISH : NONE
H.T. : NONE
QTY. : 4 PER ASSY



11

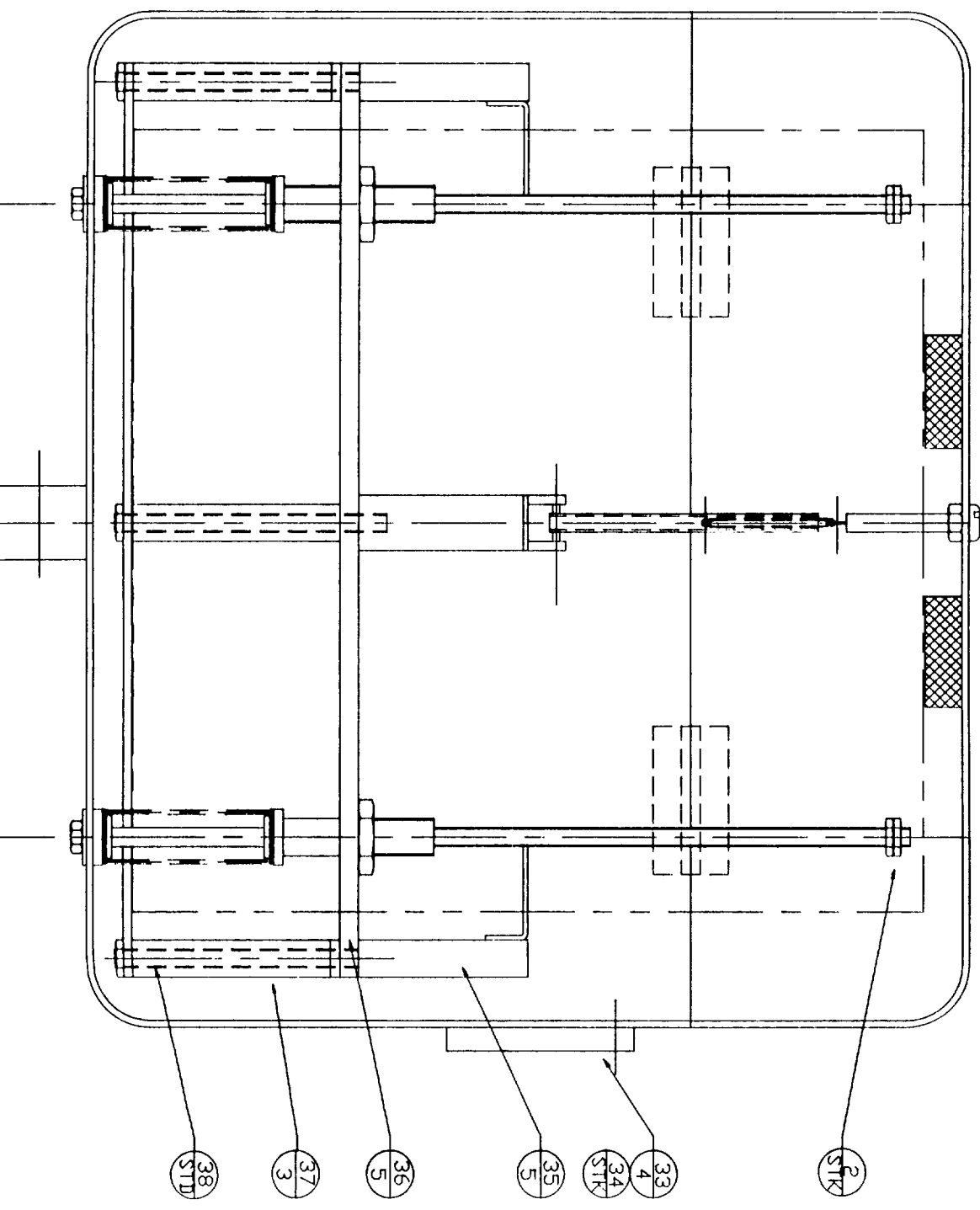
SPRING SEAT
MATL. : 1 DIA ST. STEEL ROD X 3/4 LG.
FINISH : NONE
H.T. : NONE
QTY. : 4 PER ASSY

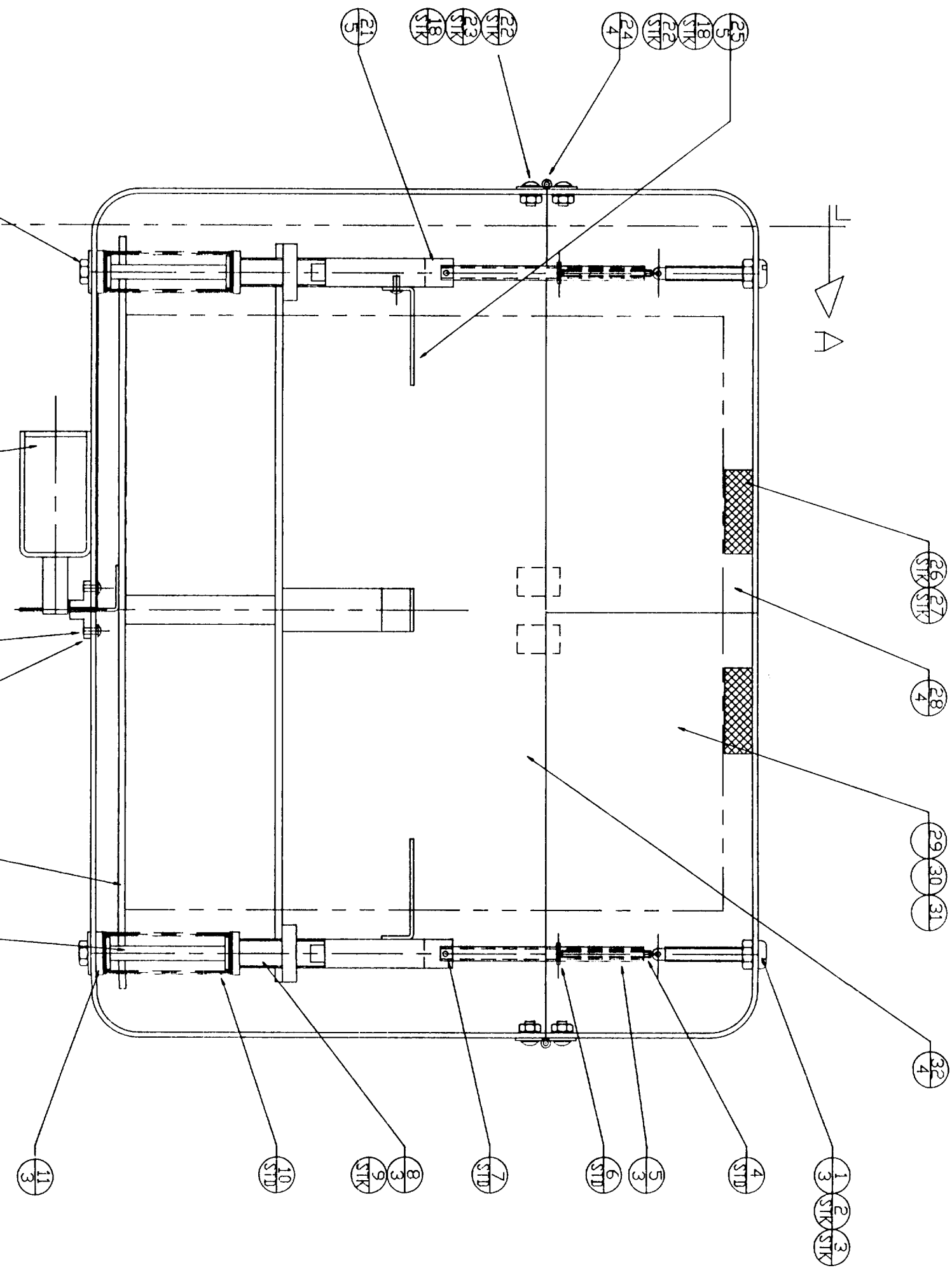


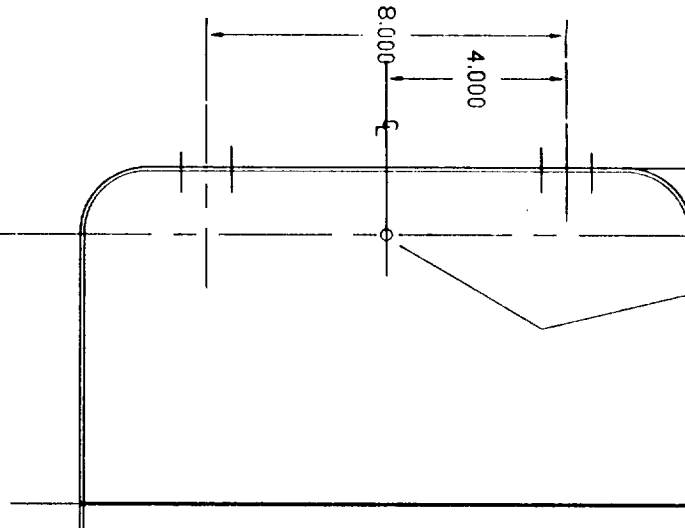
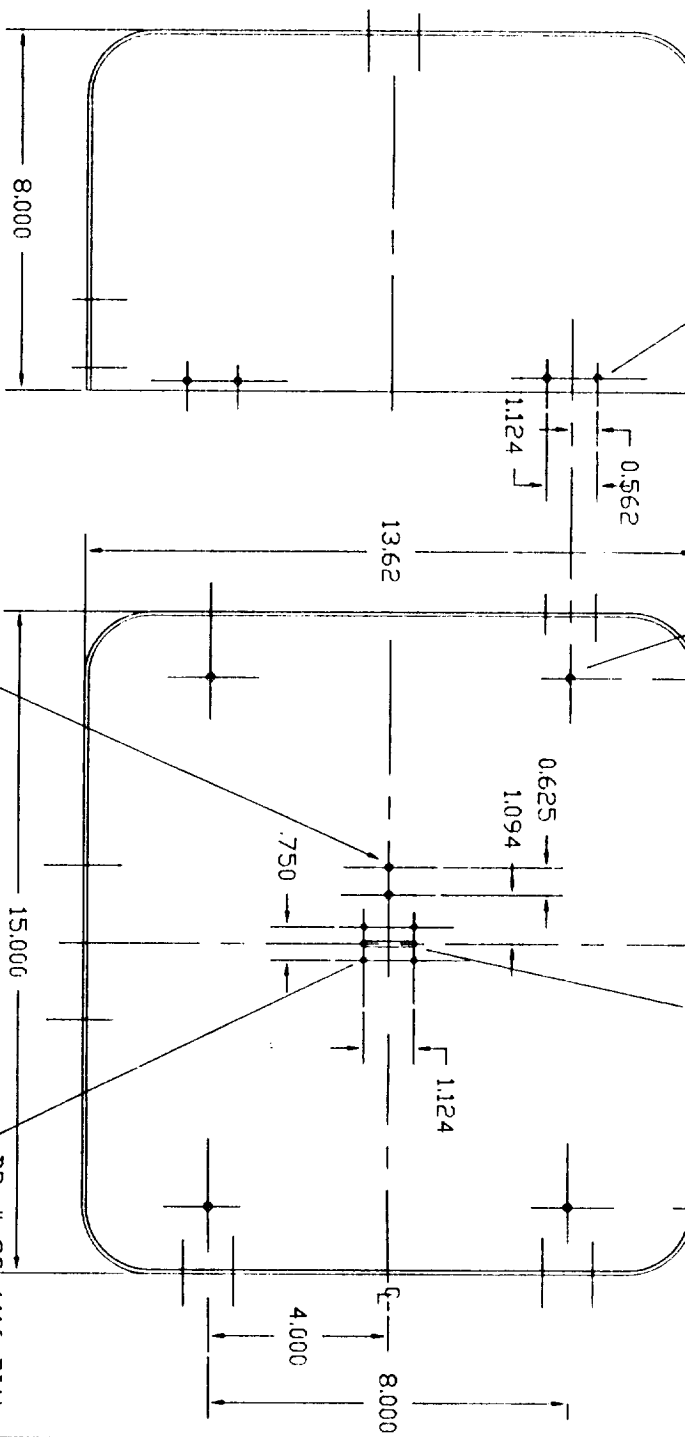
37

SPACER TUBE
MATL. : 1/2 DIA X .049 WALL X 3.0 LG ALUM.
FINISH : BLACK ANODIZE
H.T. : NONE
QTY. : 4 PER ASSY

1.
FOLDOUT FRAME





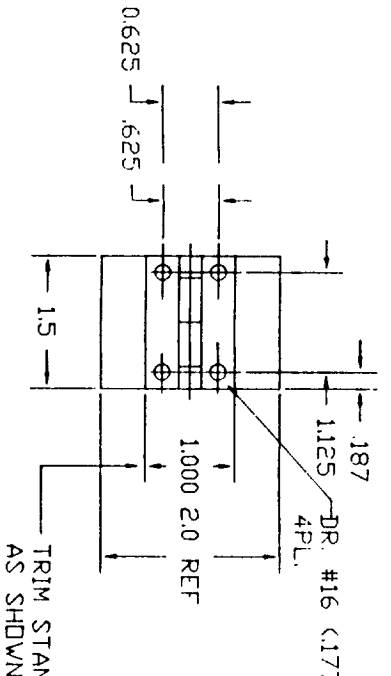
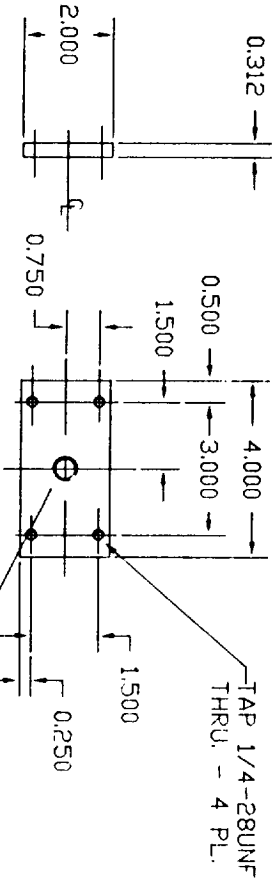


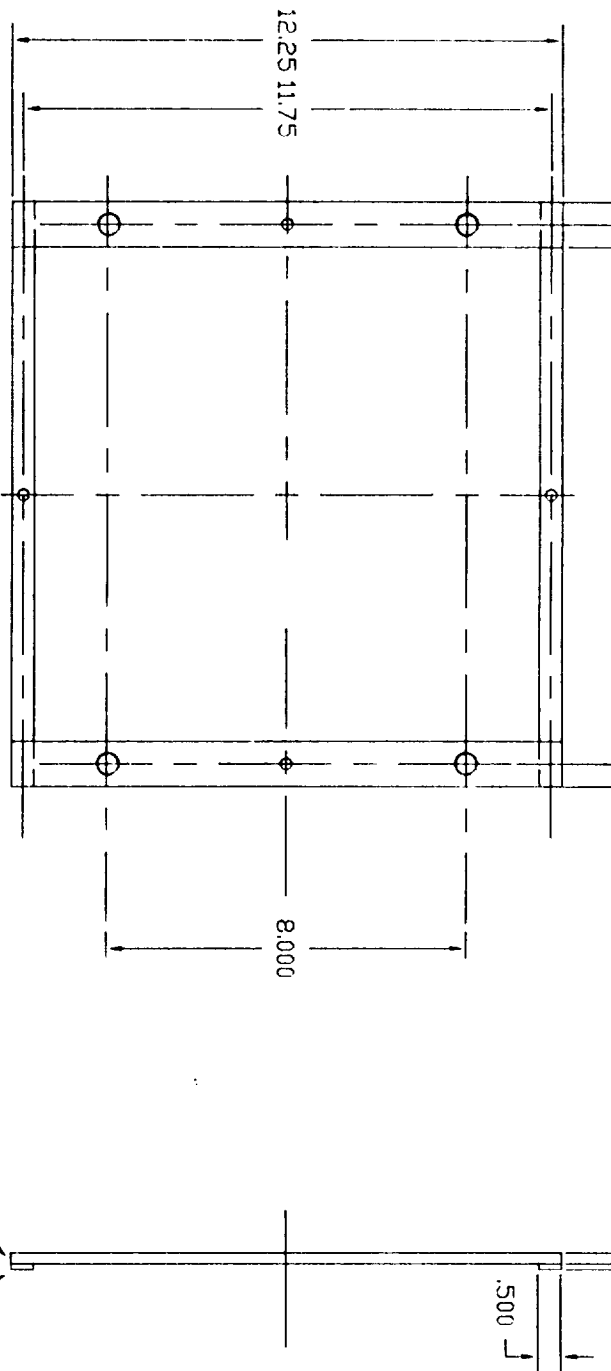
32

CANISTER BASE
 MATL. : ZERO CORP. # Z218-240 RECT. BDX. TRIMMED 8.00 LG.
 FINISH : BLACK ANODIZE
 H.T. : NONE
 QTY. : 1 PER ASSY

HALF FULL SCALE

HALF FULL SCALE





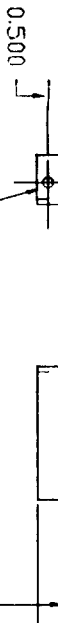
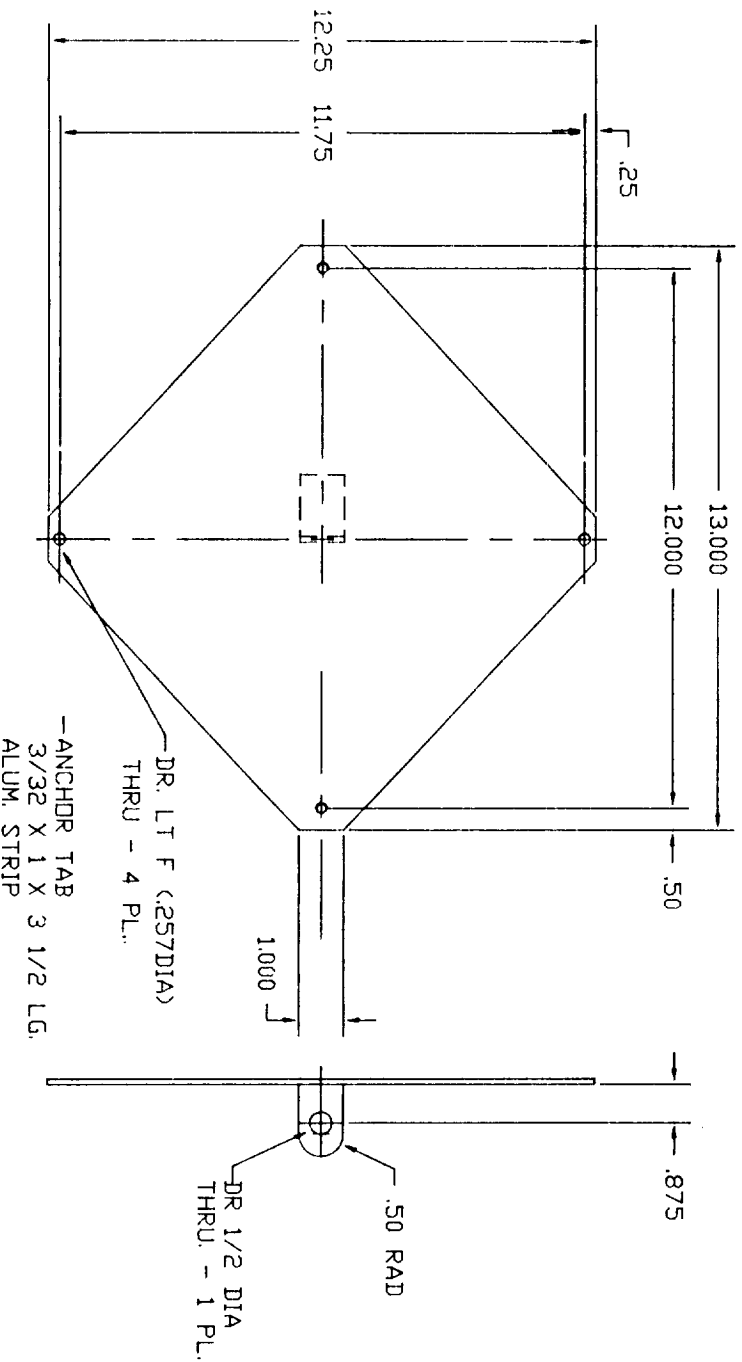
(36)

UPPER FRAME ASSY
 MATL. : AS NOTED
 FINISH : BLACK ANODIZE
 H.T. : NONE
 QTY. : 1 PER ASSY

1/4 X 1 X 12 1/4 LG ALUM. BAR

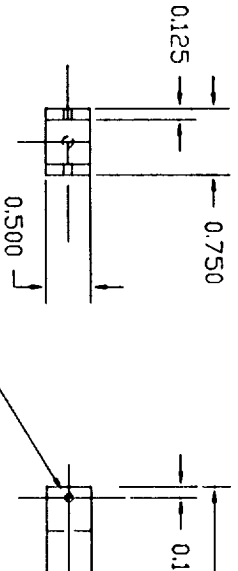
1/8 X 1/2 X 13 LG. ALUM. BAR

DR. LT F (.257DIA)
 THRU - 4 PL.



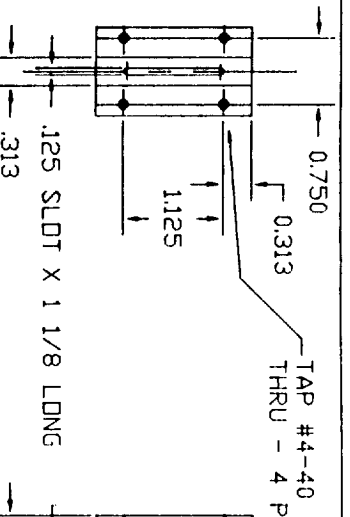
(25)

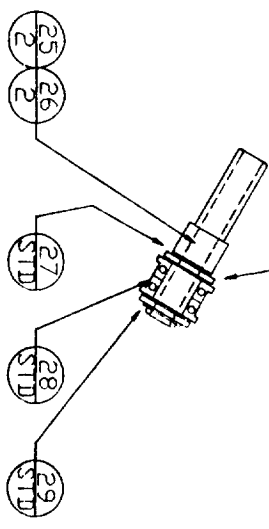
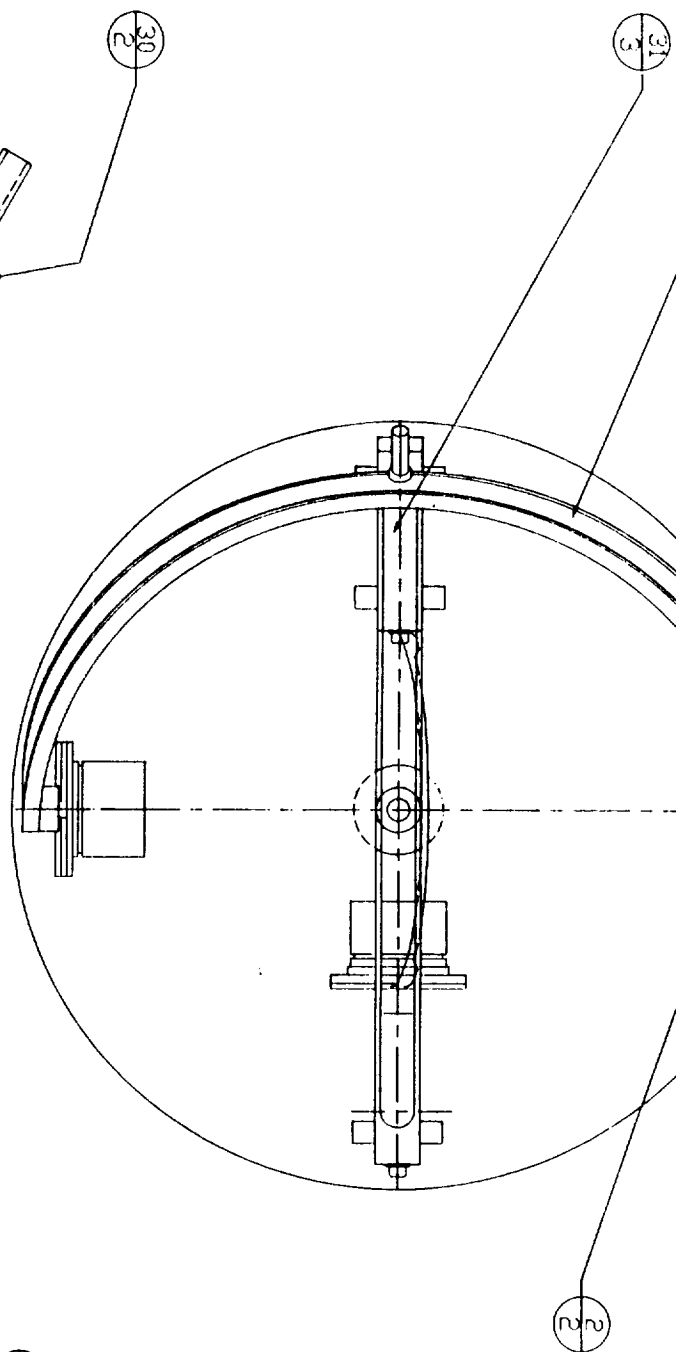
MODULE SUPPORT PLATE
 MATL. : 3/4 X 1/16 X 2 LG ALUM.
 FINISH : BLACK ANODIZE
 H.T. : NONE
 QTY. : 4 PER ASSY



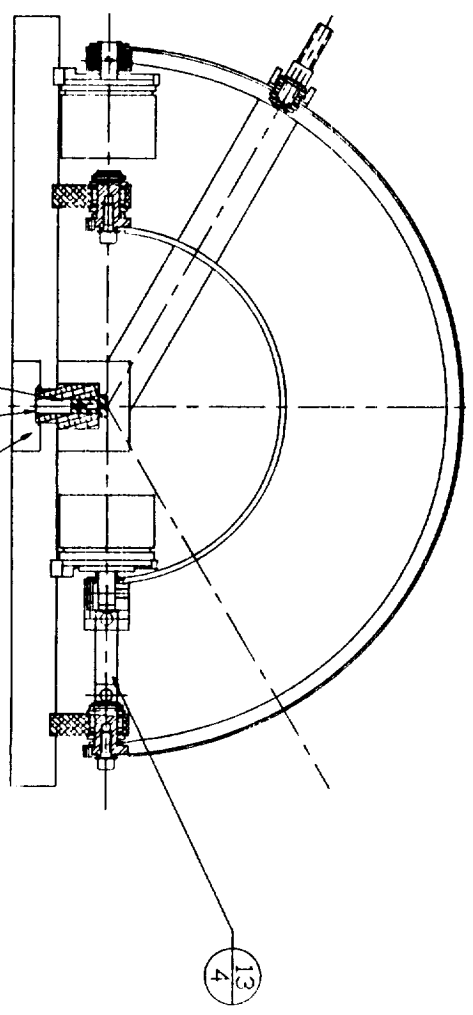
(21)

CLEVIS BAR
 MATL. : 1/2 X 3/4 X 3 LG ALUM.
 FINISH : BLACK ANODIZE
 H.T. : NONE
 QTY. : 2 PER ASSY

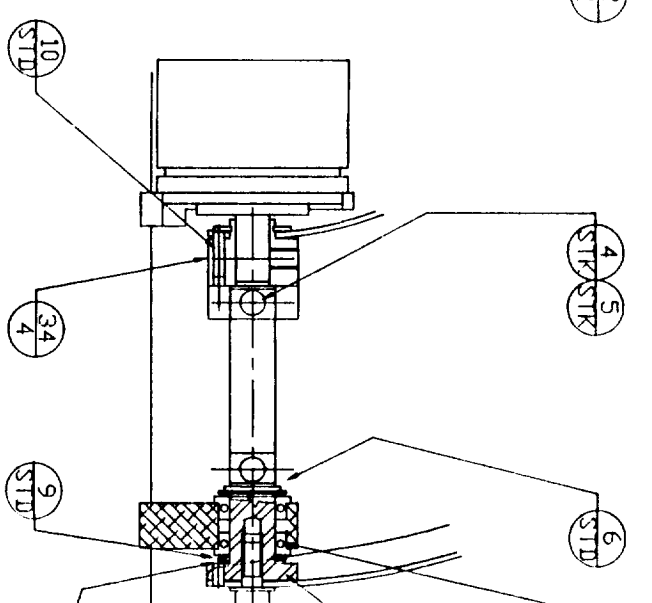




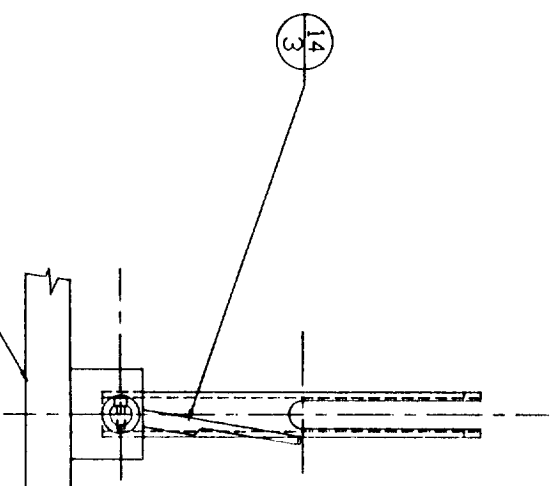
2 X FULL SCALE



1.
FOLDOUT FRAME



2 X FULL SCALE

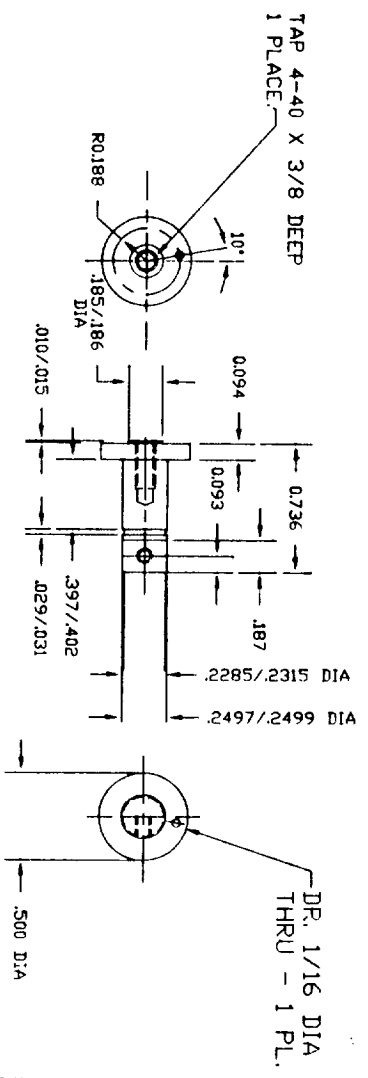


33

PIVOT SHAFT

MATL: 1/2 DIA X 1 1/2 LG ST. STL. BAR
FINISH: NONE
H.T.: NONE
QTY: 2 PER ASSEMBLY

SCALE: 2 X FULL SCALE

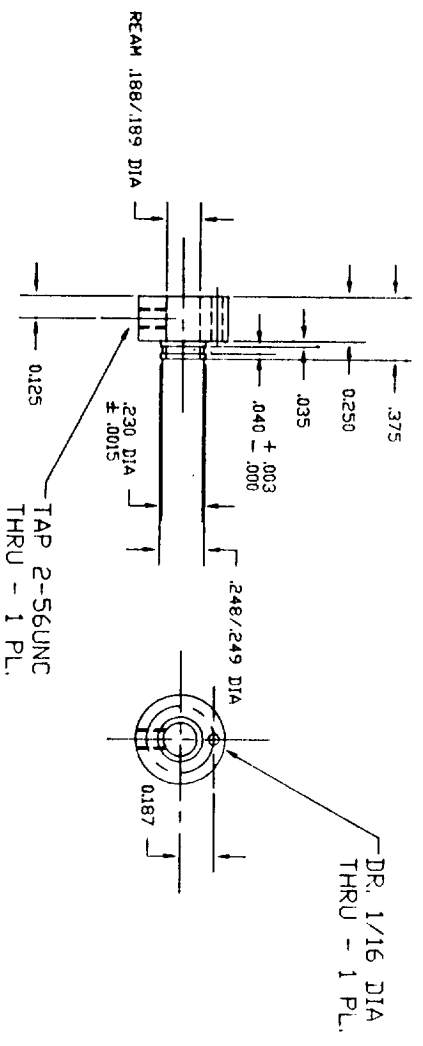


7

PIVOT (TENSION SENSING)

MATL: 1/2 DIA X 1 1/2 LG ST. STL. BAR
FINISH: NONE
H.T.: NONE
QTY: 1 PER ASSEMBLY

SCALE: 2 X FULL SCALE



24

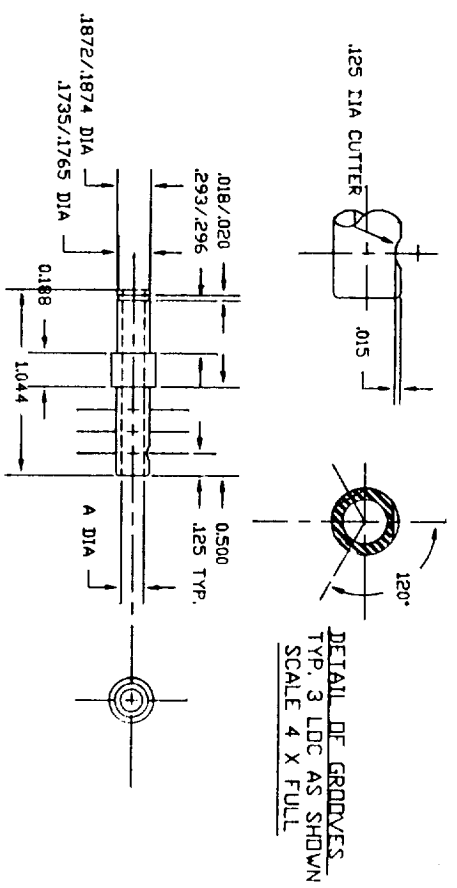
RVDT ATTACHMENT BUSH

16

DRILL BUSHING POST

MATL: 1/2 DIA X 1 LG 1018 CR STL. BAR
FINISH: CAD PLATE
H.T.: NONE
QTY: 2 PER ASSEMBLY

SCALE: 2 X FULL SCALE



25

NOZZLE GUIDE

A= 0.120 DIA (#31)
QTY: 1 PER ASSY

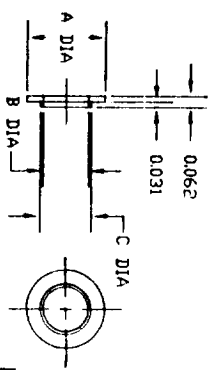
26

NOZZLE GUIDE

A= 0.0XX DIA
QTY: 1 PER ASSY

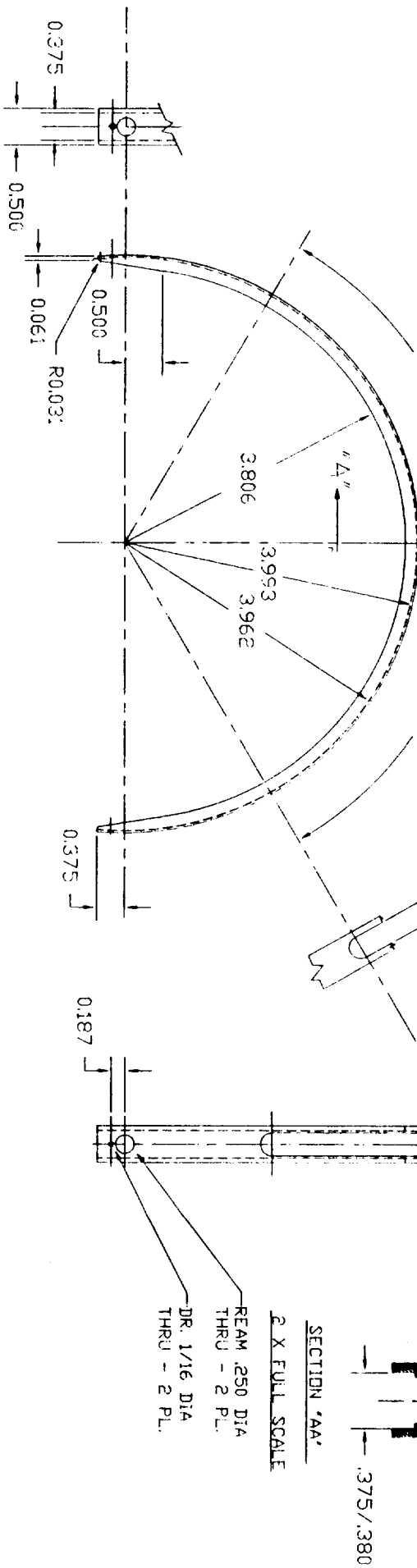
MATL: 1/4 DIA X 1 1/4 LG 303 ST. STL. BAR
FINISH: NONE
H.T.: NONE

SCALE: 2 X FULL SCALE



ITEM	A	B	C	QT
9	.437	.251/.253	.281	6
30	.312	.188/.189	.218	?

BEARING WASHER

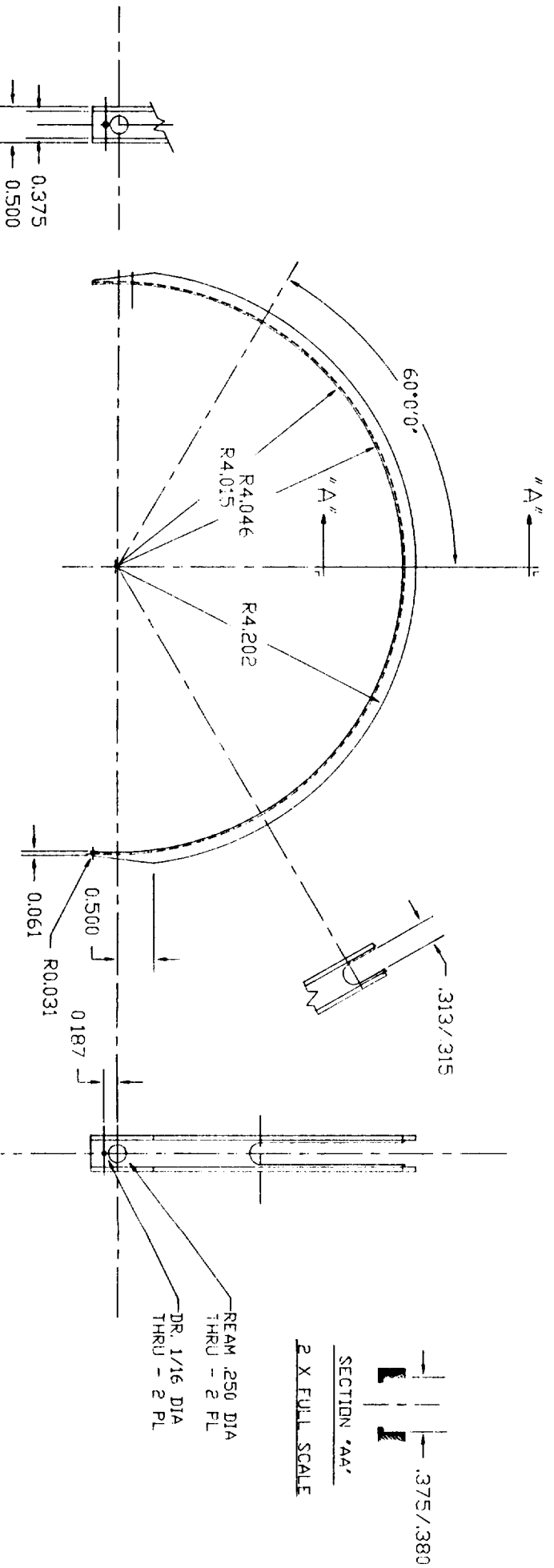


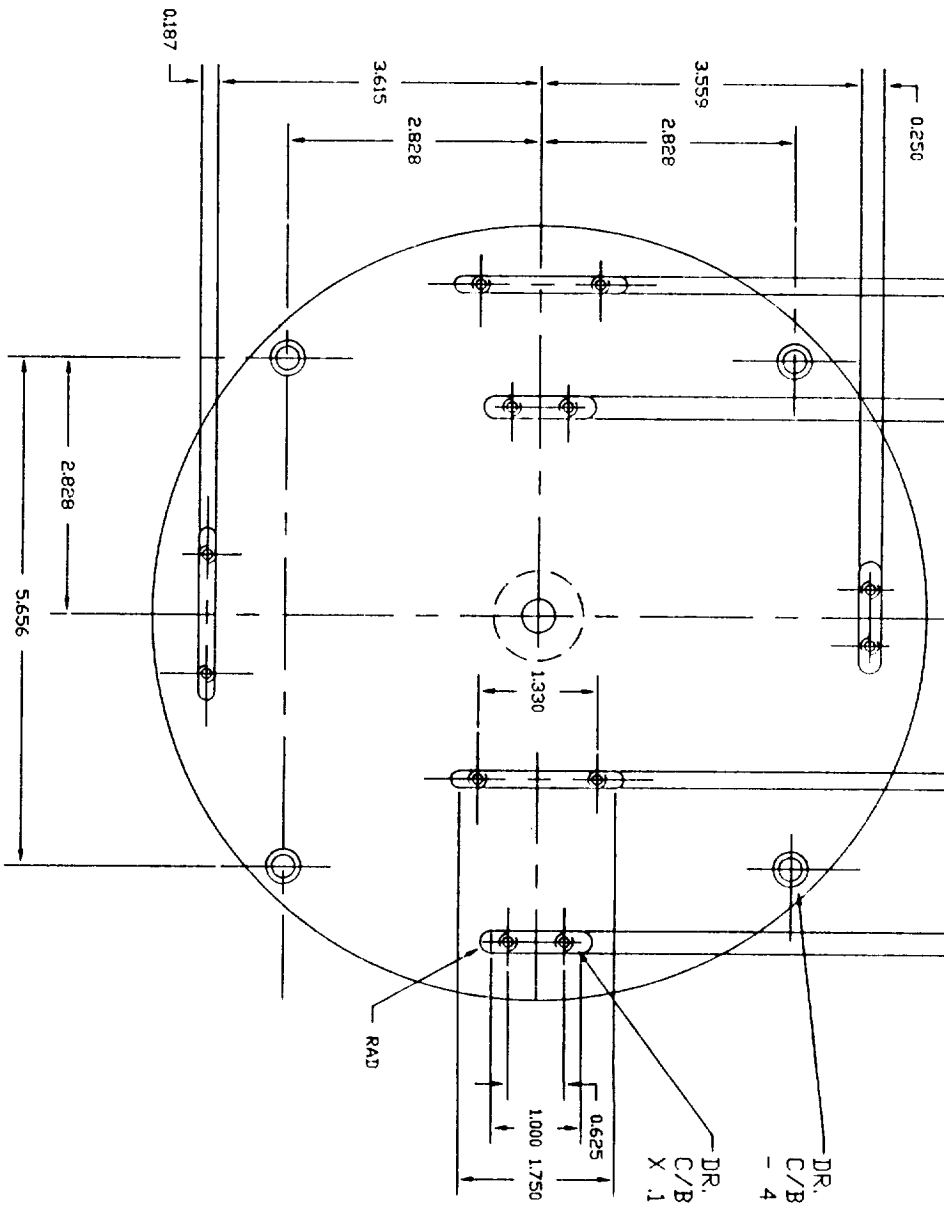
31

TRACKING HOOP (INNER)

MATL: 8 1/4 DIA X 1/4 WALL ROUND STL. TUBING
 FINISH: CAD. PLATE
 HT: NONE
 QTY: 1 PER ASSEMBLY

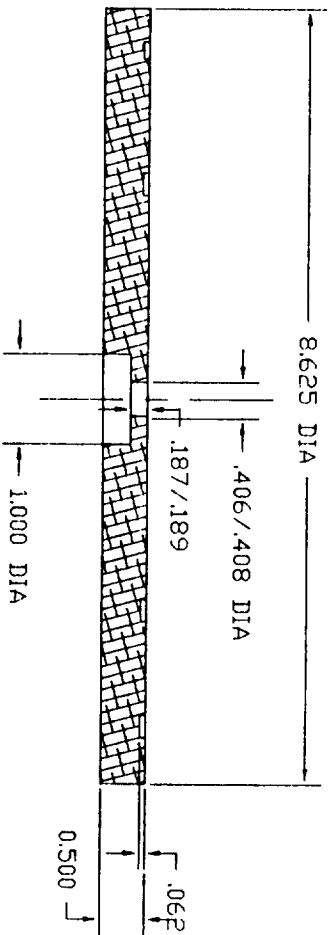
SCALE: FULL SCALE





DR. LT P (.323 DIA) THRU
 C/BORE 31/64 DIA X .32 DP.
 - 4 PL.

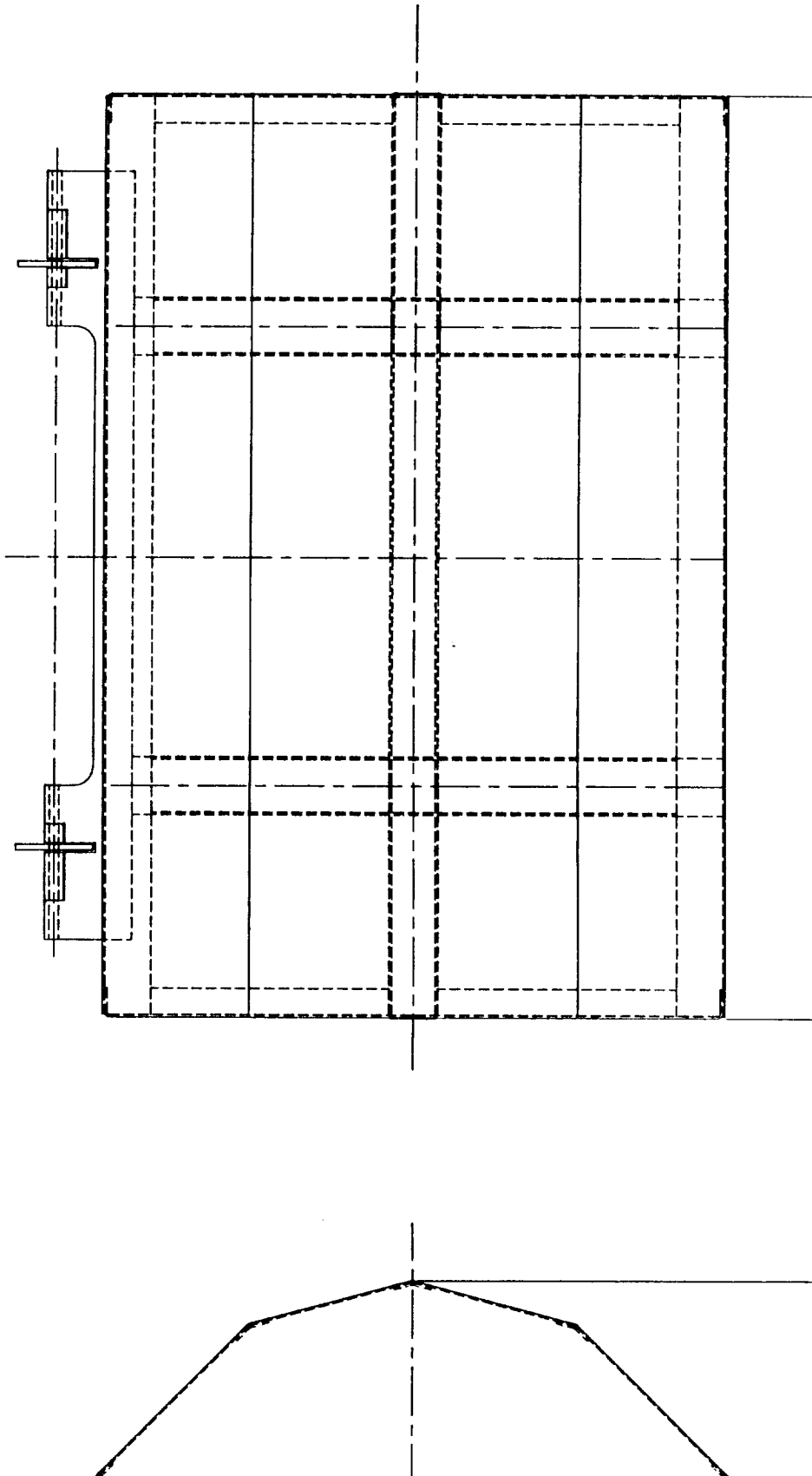
DR. #32 (.116 DIA) THRU
 C/BORE (FAR SIDE) 13/64 DIA
 X .125 DEEP - 12 PL.



1

BASEPLATE
 MATL: 1/2 THICK ALUMINUM TOOLING PLATE
 FINISH: BLACK ANODIZE
 H.T.: NONE

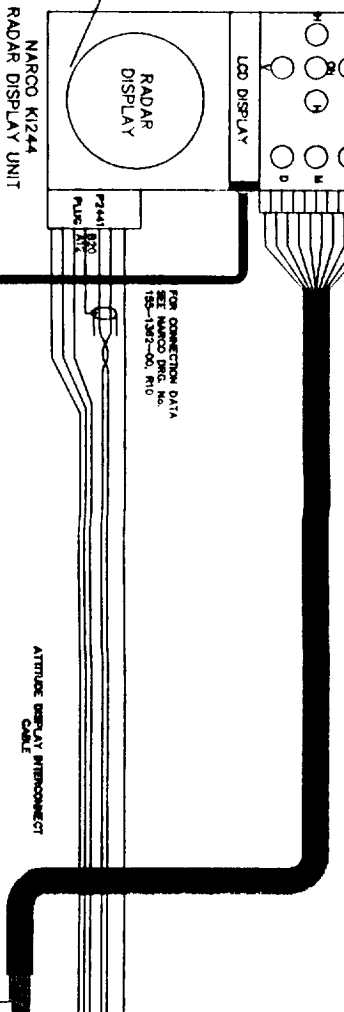
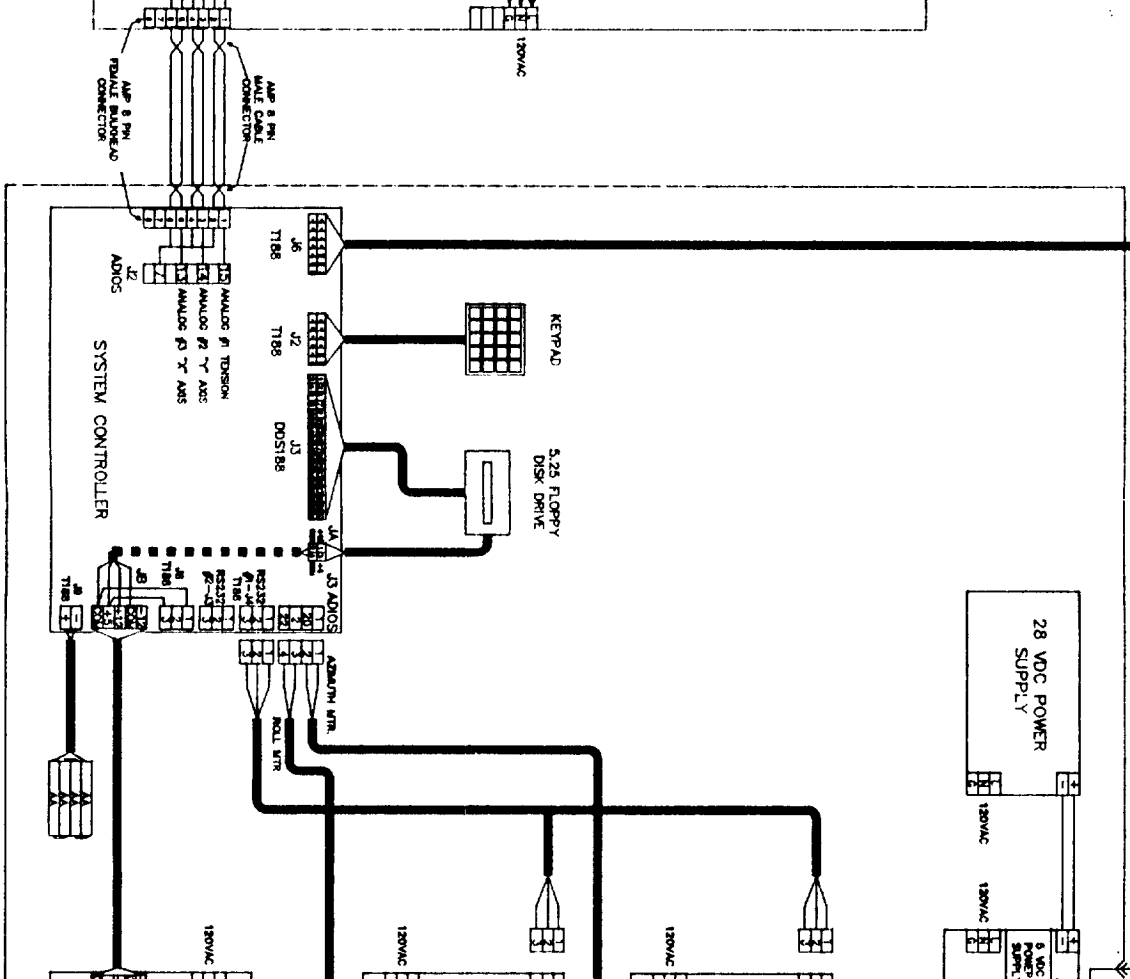
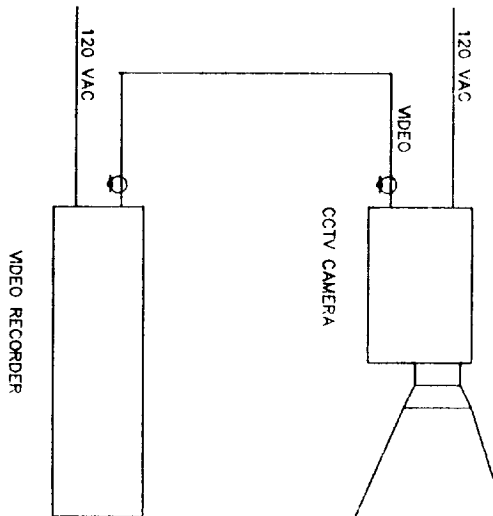
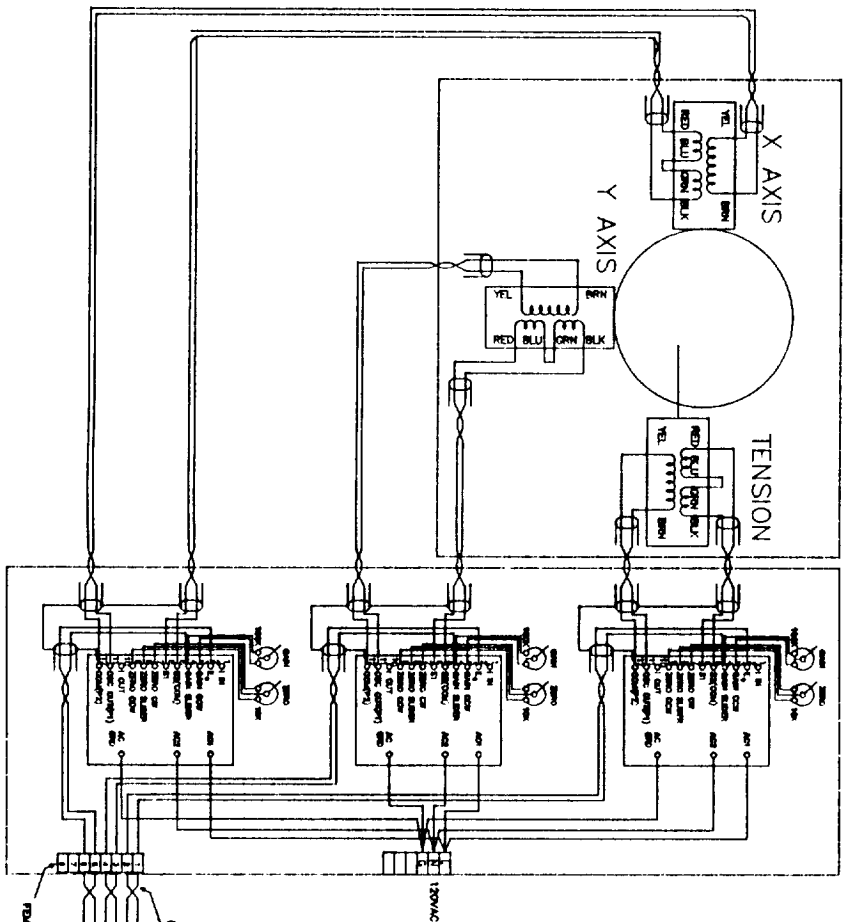
230 ± .0015 T
 RE/

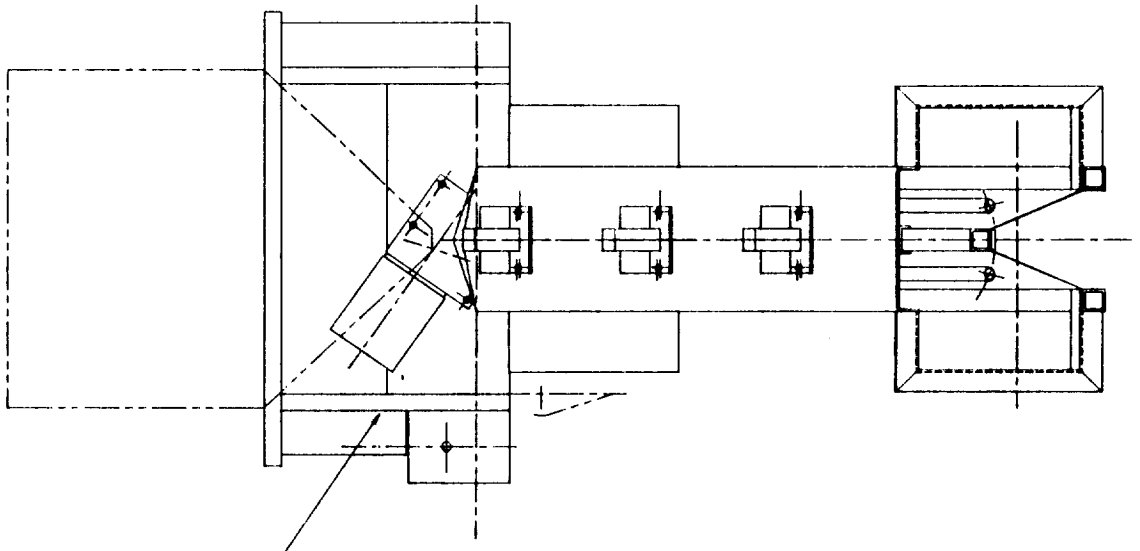


G1

CLAMSHELL MODULE ASSEMBLY

SCALE: FULL SIZE





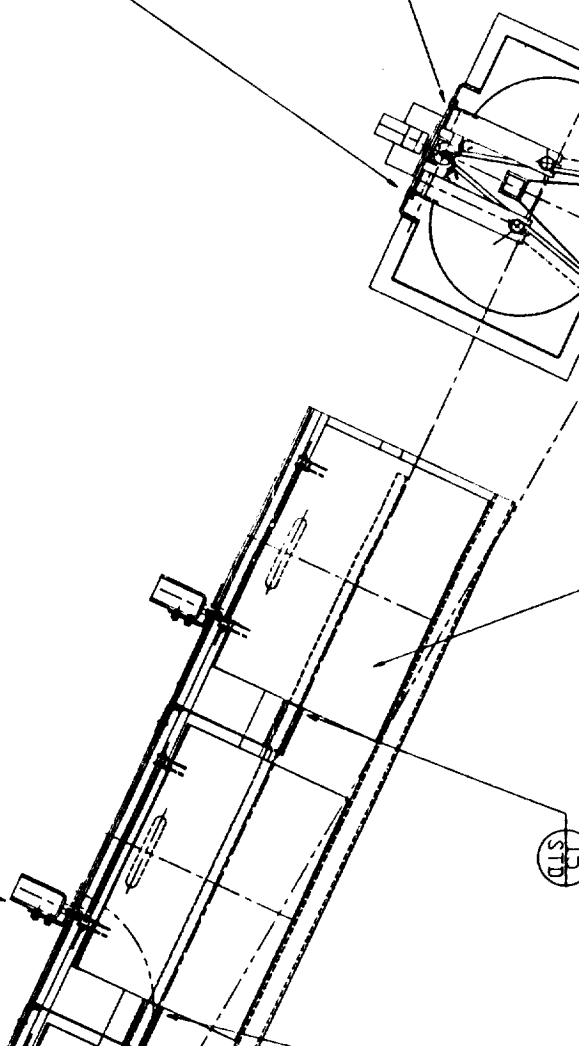
1

21
3
22
STD

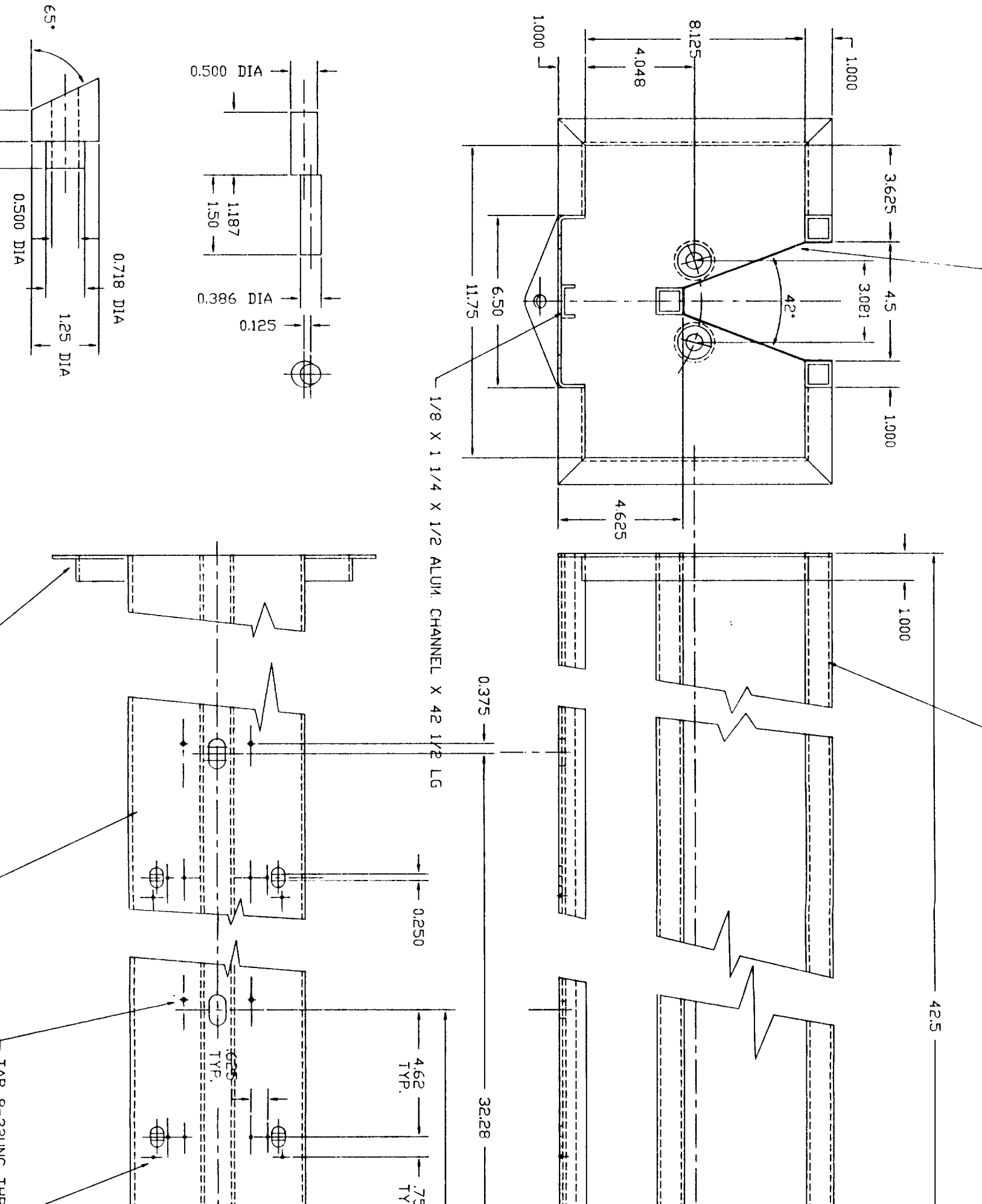
17
3
18
3
19
STD
20
STD

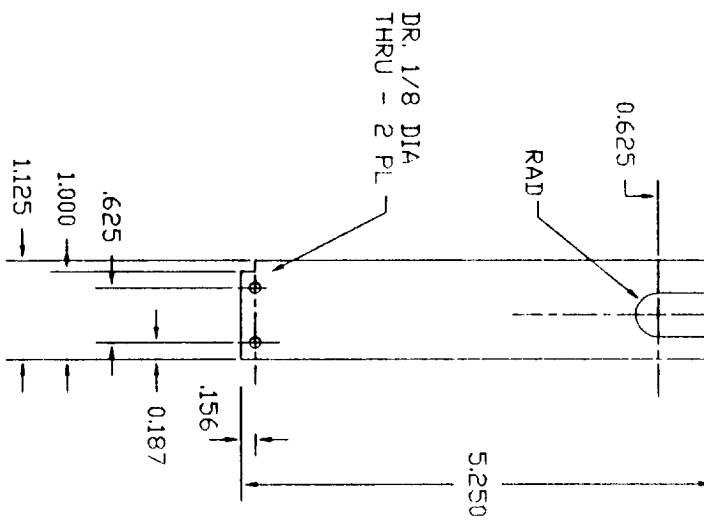
2
3
3
STD
4
STD
5
STD

6
STD



13
STD

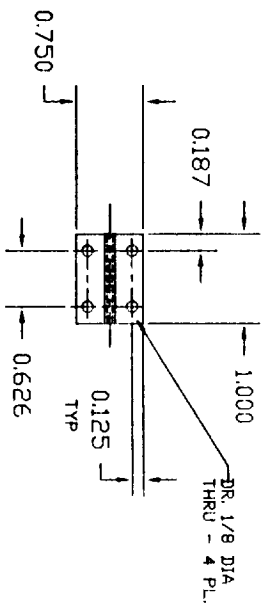




17

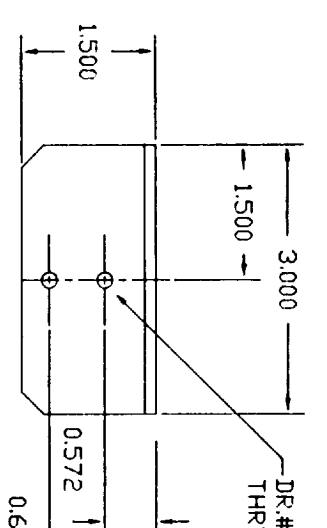
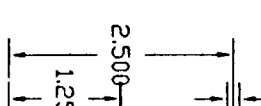
POSITION PLATE

MATL: 1/16 X 1 1/8 X 6 LG ALUM. STRIP
FINISH: BLACK ANODIZE
QTY: 6 PER ASSEMBLY



18

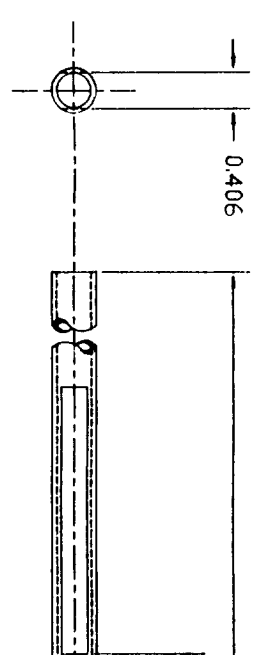
HINGE



2

SDL

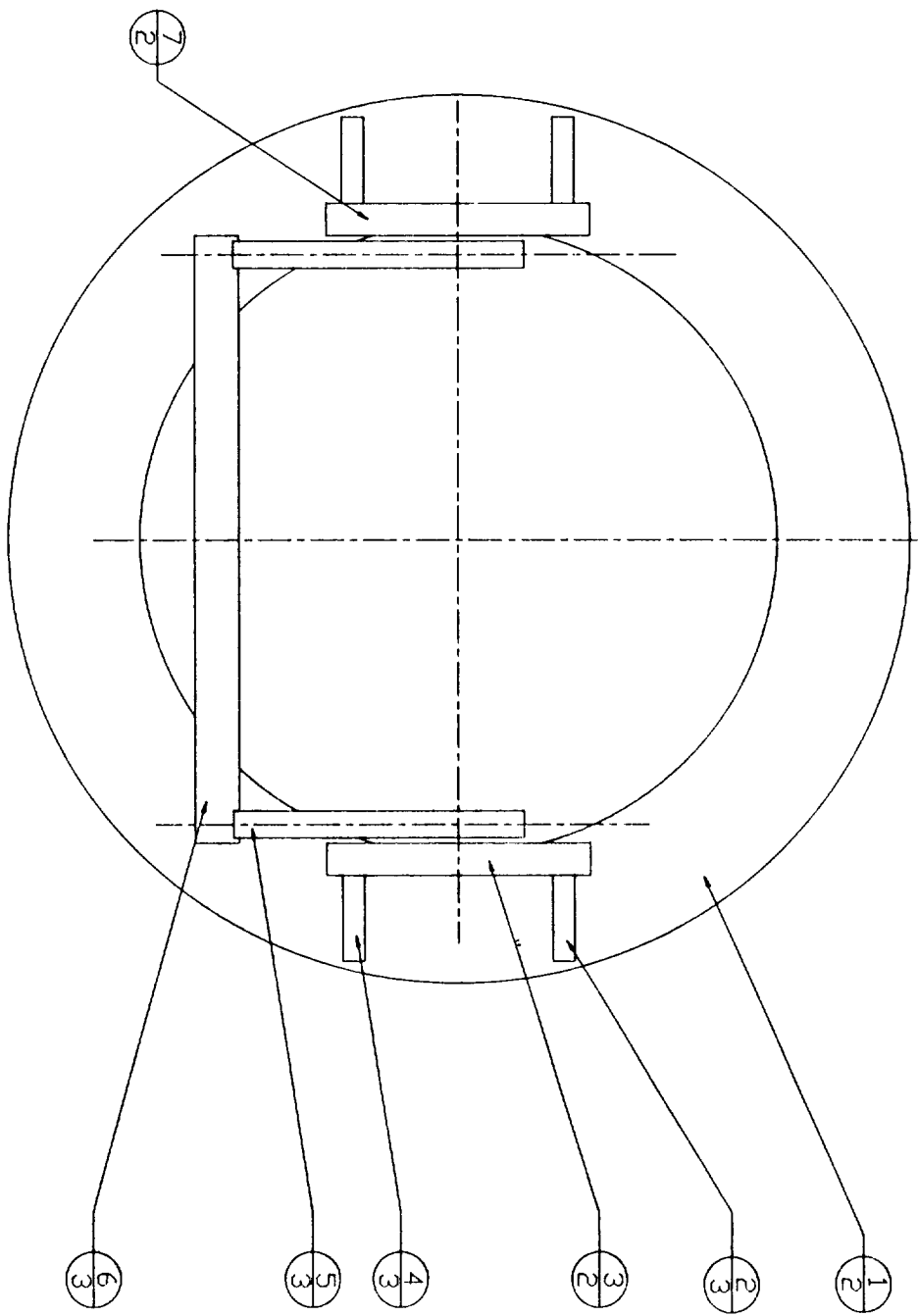
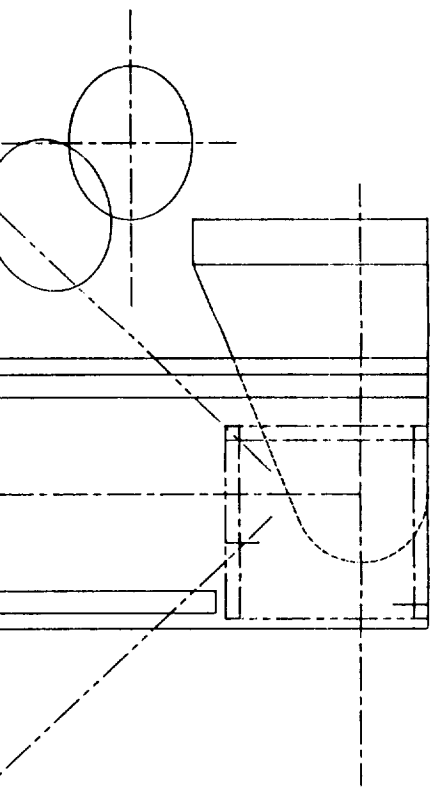
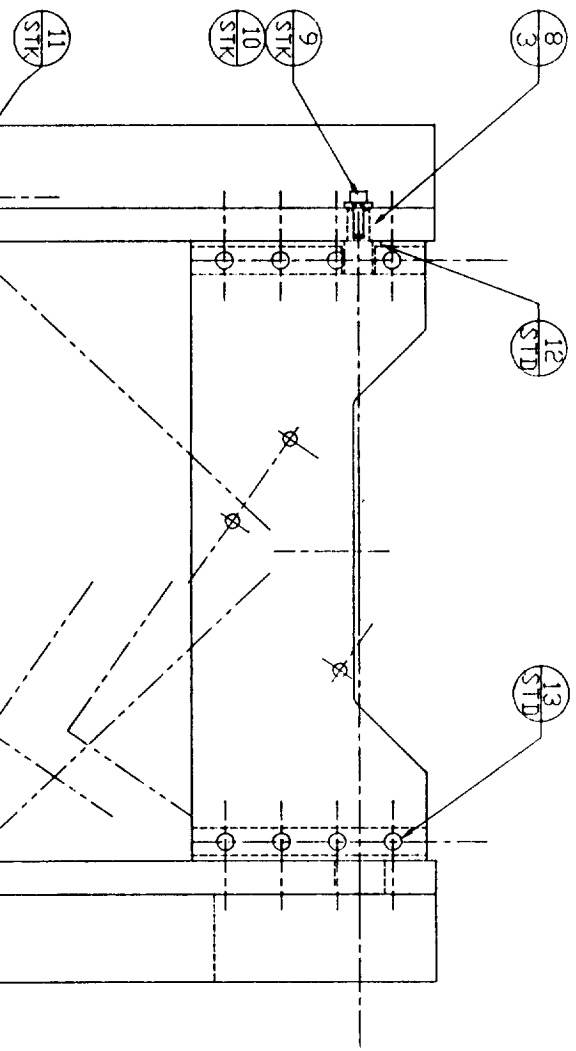
MAT
FIN
QTY

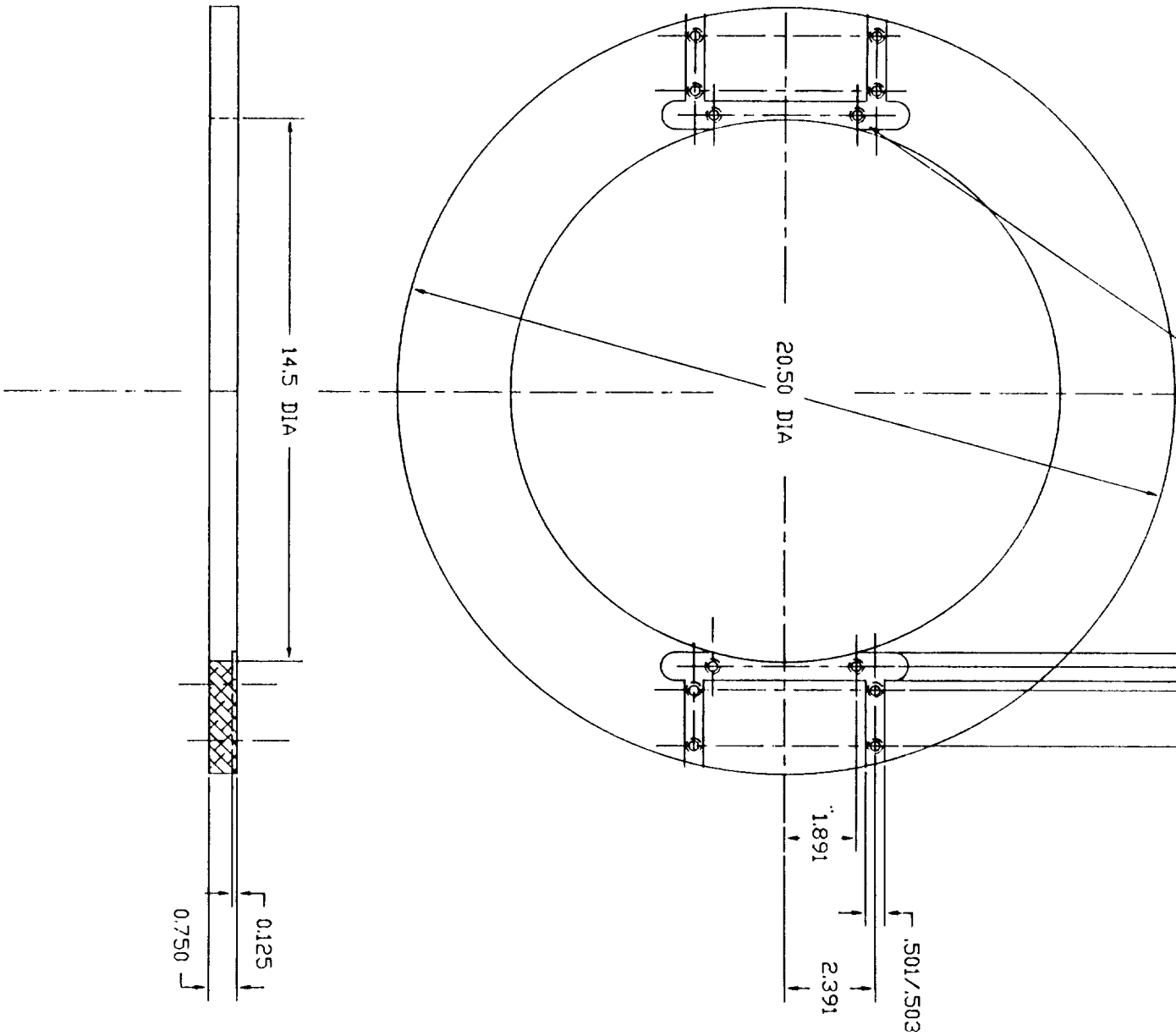


12

GUT

MAT
FIN
QTY





1

BASEPLATE

MATL: 20 1/2 DIA X 3/4 ALUM. PLATE

H.T.: NONE

FINISH: BLACK ANODIZE

QTY: 1 PER ASSEMBLY

SCALE: HALF FULL SCALE

3

MOTOR PLATE

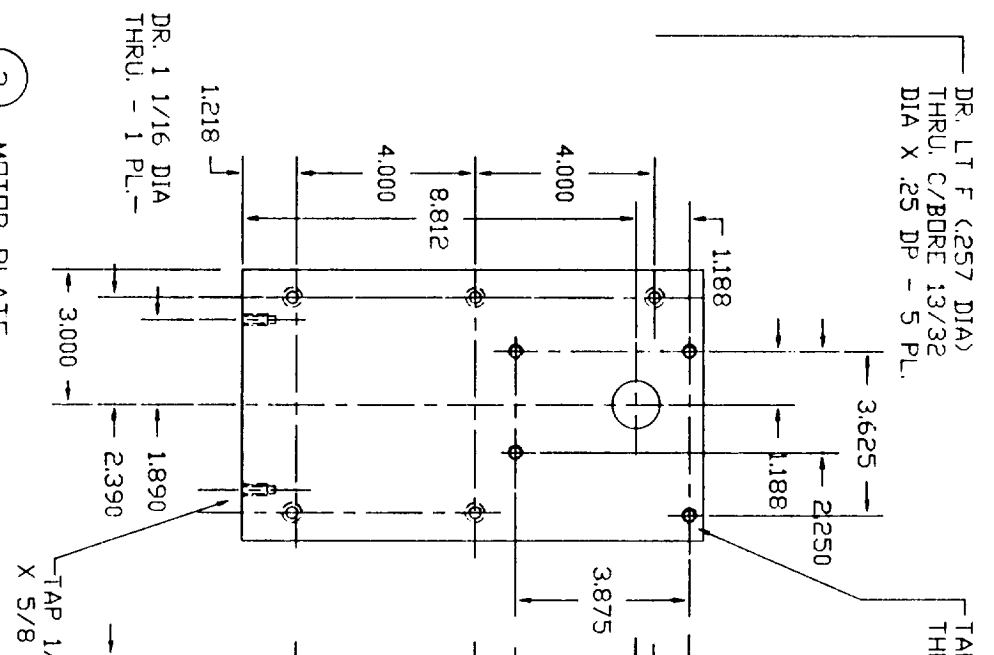
MATL: 3/4 X 6 X 10 1/2 LG ALUM.

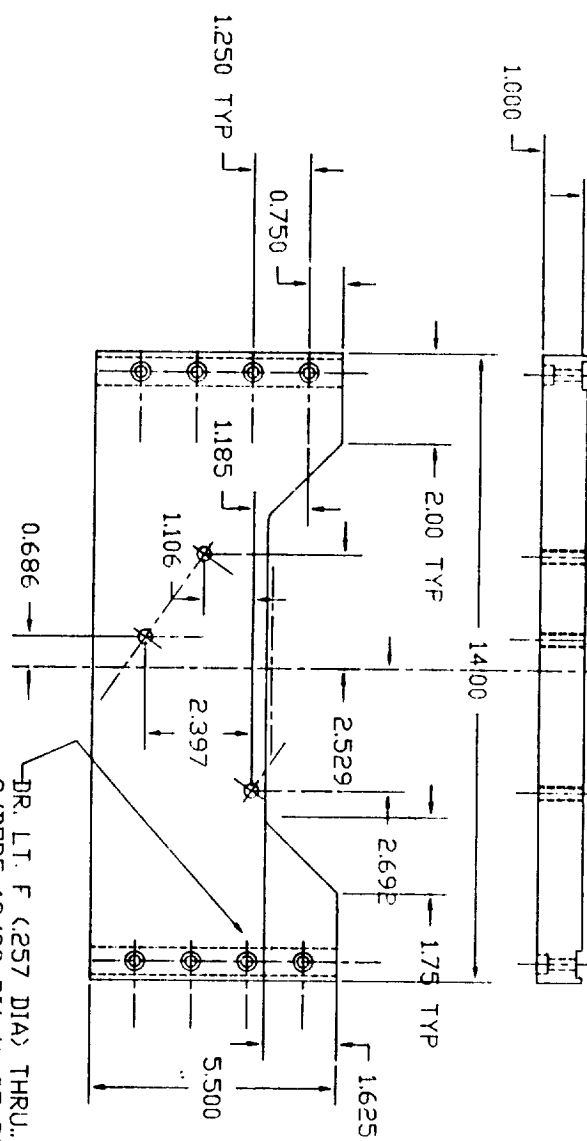
H.T.: NONE

FINISH: BLACK ANODIZE

QTY: 1 PER ASSEMBLY

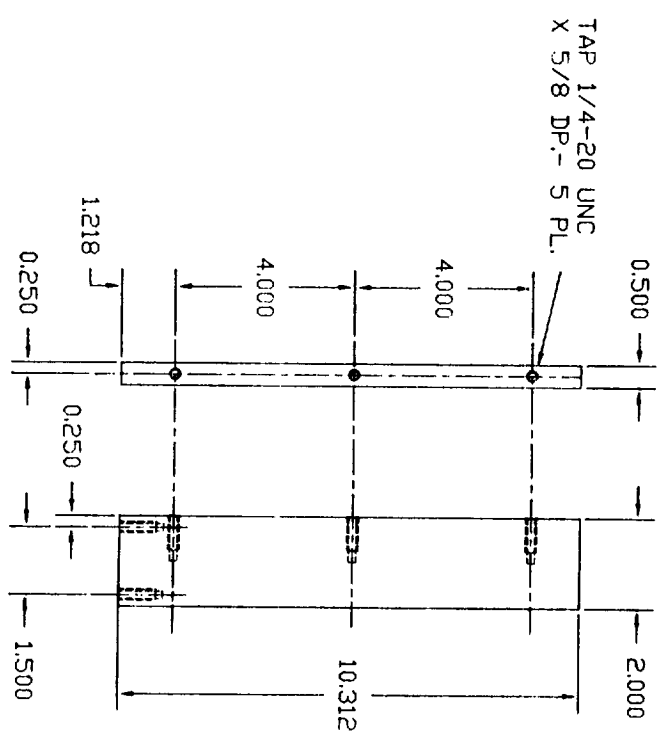
SCALE: HALF FULL SCALE



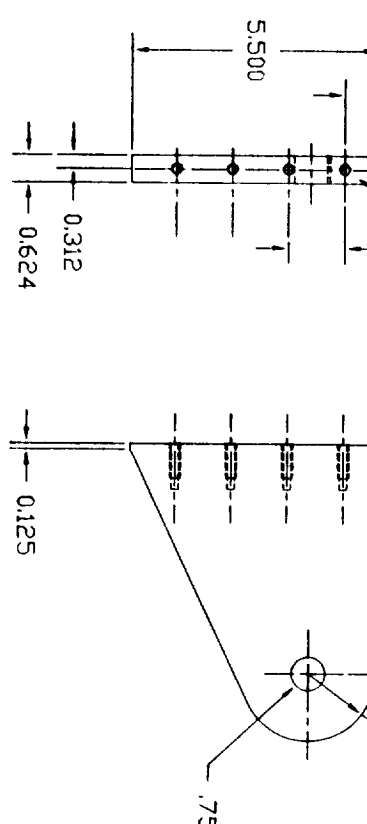


6 CROSS PLATE

MATL: 1 X 5 1/2 X 13 1/8 LG 2024T531 ALUM. BAR
H.T.: NONE
FINISH: BLACK ANODIZE
QTY: 1 PER ASSEMBLY
SCALE: HALF FULL SCALE

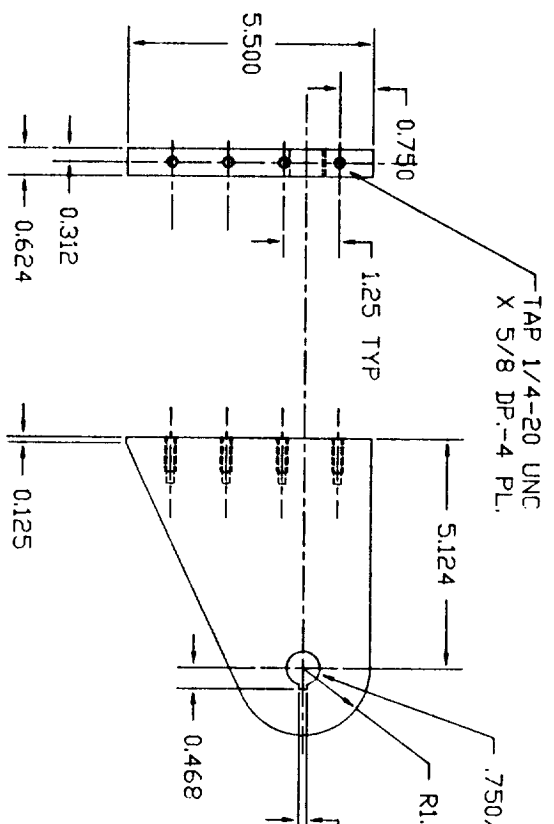


4 SUPPORT PLATE



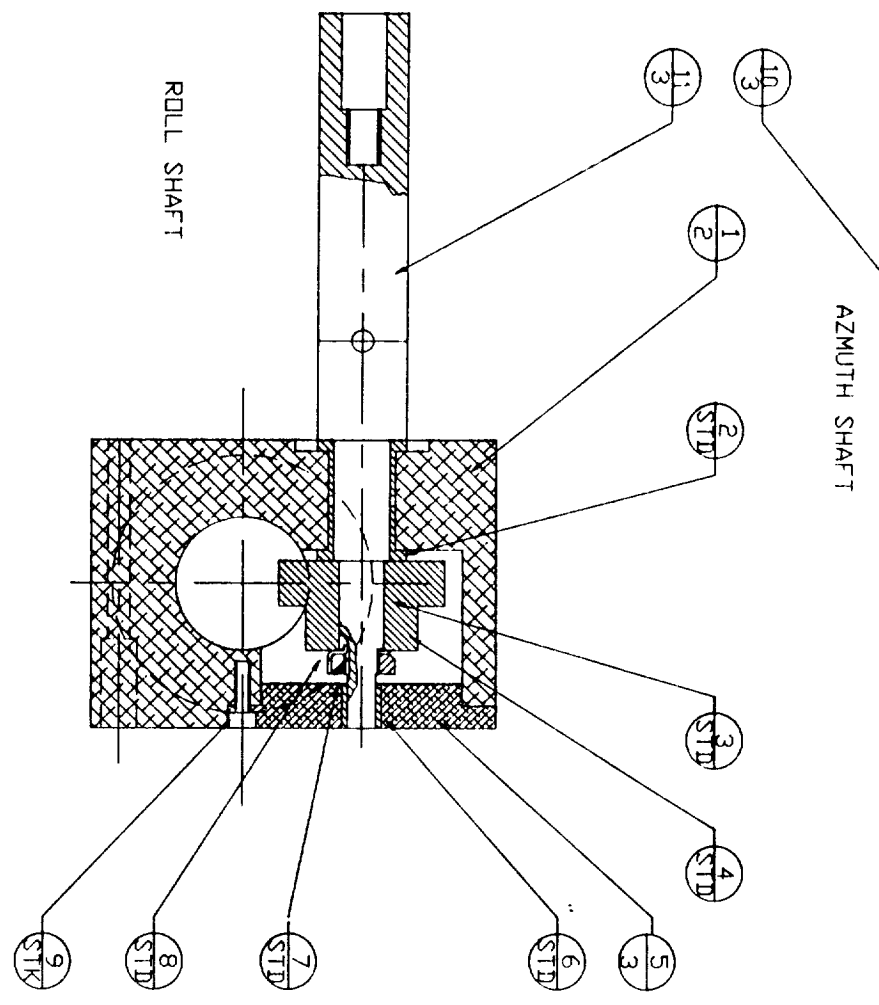
7 BEARING PLATE

MATL: 5/8 X 5 1/2 X 6 3/4 LG. 2024T351 ALU.
H.T.: NONE
FINISH: BLACK ANODIZE
QTY: 1 PER ASSEMBLY
SCALE: HALF FULL

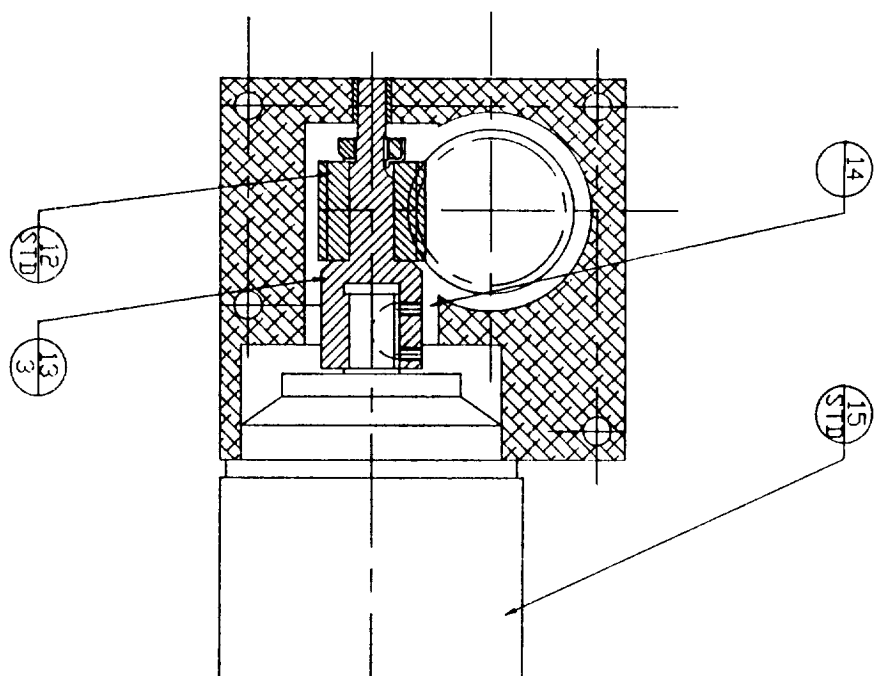


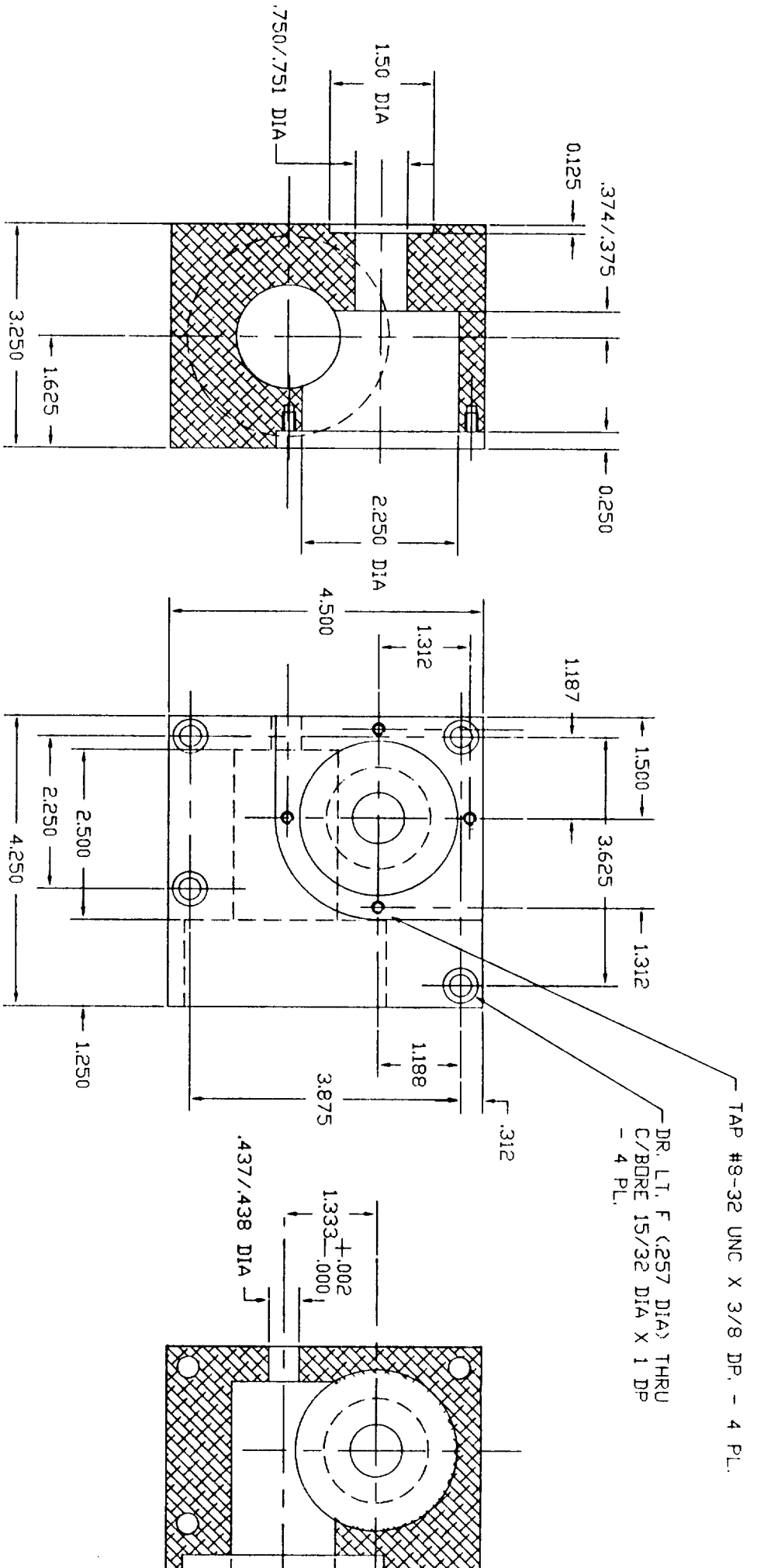
5 PIVOT PLATE

MATL: 5/8 X 5 1/2 X 6 3/4 LG. 2024T351 ALU.
H.T.: NONE
FINISH: BLACK ANODIZE
QTY: 1 PER ASSEMBLY
SCALE: HALF FULL



- G1 GEARBOX (AZMUTH)
- G2 GEARBOX (ROLL)



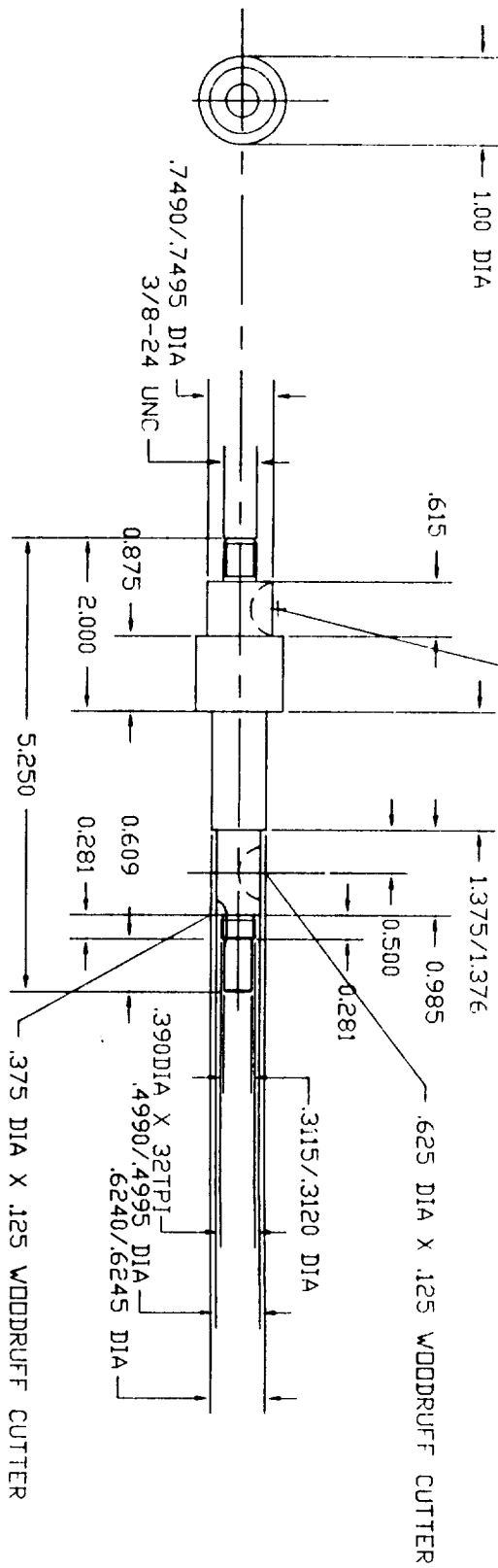


1

GEARBOX HOUSING

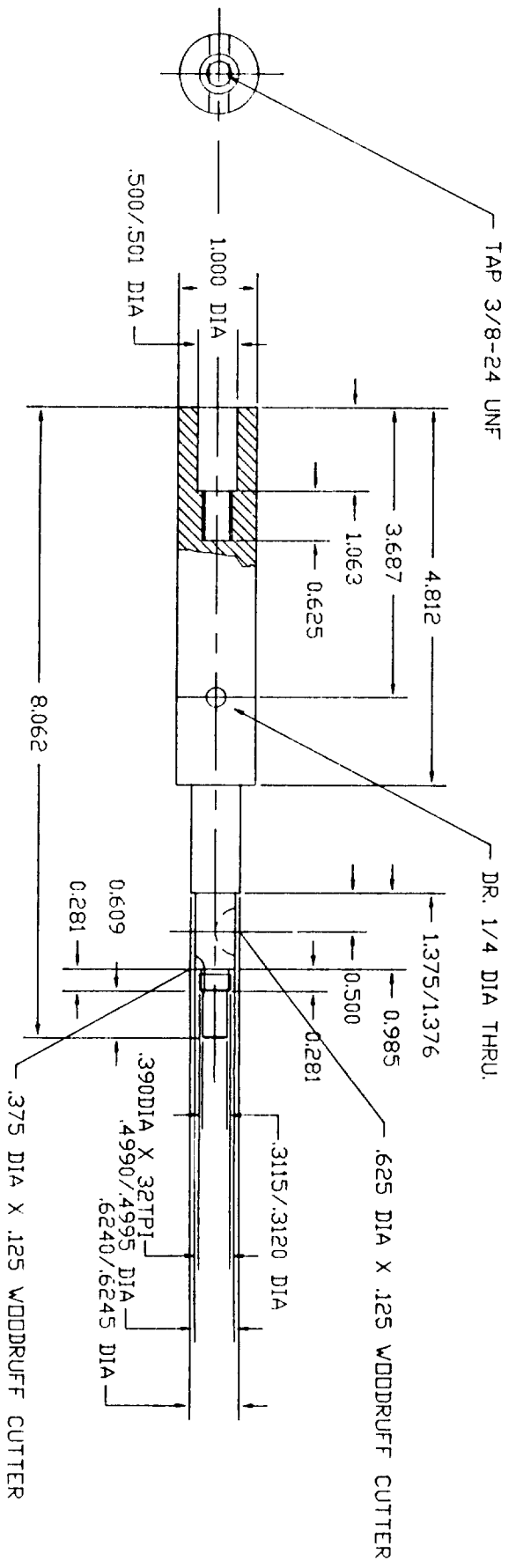
MATL: 3 1/4 X 4 1/2 X 4 1/4 ALUM. BAR
 H.T.: NONE
 FINISH: BLACK ANODIZE
 QTY: 1 PER ASSEMBLY

SCALE: FULL SIZE



10

SHAFT (AZMUTH)
 MATL: 1 DIA X 5 1/2 LG HEAT TREATED 4140 STEEL BAR
 H.T.: NONE
 FINISH: NONE
 QTY: 1 PER ASSEMBLY
 SCALE: FULL SCALE



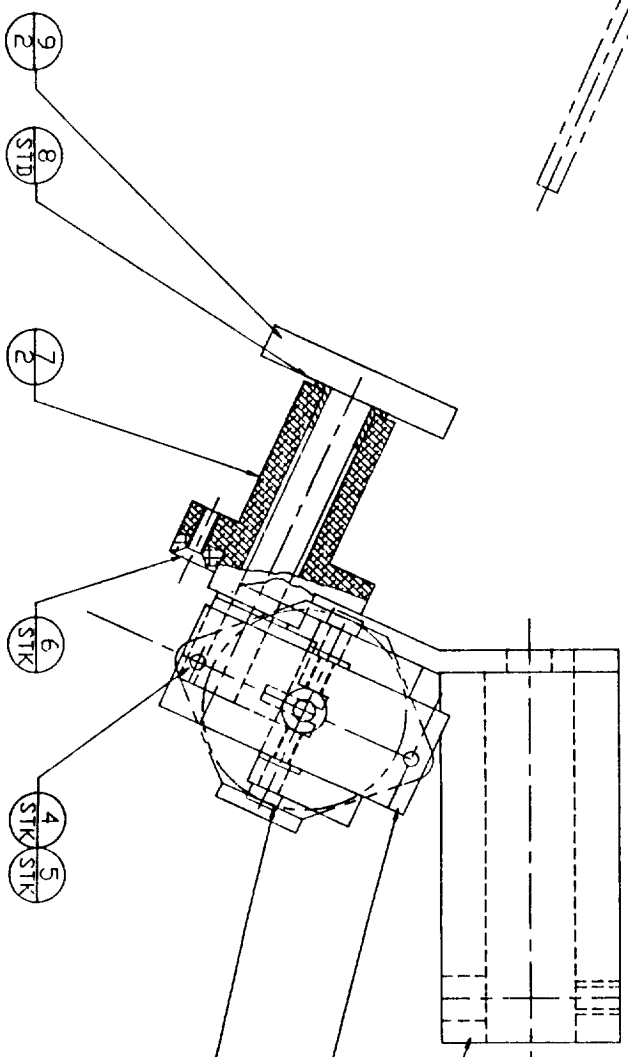
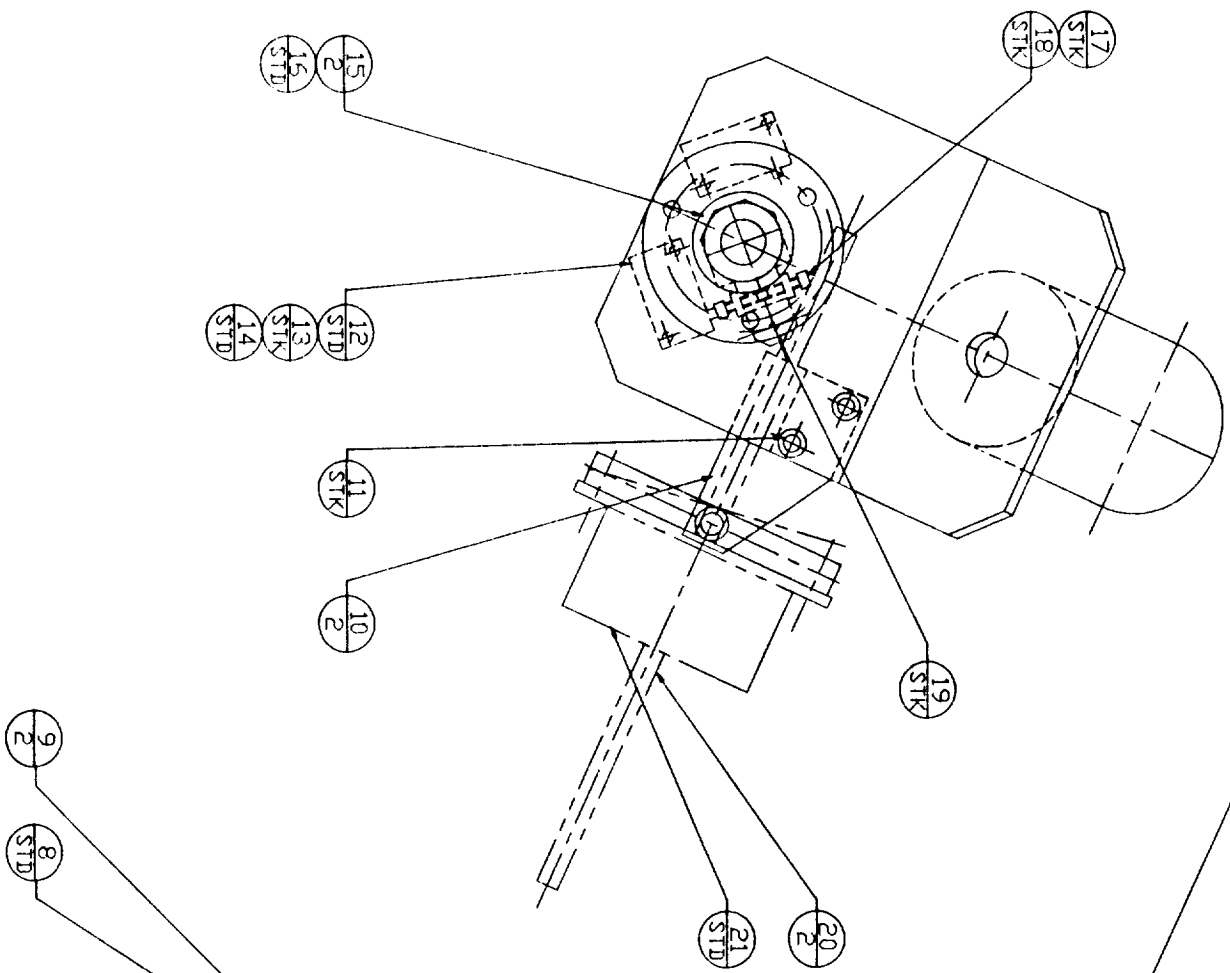
11

SHAFT (ROLL)
 MATL: 1 DIA X 8 1/4 LG. HEAT TREATED 4140 STEEL BAR
 H.T.: NONE

13



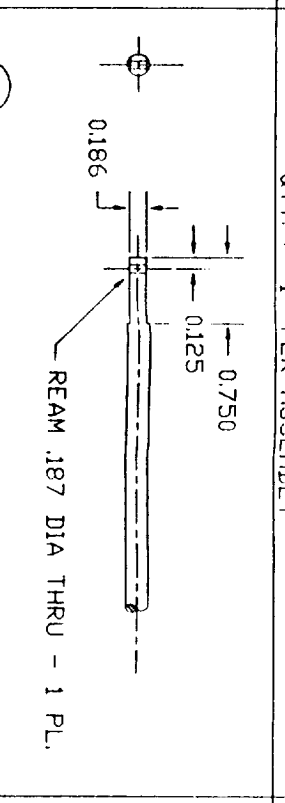
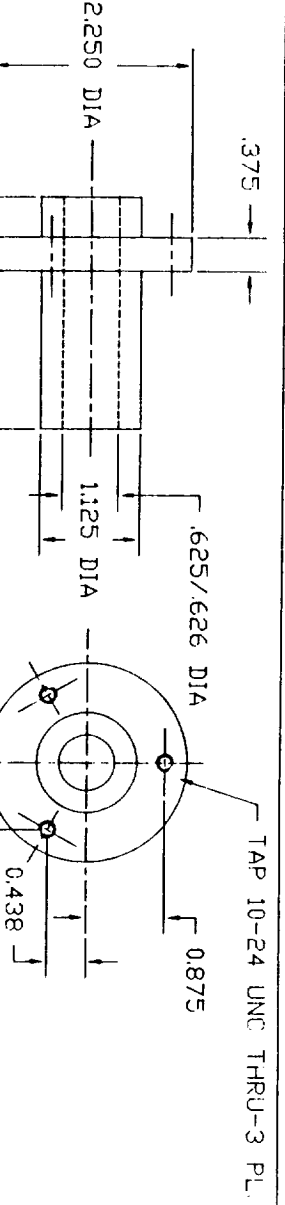
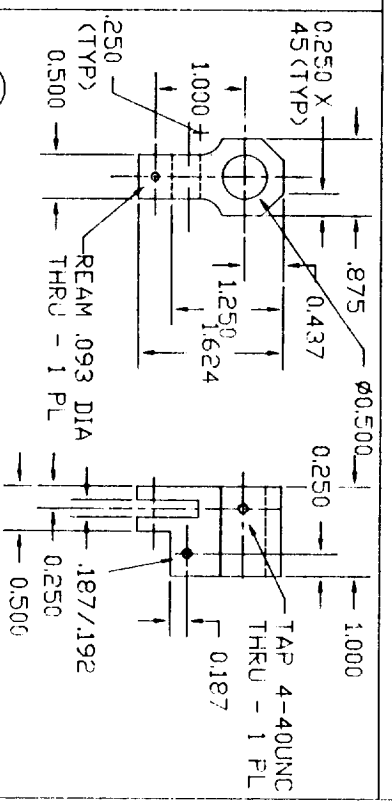
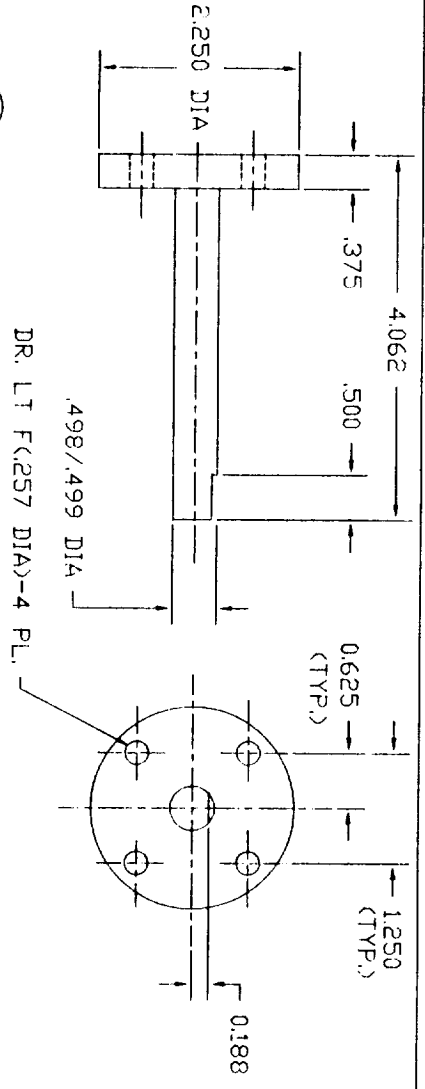
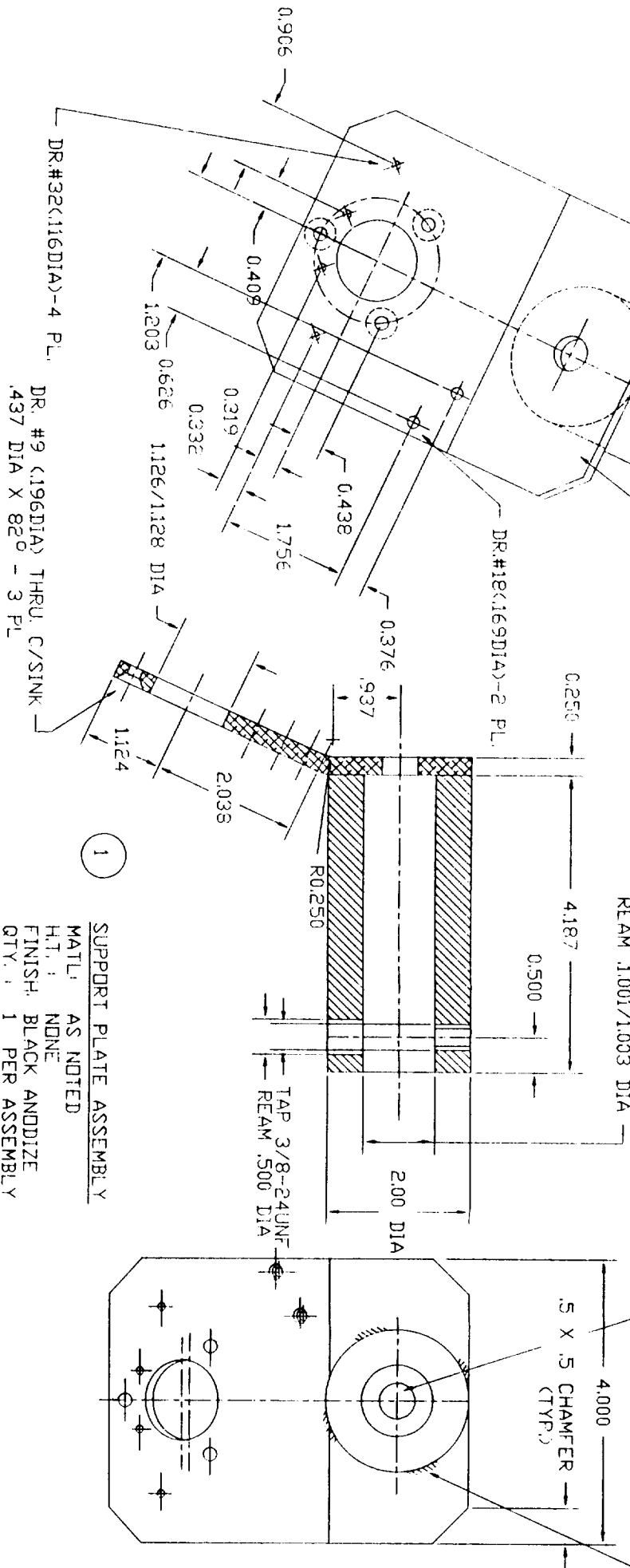
5



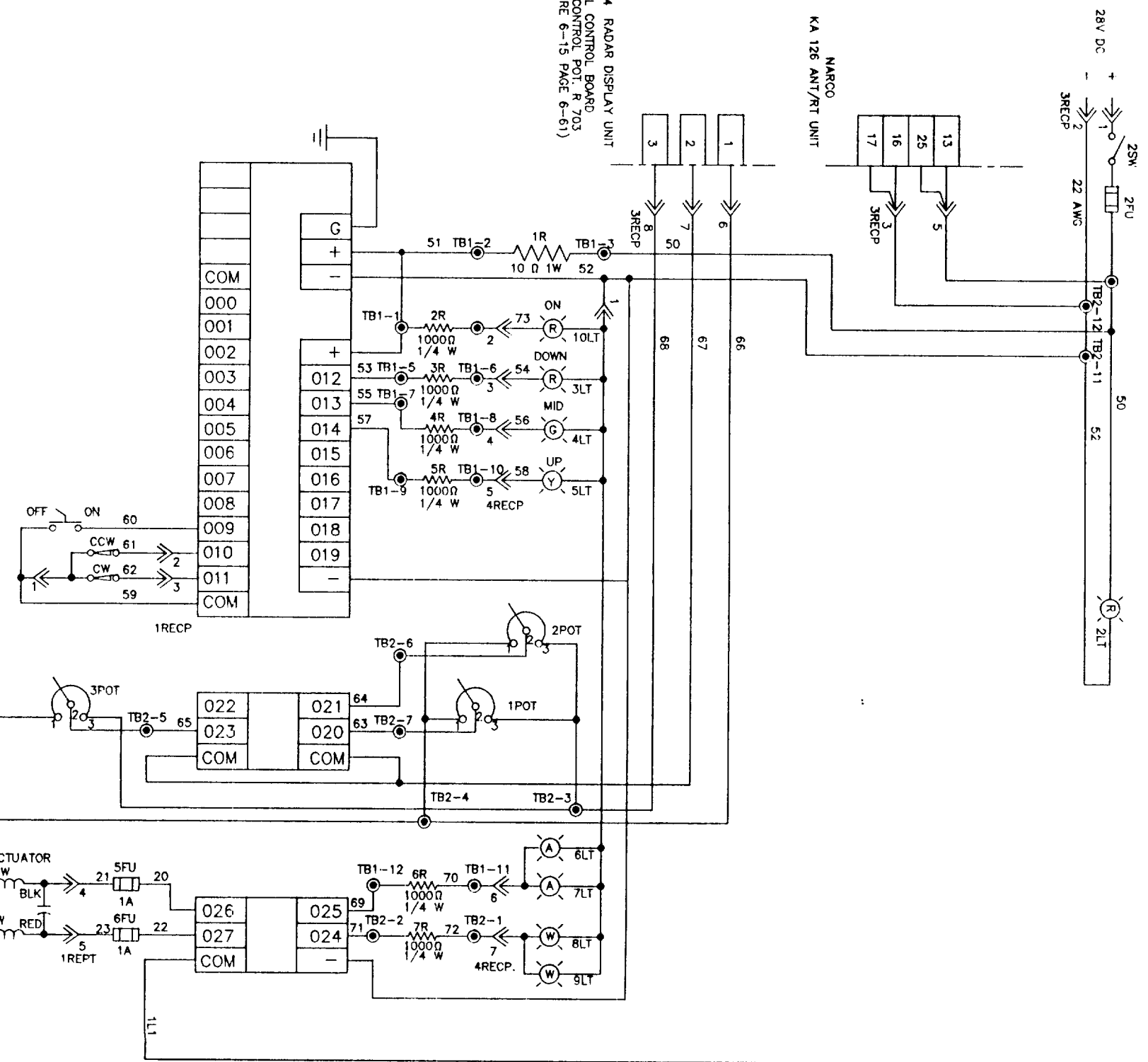
GENE

TRAVEL EXTREME

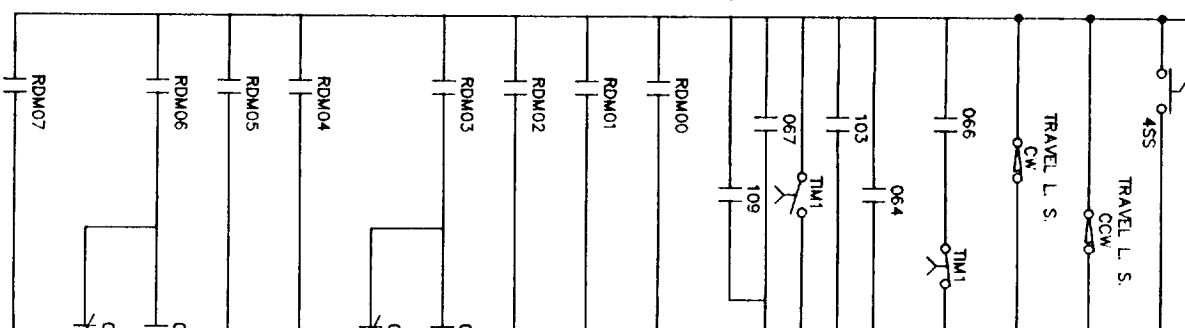
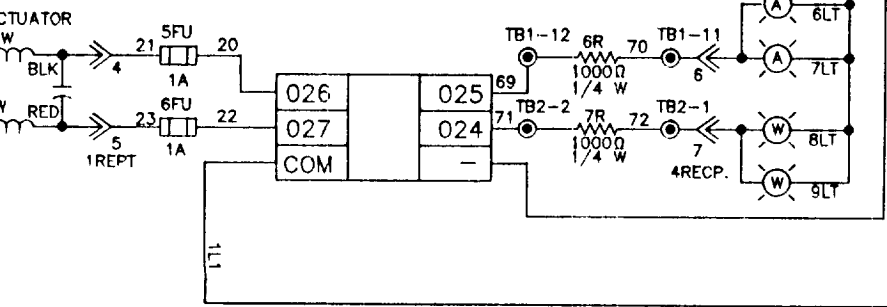
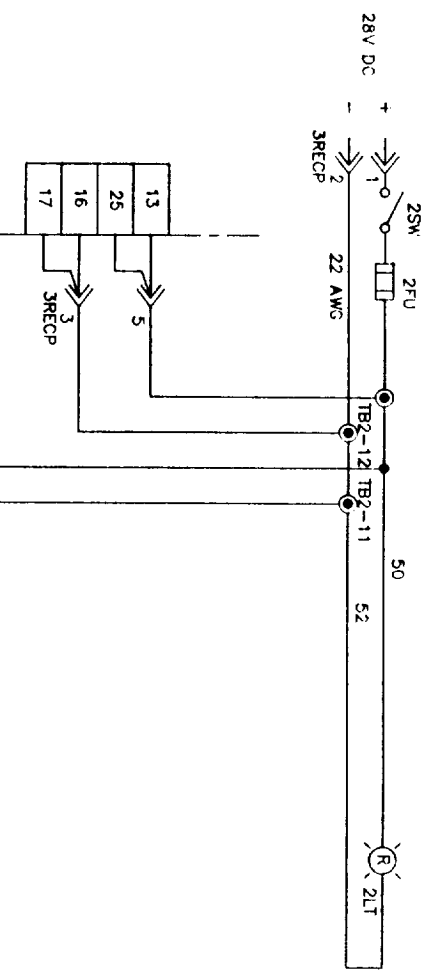


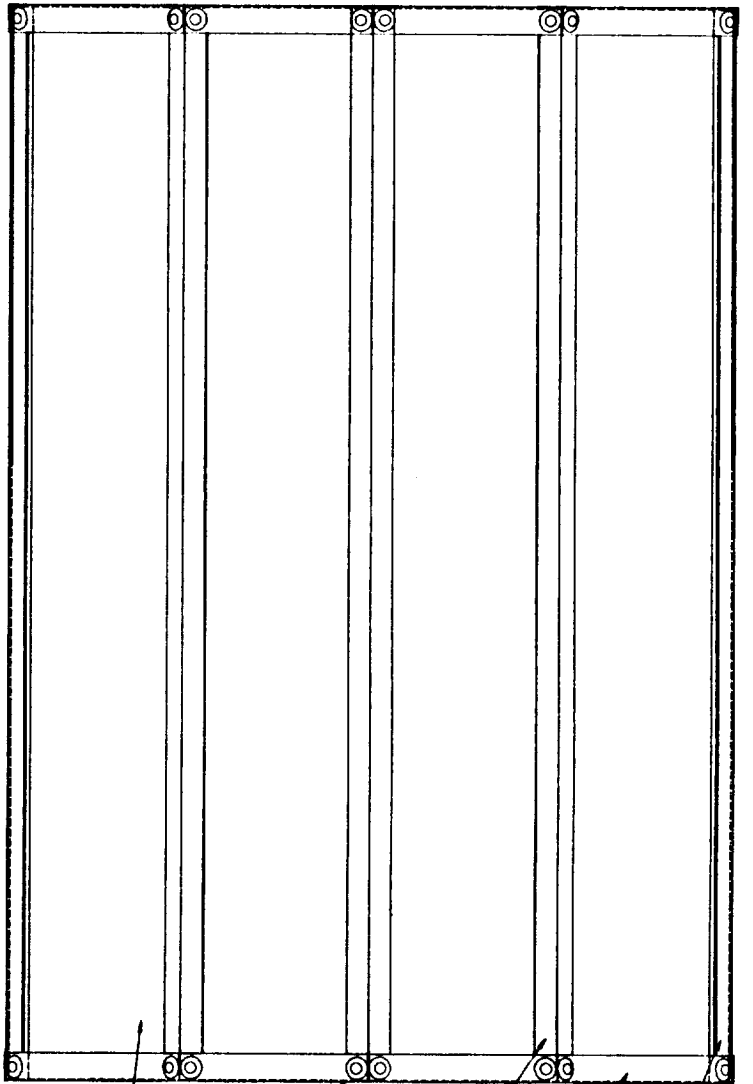


KI 244 RADAR DISPLAY UNIT
 PANEL CONTROL BOARD
 TILT CONTROL POT R 703
 (FIGURE 6-15 PAGE 6-61)



NARCO
 KA 126 ANT/RT UNIT





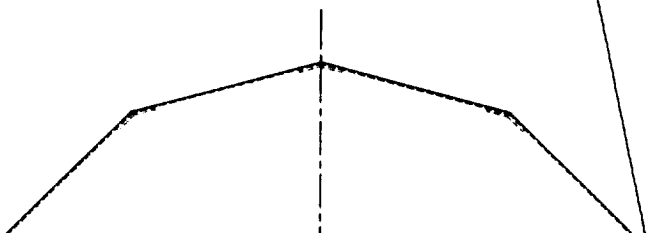
2
3
4
5
6
STD

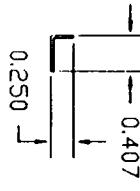
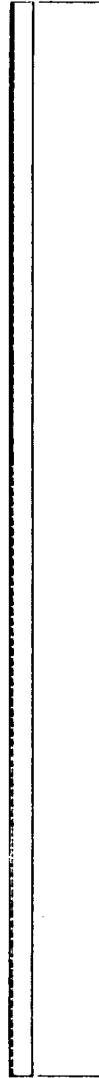
G1

COVER ASSEMBLY

SCALE - FULL SIZE

1
2

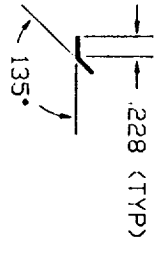
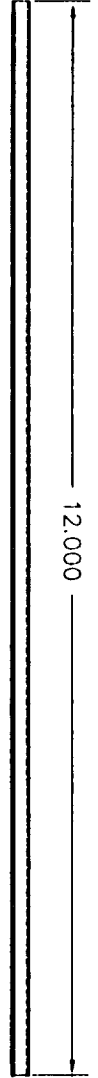




1

RAIL
 MATL: .020 X 19/32 X 12 ALUM. SHEET
 HT: NONE
 FINISH: WHITE ANODIZE
 QTY: 4 PER ASSEMBLY

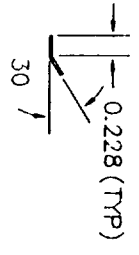
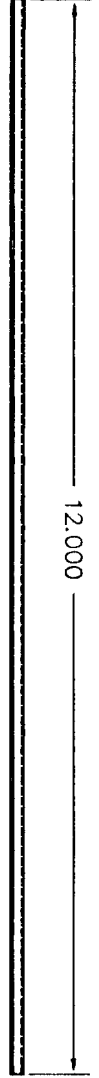
SCALE - FULL SIZE



2

SIDE ANGLE
 MATL: .020 X 15/32 X 12 ALUM. SHEET
 HT: NONE
 FINISH: WHITE ANODIZE
 QTY: 4 PER ASSEMBLY

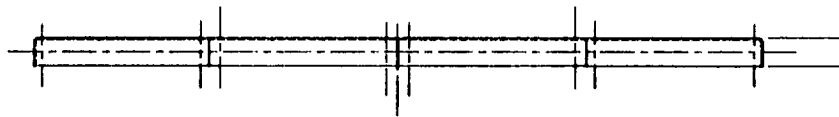
SCALE - FULL SIZE



4

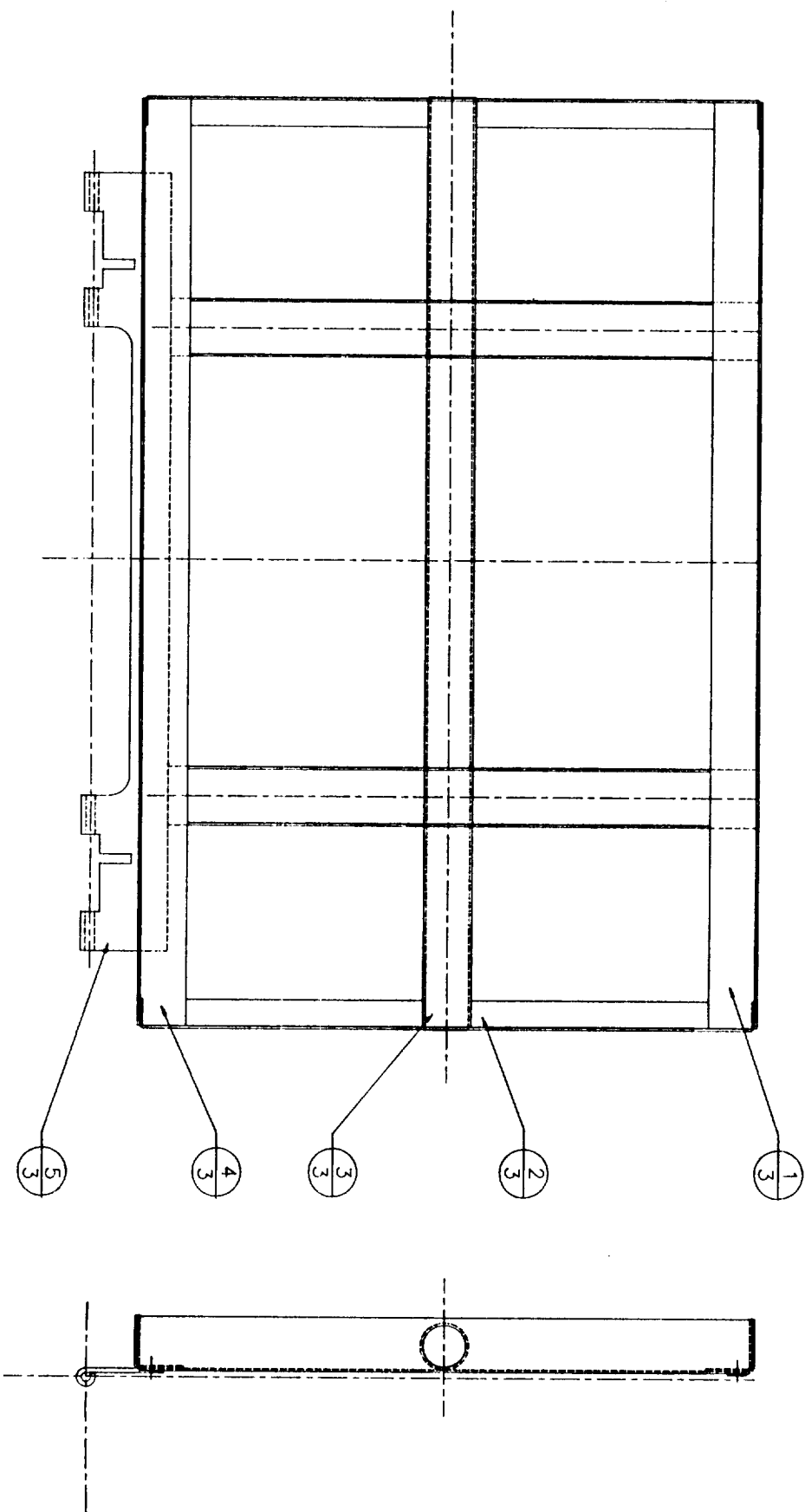
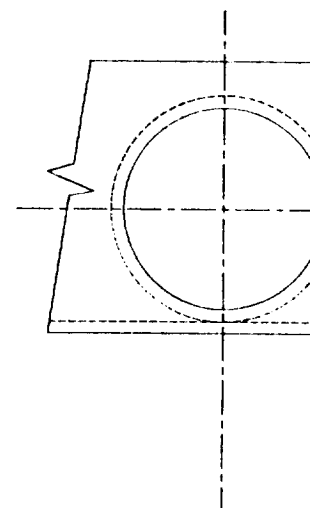
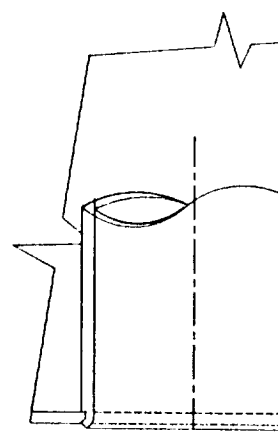
TOP ANGLE
 MATL: .020 X 15/32 X 12 ALUM. SHEET
 HT: NONE
 FINISH: WHITE ANODIZE
 QTY: 2 PER ASSEMBLY

SCALE - FULL SIZE



3

END PLATE
 MATL: .020 X 15/32 X 12 ALUM. SHEET
 HT: NONE
 FINISH: WHITE ANODIZE
 QTY: 4 PER ASSEMBLY

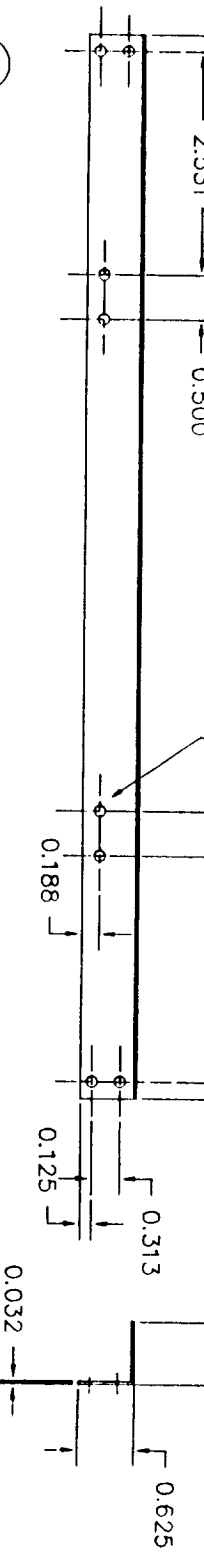


G1

BASE ASSEMBLY
QTY: 2 PER MODULE

1

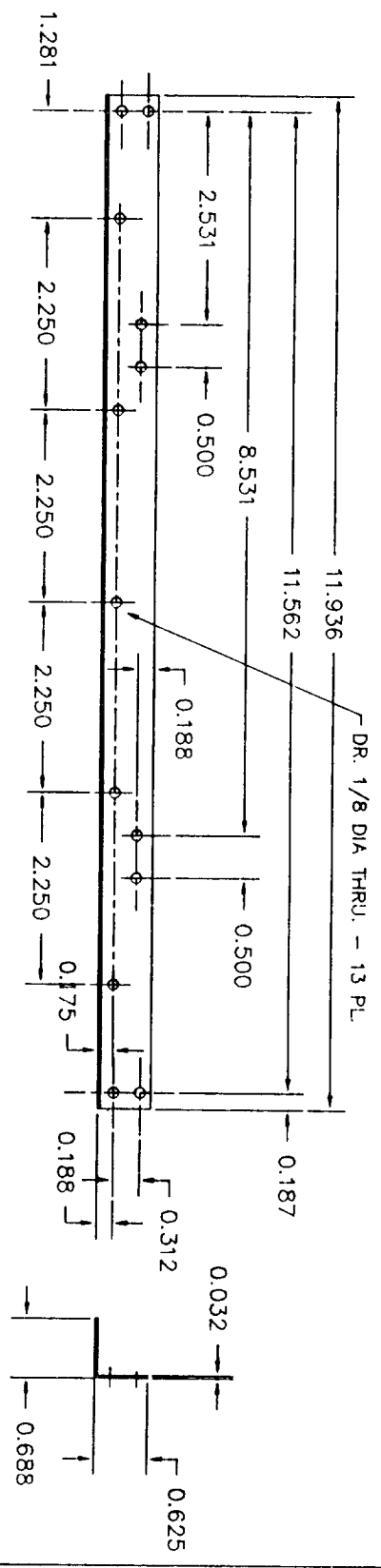
TOP RAIL
MATL: .020 X 1 1/4 X 11.94 ALUM. SHEET
HT: NONE
FINISH: WHITE ANODIZE
QTY: 2 PER ASSEMBLY



4

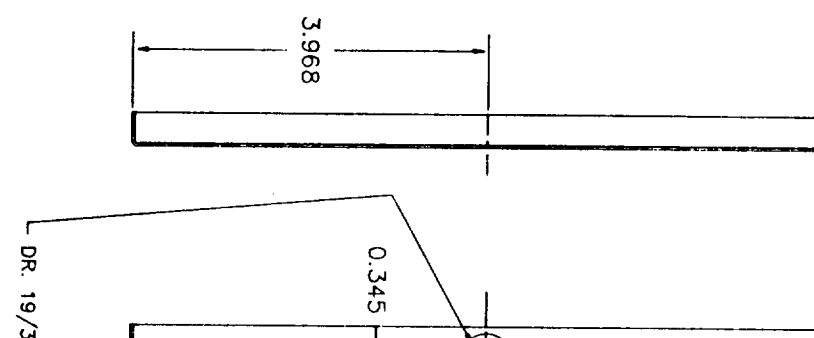
LOWER RAIL
MATL: .020 X 1 1/4 X 11.94 ALUM. SHEET
HT: NONE
FINISH: WHITE ANODIZE
QTY: 2 PER ASSEMBLY

SCALE - FULL SIZE



2

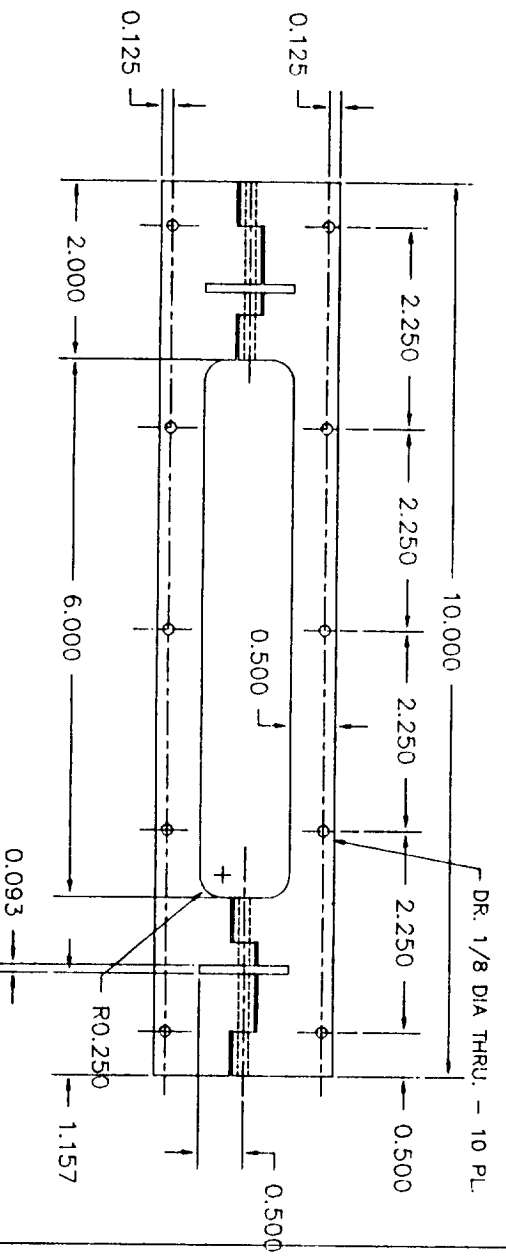
END ANGLE
MATL: .020 X 1 1/4
HT: NONE
FINISH: WHITE ANOD
QTY: 4 PER ASS
SCALE - FULL SIZE



3

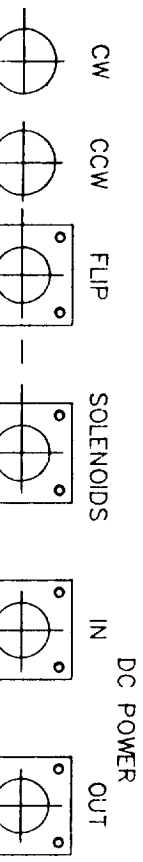
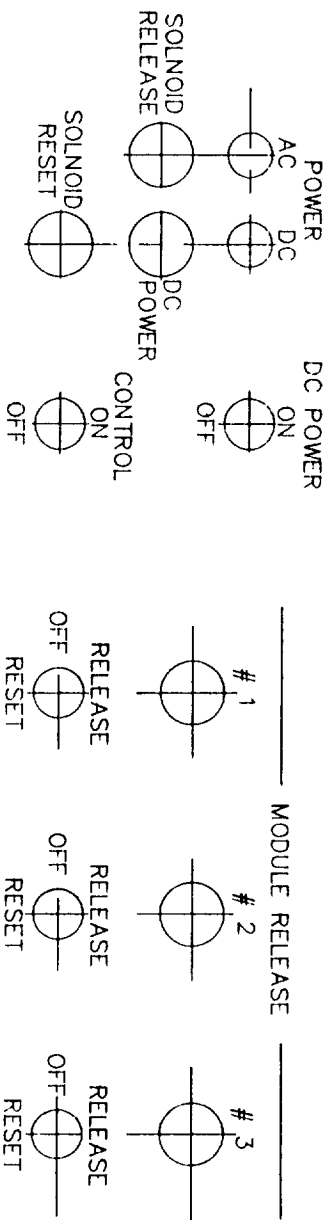
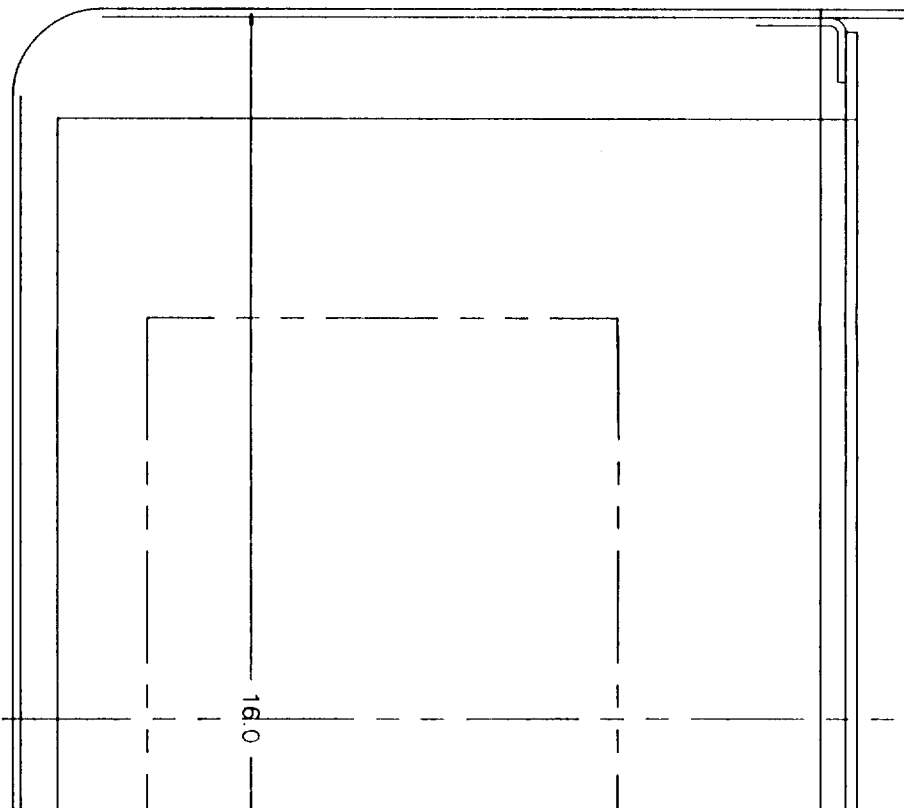
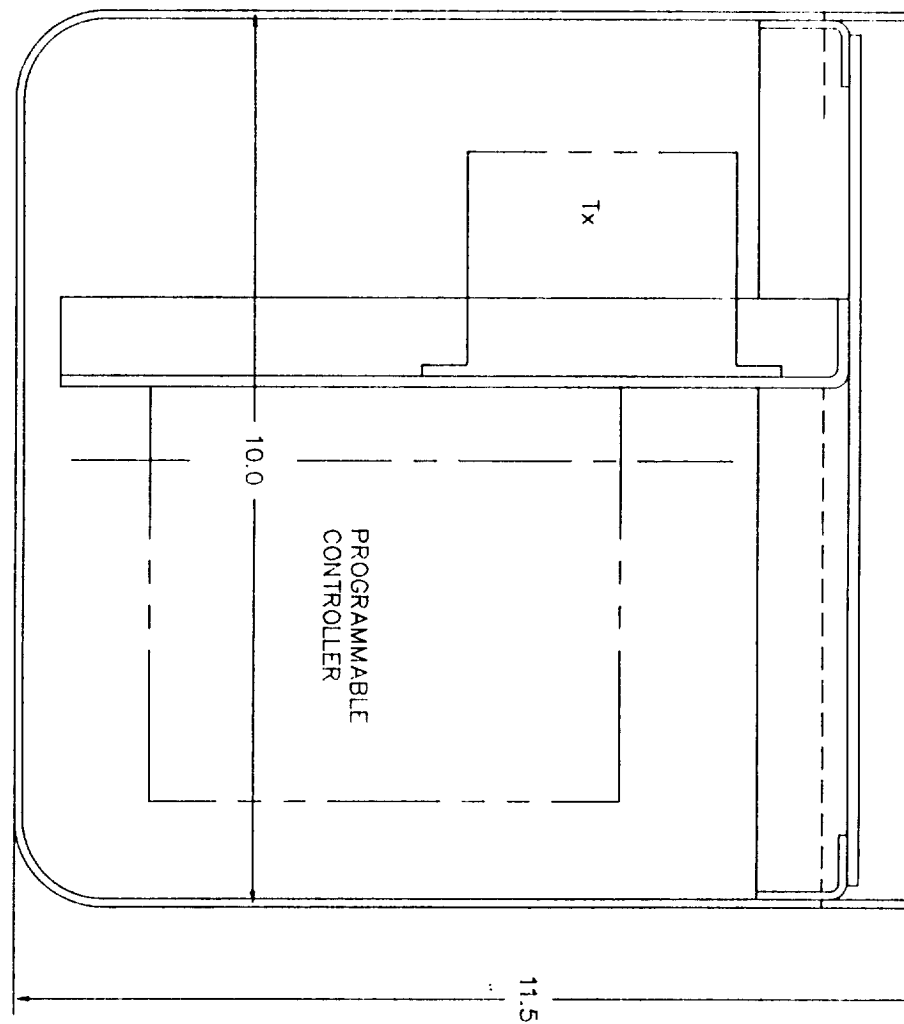
TUBE
MATL: 5/8 O/DIA X .035 WALL X 12 1/4 LC
HT: NONE
FINISH: WHITE ANODIZE
QTY: 2 PER ASSEMBLY

SCALE -

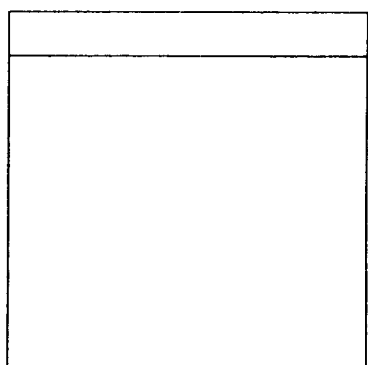
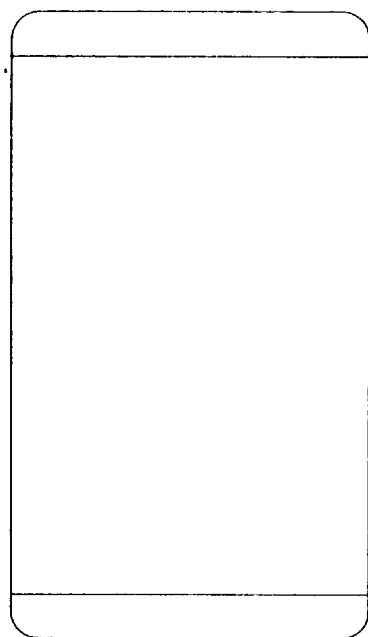
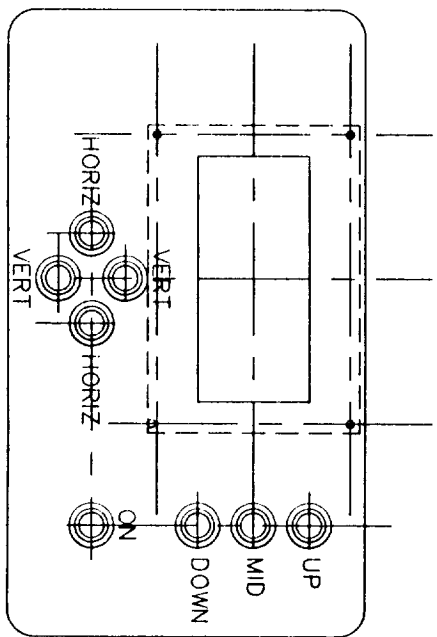


5

UNIDOT

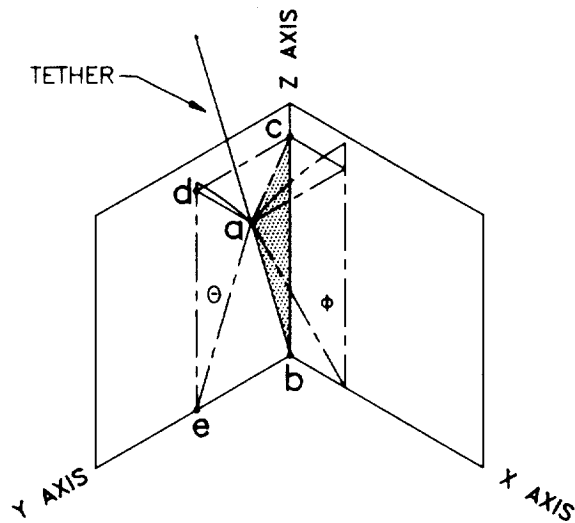


COMPONENT
MOUNTING
PLATE
(FULL SCALE)



ANCO

APPENDIX C
CALCULATIONS



$ab = \text{Radius of Attitude Detector Hoops} = 4.000 \text{ inches}$

$$ad = de \tan \theta \tag{C-1}$$

$$dc = de \tan \phi \tag{C-2}$$

$$ad^2 + dc^2 = ac^2$$

Substituting (C-1) and (C-2):

$$(de \tan \theta)^2 + (de \tan \phi)^2 = ac^2 \tag{C-3}$$

Also: $ac^2 + bc^2 = ab^2$; $bc = de$; and $ab = 4.000$

$$\text{Therefore: } ac^2 + de^2 = 4^2$$

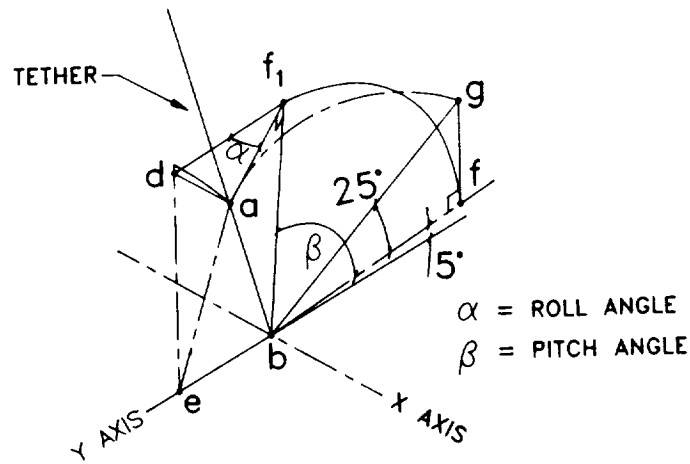
Substituting from (C-2):

$$(de \tan \theta)^2 + (de \tan \phi)^2 + de^2 = 4^2$$

Expanding and simplifying:

$$de^2(\tan^2 \theta + \tan^2 \phi + 1) = 4^2$$

$$de = \frac{4}{(\tan^2 \theta + \tan^2 \phi + 1)^{1/2}} \tag{C-4}$$



For this calculation the following are constants:

$$af_1 = 1.6905 \text{ inches}$$

$$bf = bf_1 = 3.6252 \text{ inches}$$

$$\text{angle } fbg = 25^\circ, \quad \text{angle } af_1b = 90^\circ$$

Let angle $(af_1d) = \text{Roll angle} = \alpha$

and angle $(fbf_1) = \text{Pitch angle} = \beta$

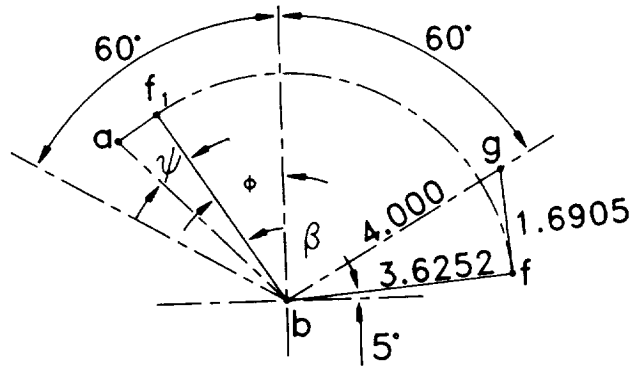
Note from (C-1), $ad = de \tan \theta$; and from (C-4) $de = \frac{4}{(\tan^2 \theta + \tan^2 \phi + 1)^{1/2}}$

$$\text{Therefore, } ad = \frac{4 \tan \theta}{(\tan^2 \theta + \tan^2 \phi + 1)^{1/2}}$$

$$\text{Roll angle} = \sin \alpha = \frac{ad}{af_1}$$

$$\sin \alpha = \frac{4 \tan \theta}{1.6905(\tan^2 \theta + \tan^2 \phi + 1)^{1/2}}$$

$$\alpha = \sin^{-1} \frac{4 \tan \theta}{1.6905(\tan^2 \theta + \tan^2 \phi + 1)^{1/2}} \quad (C-5)$$



Angle $fbf_1 = \text{Pitch angle} = \beta$

$$af_1 = 1.6905 \cos \alpha$$

$$\tan \psi = \frac{1.6905 \cos \alpha}{3.6252}$$

$$\psi = \tan^{-1} \frac{1.6905 \cos \alpha}{3.6252}$$

$$\begin{aligned} \text{Pitch angle} &= 180^\circ - 5^\circ - (90^\circ - \theta + \psi) \\ &= 85^\circ + \psi - \theta \end{aligned}$$

ANCO

APPENDIX D

ANALYSIS OF DEPLOYMENT OF THE
EXPENDABLE TETHERED SYSTEM

**Analysis of Deployment of the
Expendable Tethered System**

ANCO Contract 2836

Final Report

For the period 22 April 1988 through 30 July 1988

**Principal Investigator
Dr. Enrico C. Lorenzini**

**Co-Investigator
Dr. Mario Cosmo**

August 1988

**Prepared for
ANCO Engineers, Inc.
9937 Jefferson Boulevard
Culver City, California 90232-3591**

**Smithsonian Institution
Astrophysical Observatory
Cambridge, Massachusetts 02138**

**The Smithsonian Astrophysical Observatory
is a member of the
Harvard-Smithsonian Center for Astrophysics**

CONTENTS

	Page
Summary	1
Figure Captions	2
SECTION 1. INTRODUCTION	3
2. DEPLOYMENT DYNAMICS	3
2.1 Introductory Remarks	5
2.2 Dynamics Simulation Model	6
2.3 Deployment Control Law	10
2.4 Computer Code Validation	11
2.5 Simulation Of SEDS Deployment Dynamics	15
2.5.1 Without Radar Targets	15
2.5.2 With Radar Targets	26
2.6 Tether Discretization And Accuracy	34
2.7 Conclusions And Recommendations	39

Summary

Three radar reflectors, each with a mass of 100 gr, are attached to the tether of the Small Expendable Deployer System (SEDS) during deployment. The reflectors are attached to the tether at the 5, 10, and 15 km points. They are expected to impact the tether, at attachment, with a longitudinal and a transverse (in-plane) velocity mismatch of $\pm 10\%$ of the predicted tether deployment velocity. This report investigates the impact of the attachment of the radar targets upon the deployment dynamics of *SEDS*. The investigation is carried out by running numerical simulations with one of the Smithsonian Astrophysical Observatory (SAO) bead-model computer codes (*MASTER20*) specially developed for simulating the dynamics of tethered systems in space. In particular the report assesses the effect of the radar targets upon the shape of the tether and evaluates the relative error between the tether shapes with and without radar targets.

Figure Captions

- Figure 1. Reference Frames and Coordinates.
- Figures 2(a)-2(d). *SEDS* dynamic response during deployment, obtained by means of SAO computer code (simulation 1), is compared to the results obtained by Energy Science Lab's. No aerodynamics, spherical gravity field.
- Figure 3. System Discretization Models.
- Figures 4(a)-4(n). Baseline simulation run. Dynamics response of *SEDS* without radar targets (simulation 2). 9-lump model. No aerodynamics, oblate Earth gravity field.
- Figures 5(a)-5(i). Dynamic response of *SEDS* with three radar targets attached to the tether with a differential longitudinal and transverse (in-plane) velocity components of +10% of the predicted tether payout velocity (simulation 3). 9-lump model. No aerodynamics, oblate Earth gravity field.
- Figures 6(a)-6(i). Dynamic response of *SEDS* like in simulation 3 but the model is a 17-lump model (simulation 4). This simulation runs covers 75% of the deployment maneuver.

1. INTRODUCTION

This is the Final Report submitted by the Smithsonian Astrophysical Observatory (SAO) under contract 2836 from ANCO Engineers, Inc., for "Analysis of Deployment of Expendable Tethered System." This report covers the period from 22 April 1988 through 30 July 1988. The Principal Investigator for this contract is Dr. Enrico C. Lorenzini and the Co-Investigator is Dr. Mario Cosmo.

2. DEPLOYMENT DYNAMICS

SEDS deployment has dynamic features different from other tethered systems such as the Tethered Satellite System. The main characteristics of *SEDS* deployment are the following:

- Low tension
- Limited tether control
- Expendable tether

The low tension deployment is required to minimize the momentum transfer to the tethered payload. Since there is no retrieval phase an expendable tether poses less constraints on the system hardware such as actuators on the payload and adequate sensors on the mother satellite [e.g. the space shuttle (STS)] and on the payload itself. It is well known that the retrieval maneuver is

intrinsically unstable and requires more time than the deployment.

From reference [1], the major events in a typical *SEDS* operation are:

1. Payload separation from the *STS* is initiated by a spring.
2. The payload drifts away and pulls tether out under low tension.
3. Small tension adjustments maintain the deployment schedule.
4. Braking reduces the range rate at the end of the 20 km tether.
5. Wide libration ensues, with payload released near the vertical.
6. The payload ends up 20 km to ~270 km below (or above) the *STS*.
7. The tether is released into a safe short-lived orbit.

The first *SEDS* experiment will consist of deploying from the mother satellite a 50 kg-mass payload on a 20-km long tether. The deployment dynamics, following the scheme above, can be divided into three main phases, namely 1) drift phase, 2) straighten phase, and 3) brake phase. Phase 1) is characterized by low tension that ranges approximately from 0.01 N to 0.05 N. This phase takes about 100 minutes and about 50% of the final length is deployed. The long duration of this phase allows even small forces to cause noticeable perturbations of the payload trajectory.

Phase 2) reduces the tether curvature raising the tension by one order of magnitude (~0.5 N). This phase takes about 25 minutes and about 40% of the final length is deployed.

Phase 3) slows the payout velocity down in order to minimize the final stretch and the payload rebound. This phase takes about 10 minutes. During the braking maneuver because of the fast build-up of the tension relatively large tether oscillations may occur unless the straighten phase has effectively reduced the tether curvature.

2.1 Introductory Remarks

Monitoring the tether shape as well as the tension, the payout velocity and the tether length are necessary to assess *SEDS* performance during deployment. This implies that some provisions in terms of system hardware are taken. Non-intrusive tensiometers and turns counters are already planned to be part of the current hardware design. Radar targets attached to the tether have been proposed by ANCO for monitoring the tether shape by using the Space Shuttle's radar to track them.

This report addresses the dynamics of *SEDS* with three radar reflectors attached to the tether. The three radar reflectors are attached to the tether at 5, 10, 15 km points respectively. The reflectors are expected to impact the tether at the attachment time with an axial and transverse (in-plane) relative velocity equal to $\pm 10\%$ of the predicted deployment velocity. Purpose of this report is: (1) to assess that the radar reflectors do not introduce any instability in *SEDS* dynamics, such as tether slackness or payload rebound; (2) to verify that the radar reflectors

do not affect appreciably the tether tension and the payout velocity, which are fundamental control variables during the tether deployment; (3) to investigate if and how the longitudinal and lateral tether oscillations, detectable through radar tracking, are affected by the introduction of the radar reflectors.

2.2 Dynamics Simulation Model

The analysis has been carried out by means of a numerical simulation code. *MASTER20*, one of SAO computer codes for simulating tethered systems dynamics, has been modified to simulate *SEDS* dynamics in the space environment. This code models both the end-platforms and the tether by means of lumped mass.

The 3-dimensional equations of motion of *SEDS* are referred to an orbiting reference frame (*ORF*) which rotates at constant orbital rate Ω and radius R_o . The origin of this frame coincides with the initial position of the system *CM* (see Figure 1). The *x* - axis is along the *ORF* velocity vector, the *z* - axis is along the local vertical toward the Earth, and the *y* - axis completes the right-handed reference frame.

The tether is assumed to be visco-elastic and perfectly flexible (no bending stiffness). The orbit of the system is generic. In this particular case the Shuttle is assumed to follow an orbit which is initially circular.

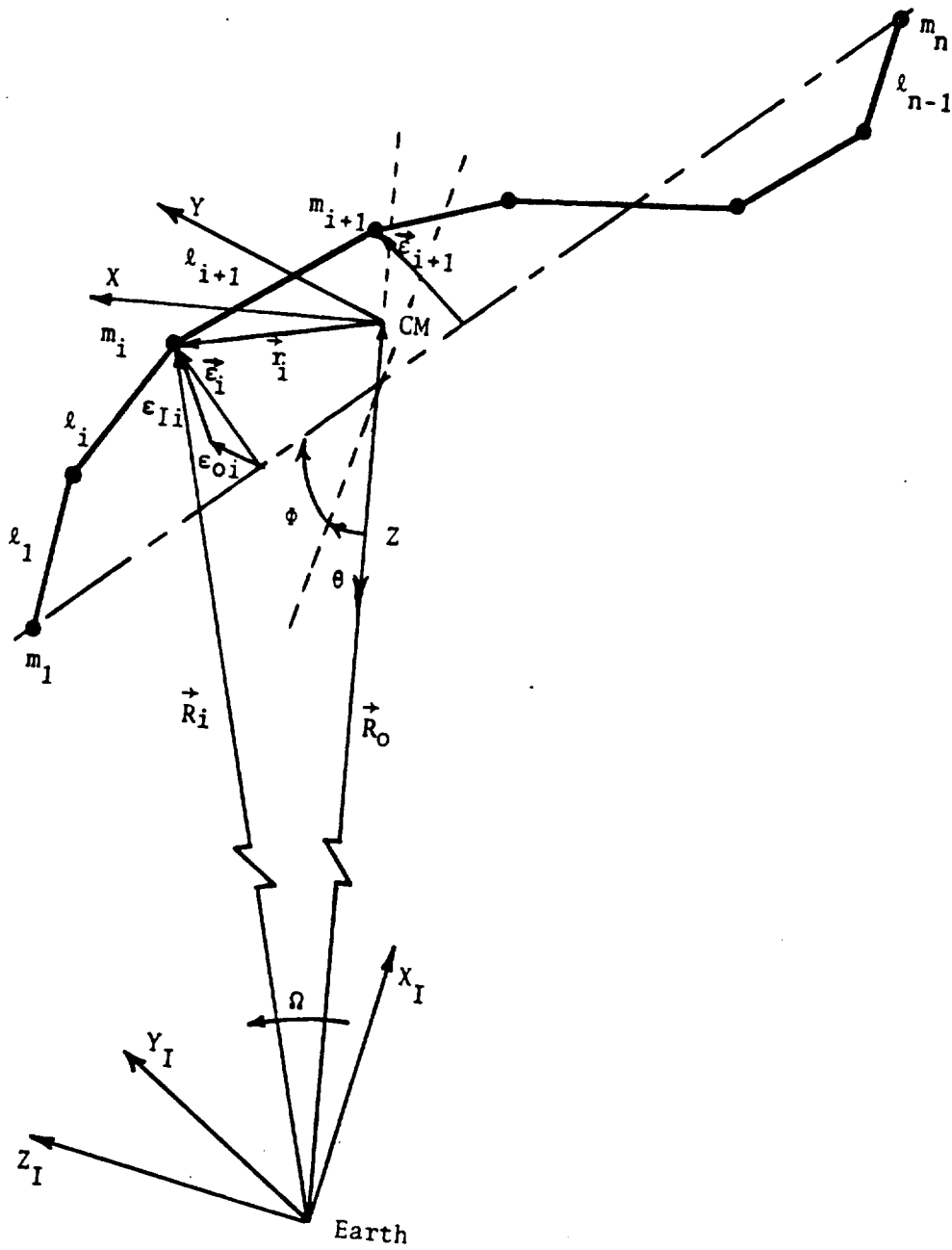


Figure 1.

The equations of motion of the N -masses of the system in vectorial form are

$$\begin{aligned} \ddot{\mathbf{r}}_i = & -\ddot{\mathbf{R}}_o - 2\boldsymbol{\Omega} \times \dot{\mathbf{r}}_i - \boldsymbol{\Omega} \times (\boldsymbol{\Omega} \times \mathbf{r}_i) + \\ & + \frac{1}{m_i} (\mathbf{F}_{g,i} + \mathbf{F}_{T,i}) \quad i = 1, \dots, N \end{aligned} \quad (1)$$

where m_i is the mass and \mathbf{r}_i the radius vector of the i^{th} -mass with respect to ORF . The above equations are a set of N vectorial equations or correspondingly a set of $3 \times N$ scalar equations which have to be integrated numerically in order to obtain the motion of the system. The external perturbations considered in the present analysis are: the gravitational forces \mathbf{F}_g , and the tensional forces \mathbf{F}_T .

The gravity model is not linearized and it also takes into account the second zonal harmonic of the gravity field (J_2 - term). The J_2 - term has a secular effect on such orbital parameters of the system as mean anomaly, argument of perigee, and right ascension of the ascending node. The J_2 - term also affects the librations and lateral oscillations (see next section) of a long tethered system such as the one under analysis.

The coordinates x_i, y_i, z_i of the point masses with respect to ORF are numerically integrated by the computer code with a 4th-order Runge-Kutta or a predictor-corrector integration routine.

A second set of coordinates has also been selected in order to provide a more direct description of the system dynamics. This set of coordinates is formed by (see Figure 1): the in-plane (in the orbital plane) θ and out-of-plane (orthogonal to the orbital plane) φ angles of libration between the line connecting the end-masses and the local vertical through the system CM ; the $N - 1$ lengths of the tether segments l_i , where N is the number of the lumped masses, and the $N - 2$ lateral deflections ϵ_i of the inner masses with respect to the line through the end-masses. The coordinates ϵ_i are further projected onto the in-plane ϵ_{Ii} and out-of-plane components ϵ_{Oi} . The ϵ_I 's and ϵ_O 's, therefore, provide a clear representation of the tether bowing both in the orbital plane and in the transverse plane. Drag forces have been neglected (the atmospheric density at the orbital altitude of *SEDS* is very small) in order to expedite the simulation runs. *MASTER20*, like all the other tethered object simulation codes, is very CPU intensive. A typical simulation run of *SEDS* with 17 lumps takes 30 hrs. of CPU time to cover less than 2 hrs. of deployment. The discontinuities introduced by the attachment of the radar targets, moreover, complicate the job of the integrator and of the computer analyst as well.

2.3 Deployment Control Law

SEDS tension control law has been implemented following reference [1]. The computation of the input tension T_{IN} expressed by Equation (2.1) is based on empirical considerations related to the geometry and dynamics of *SEDS* deployer. The controller, [see Equation (2.2)] computes the brake force using an array of user-provided break points F_i and break values c_{T_i} by interpolating the natural logarithm of the brake setting, as expressed by Equation (2.3). The exponential of that brake setting multiplied by the input tension is the tether control tension $T_{CONTROL}$ (see Equation 2.5).

Mathematically the control algorithm can be represented as

$$T_{IN} = T_{MIN} + A \dot{t}^2 \quad (2.1)$$

$$F = L_{DEP}/L \quad (2.2)$$

$$c_T = c_{T_i} + \frac{c_{T_{i+1}} - c_{T_i}}{F_{i+1} - F_i} (F - F_i) \quad (2.3)$$

$$T_{CONTROL} = T_{IN} e^{c_T} \quad (2.4)$$

where

- L_{DEP} = Actual deployed tether length
- L = Overall tether length to be deployed
- c_T = Brake tension multiplier (natural logarithm)
- T_{MIN} = Minimum deployment tension (Newton)

F	=	Fractional tether length
A	=	Constant that keeps into account the deployer geometry and inertia effects
\dot{l}	=	Deployment velocity

Since *SEDS* control law is proprietary data we refer to Energy Science Laboratories, Inc. for any further information about the control strategy.

2.4 Computer Code Validation

A first set of simulations has been run in order to compare the results obtained from *MASTER20* with Energy Science Lab's (Joe Carroll's, 1987) results which are so far the only data available in the literature on *SEDS* dynamics [ref. 1].

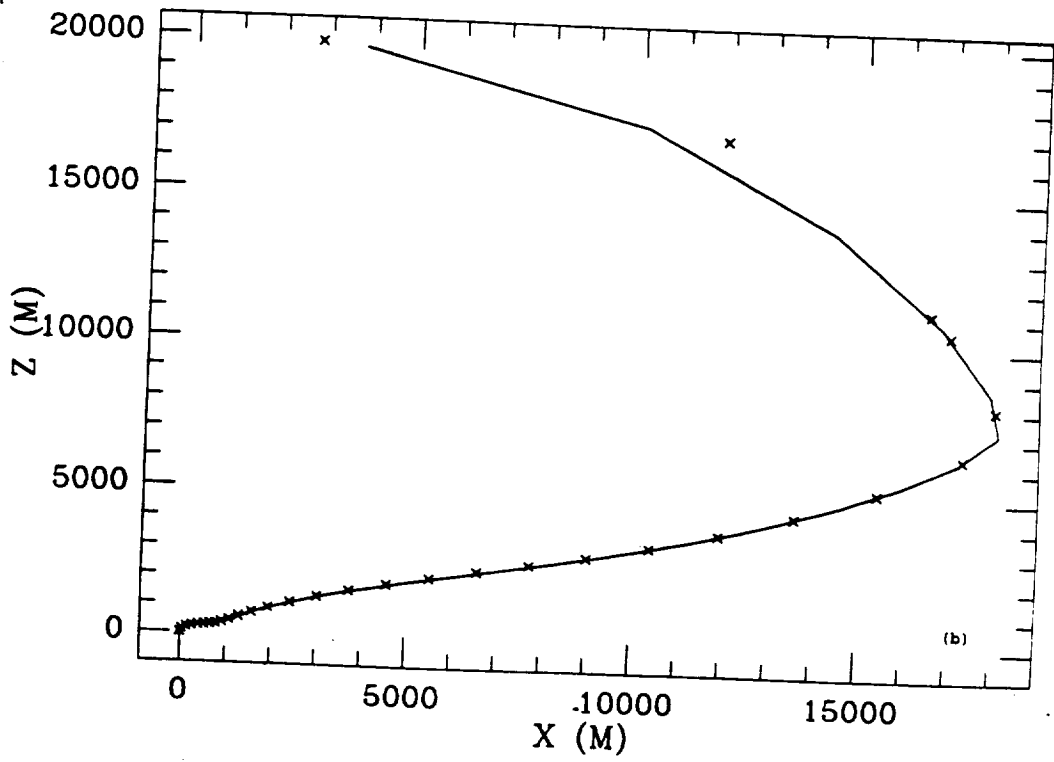
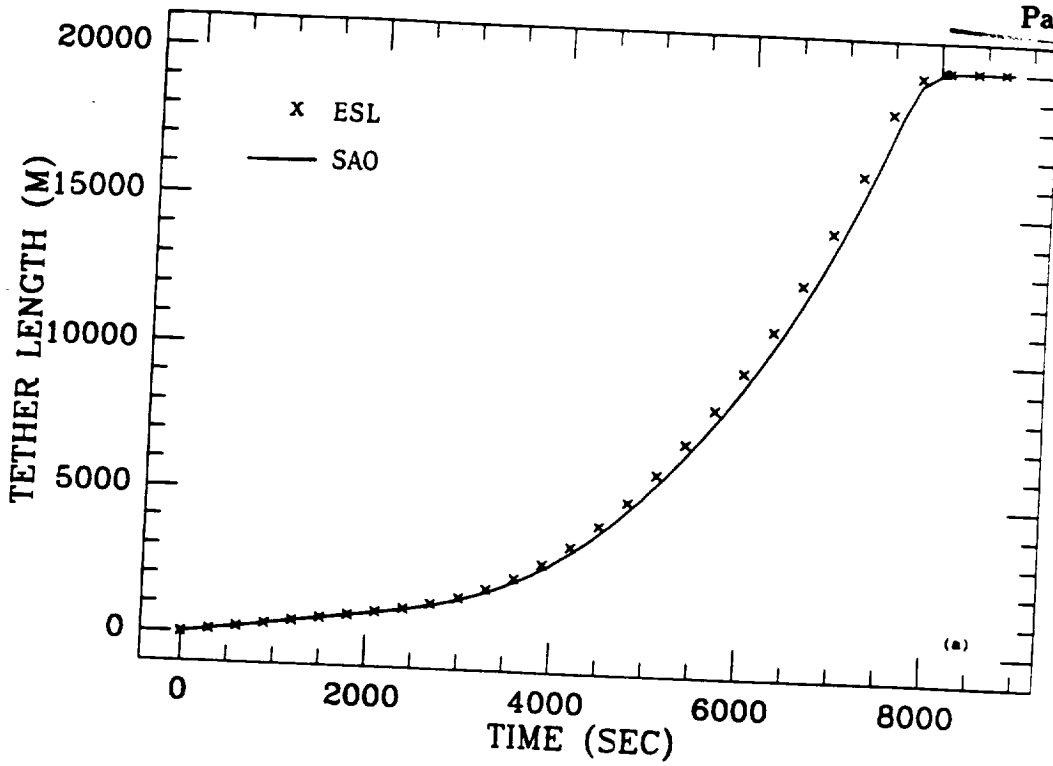
All the simulations have been run with the parameters and initial conditions listed in Table 1.

Table 1

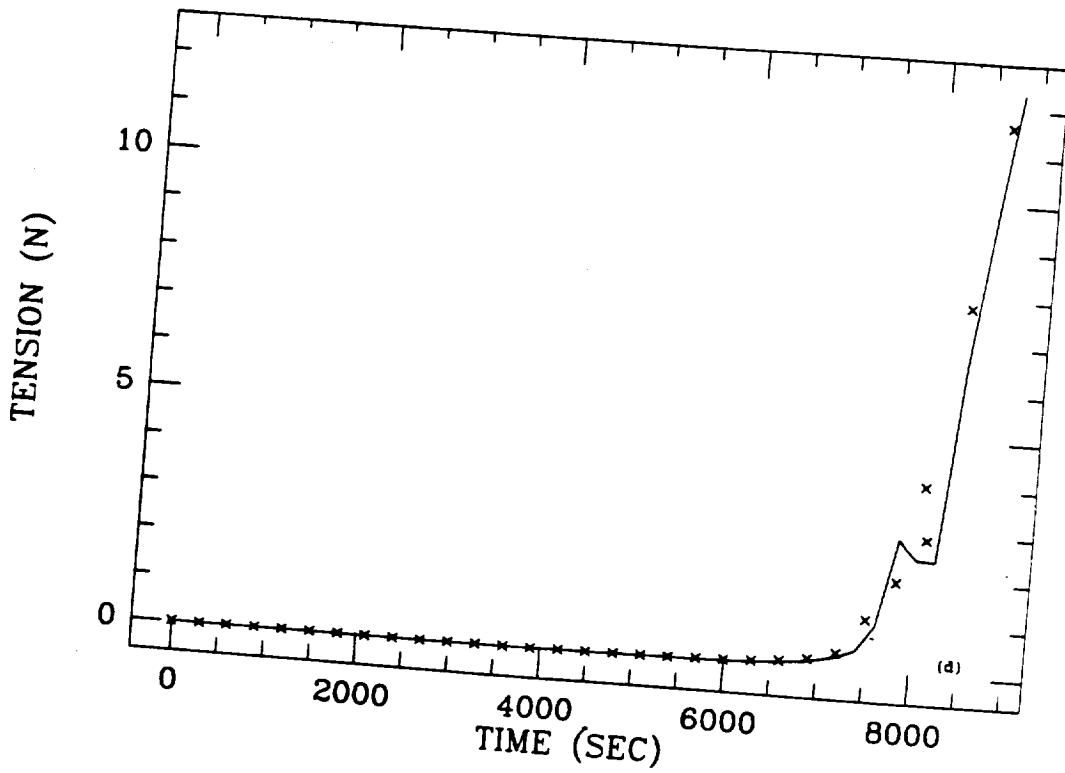
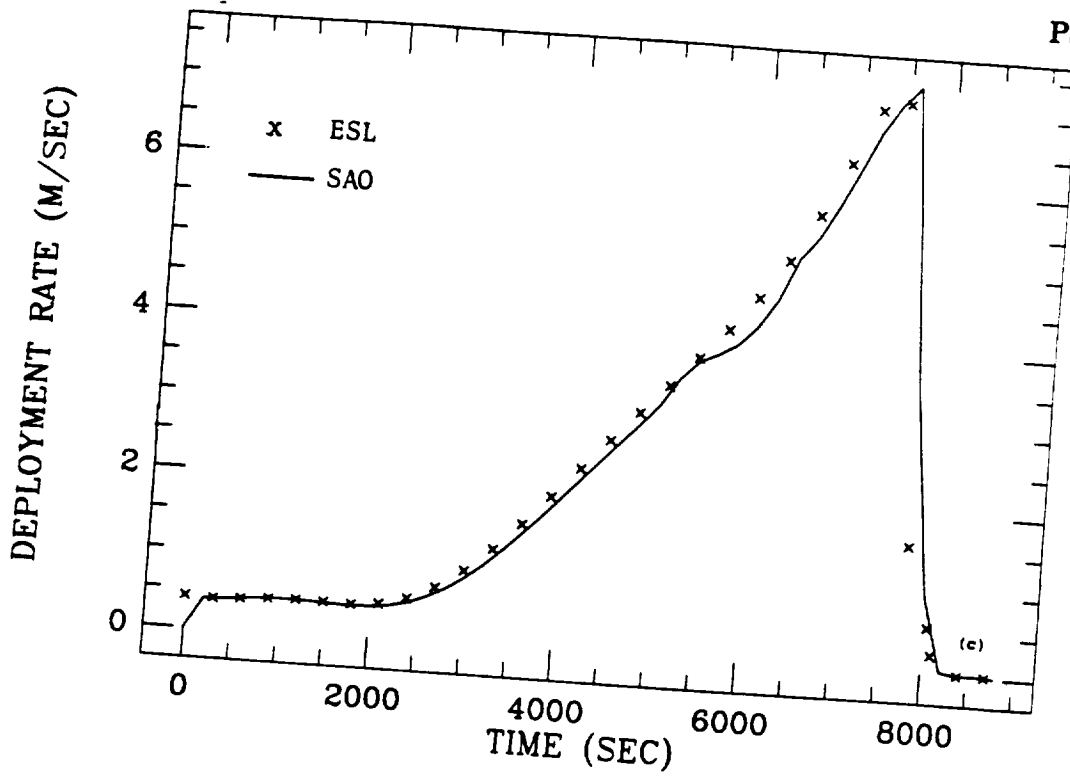
Mother Satellite Mass (i.e. Space Shuttle)	90000 kg
Payload Mass	50 kg
Orbit Inclination	28.5°
Mother Satellite Altitude	300 km
Tether Initial Length (l_0)	1 m
Tether Initial Velocity (\dot{l}_0)	0.4 m/s
Tether Radius	7×10^{-4} m
Tether Linear Density	2.9×10^{-4} kg/m
Tether Axial Stiffness (EA)	10^4 Newtons
Tether Axial Viscosity (EA')	2×10^4 Newton-sec

We have used various numbers of lumped masses in running the validation simulations and we show here the results obtained with a 5-lump model (simulation 1). Since the Energy Science Lab's (ESL) code does not have the J_2 -term the Earth gravity field has been assumed to be spherical in these validation runs. Figures 2.4(a), 2.4(b), 2.4(c), and 2.4(d) show the results of the comparison runs, namely the tether length, payload trajectory, deployment velocity, and tether tension respectively. The results agree quite satisfactorily with those published by Energy Science Laboratories. The few disagreements are due simply to different output steps (Energy Science Lab's = 300 sec; SAO = 50 sec). Other minor differences in the length and tension time histories are most probably related to small differences in generating the new lumped masses during deployment as the tether comes out of the spool.

ORIGINAL PAGE IS
OF POOR QUALITY



Figures 2(a) and 2(b).



Figures 2(c) and 2(d).

2.5 Simulation Of SEDS Deployment Dynamics

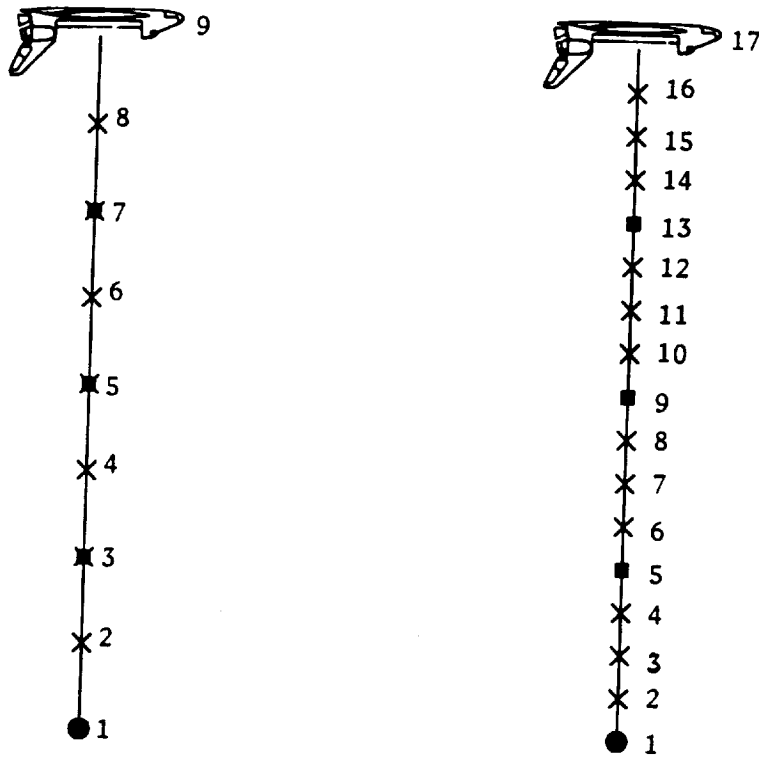
2.5.1 Without Radar Targets

After the results of our computer code had been validated we focused our effort on carrying out comparative simulation runs of SEDS deployment with and without radar targets attached to the tether. We had been informed by J. Carroll that recent tests of SEDS's tether at temperature comparable to those to be expected in space had shown that the tether material damping was much lower than the room temperature value of 20,000 N-sec. A more appropriate value at low temperature should be around $EA' = 2,000$ N-sec. We have, therefore, decided to run the comparative simulation runs according to the new value of tether axial viscosity EA' . This explains the different behavior of the tether tension during the breaking phase. Because of the lower value of material damping the tether tensions shows a significant ringing phenomenon at the end of deployment. In other words the longitudinal (along the tether) oscillations are only lightly damped. The other degrees of freedom, namely the librations θ and φ , and the lateral deflections ϵ_I 's and ϵ_O 's, are almost unaffected by the tether damping properties.

Several simulations with increasing number of lumps have been run. A finer resolution requires smaller and smaller integration steps. Furthermore, numerical instabilities appear for a large number of lumps and the CPU times, required to overcome them, become prohibitive. Thus far, from the current

9 LUMPED MASSES

17 LUMPED MASSES



x LUMPED MASS ■ RADAR TARGET

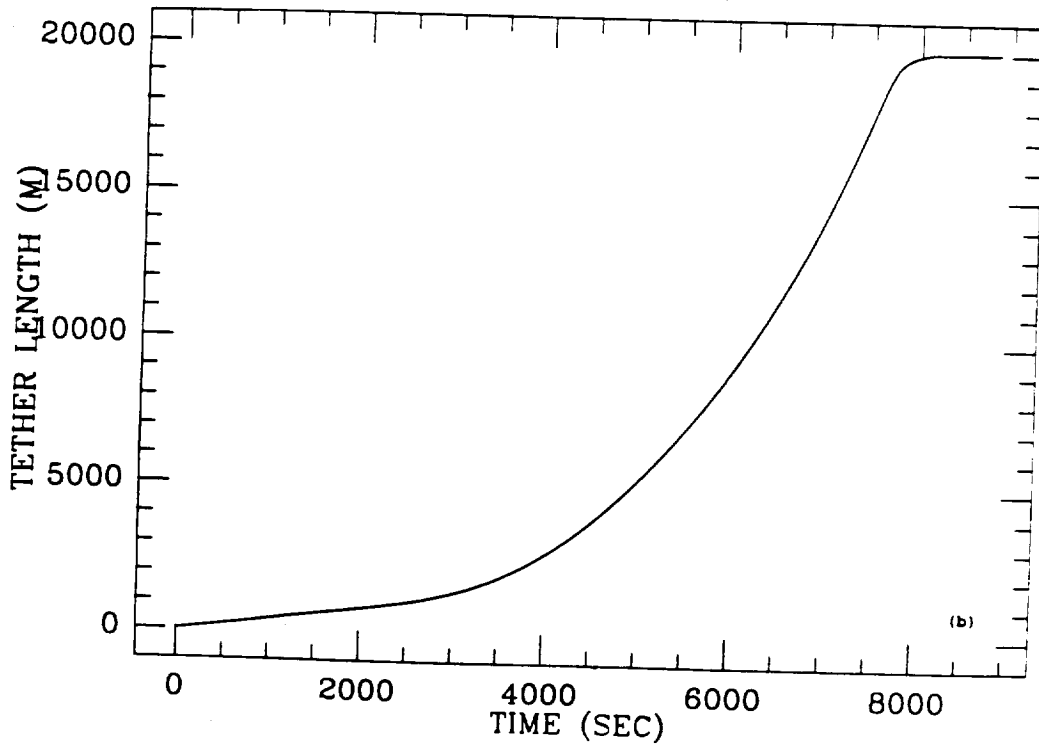
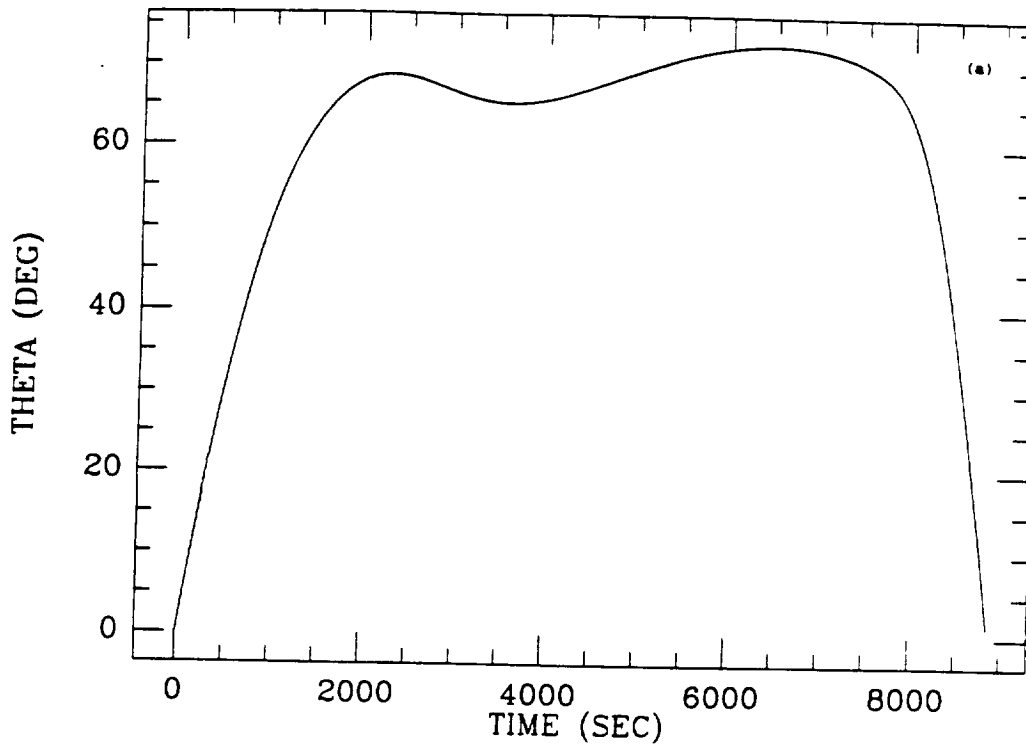
Figure 3.

ORIGINAL PAGE IS
POOR QUALITY

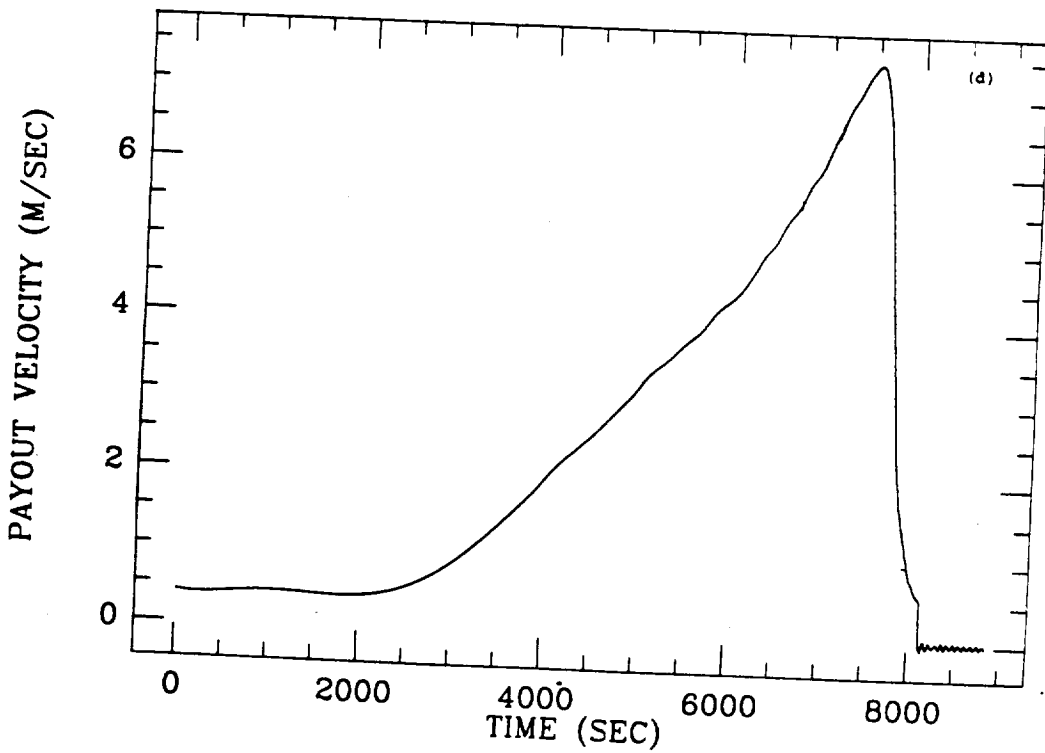
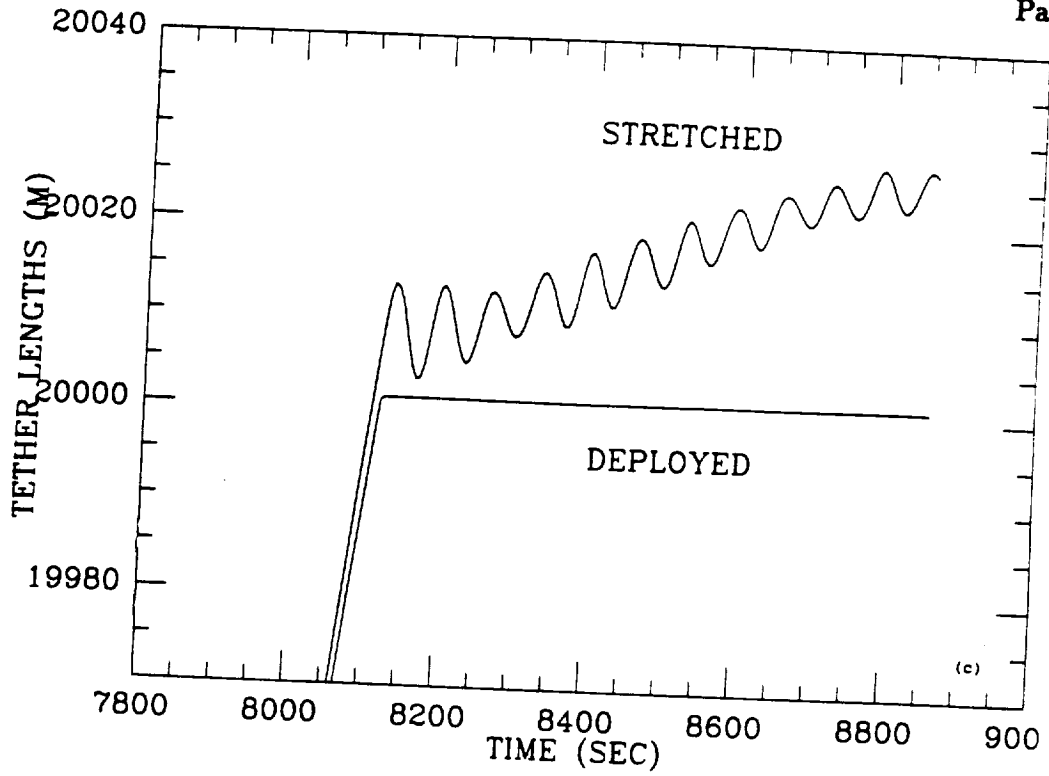
literature available on the subject, the maximum number of lumps adopted in 3-D models which do not manipulate the longitudinal tether oscillations in order to increase the computer efficiency has been 6 [ref. 2]. An important phase of our investigation has been spent looking for the "best run," that is finding the best compromise between resolution (i.e. number of lumps) and reasonable CPU times.

The discontinuities introduced by the attachment of the radar targets with mismatched velocities complicate even more the job of the integrator. After several attempts the number of lumps that provides a good compromise between resolution and CPU time has been found to be 9 (see Figure 3). The simulations require a maximum integration step of 0.1 sec for a relative accuracy of 10^{-7} . The CPU time for each run is about 4 hours.

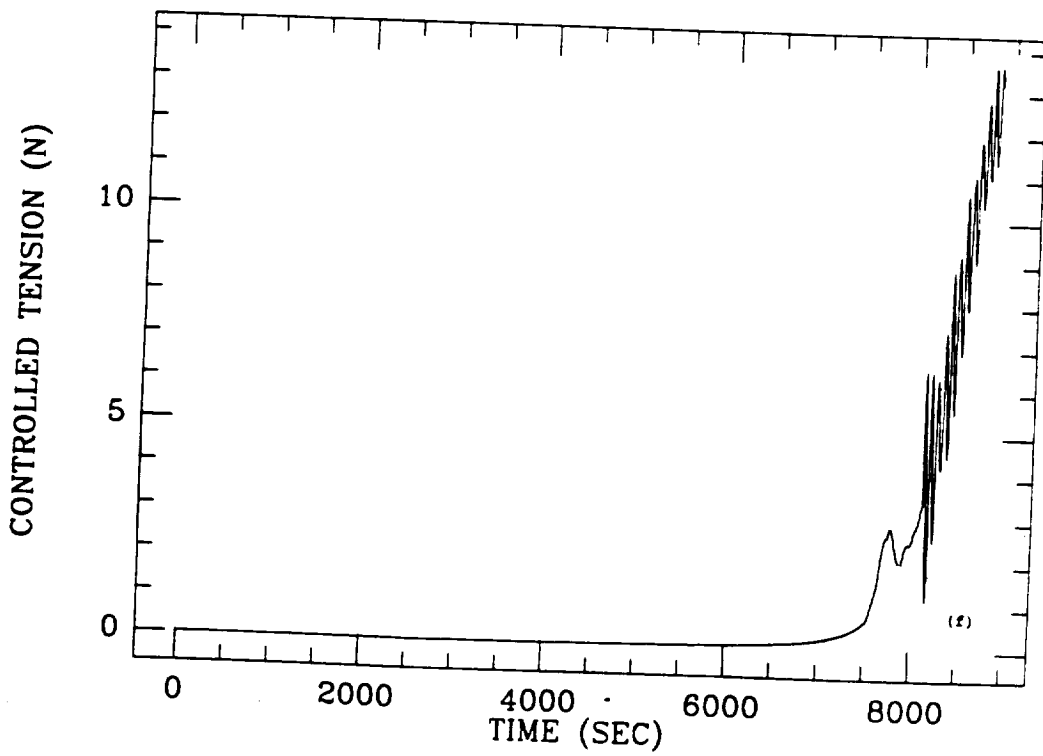
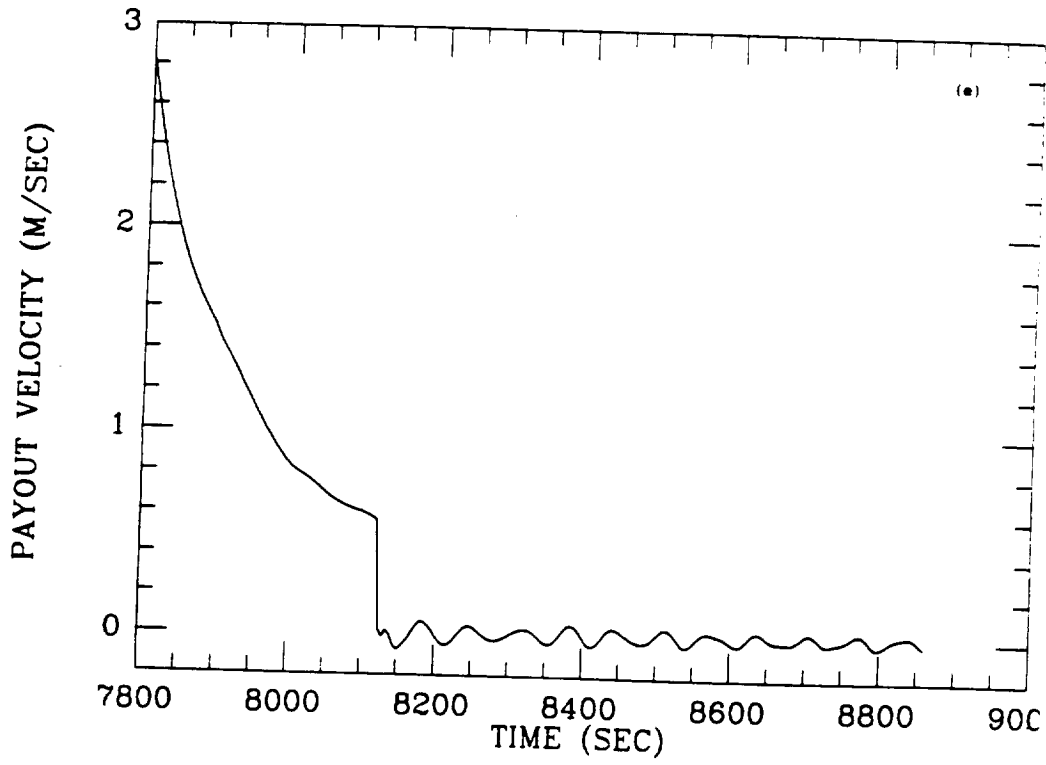
In the following the results of a typical SEDS deployment with 9 lumps and no radar targets are shown (simulation 2). The simulation run stops when the in-plane angle θ with respect to the local vertical is less than or equal to 1° . At that instant the tether is supposed to be cut and the payload released. Figure 4(a) shows the in-plane libration angle θ . The libration reaches a peak of 73° approximately 15 minutes after the payload ejection. The steep variations during the initial and final phases are a function of the balance between the gravity gradient torque and the Coriolis torque which depend upon the tether length and the tether payout velocity respectively. Figure 4(b) shows the tether length. The length follows the exponential deployment control law. Figure 4(c) depicts the



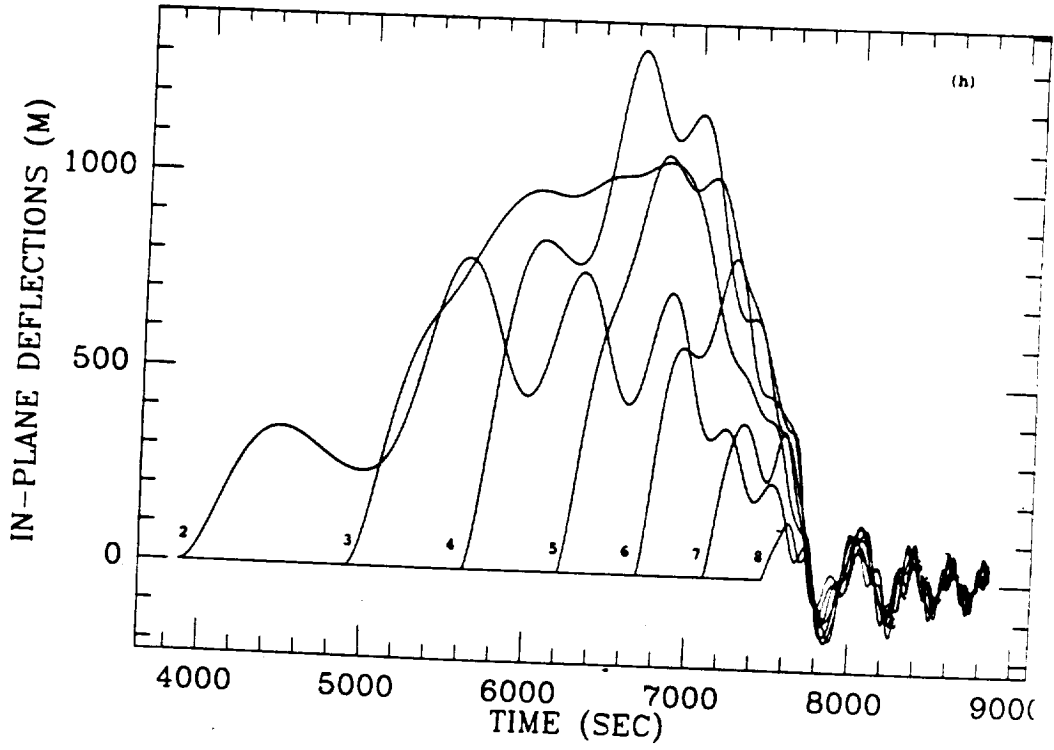
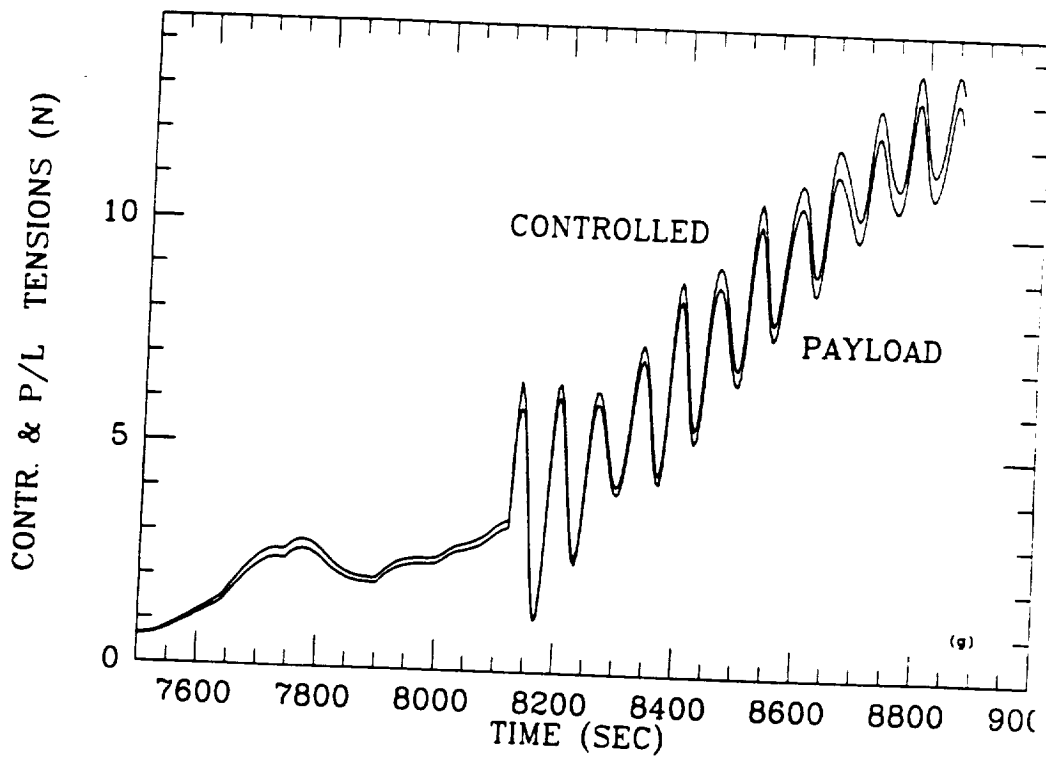
Figures 4(a) and 4(b).



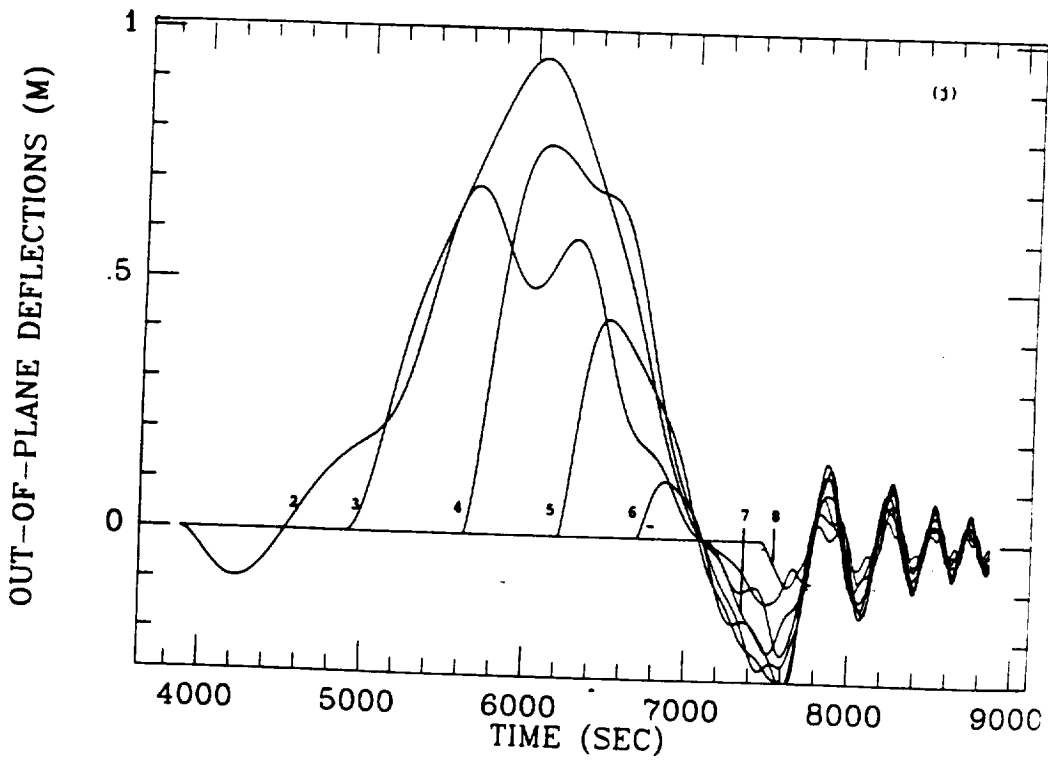
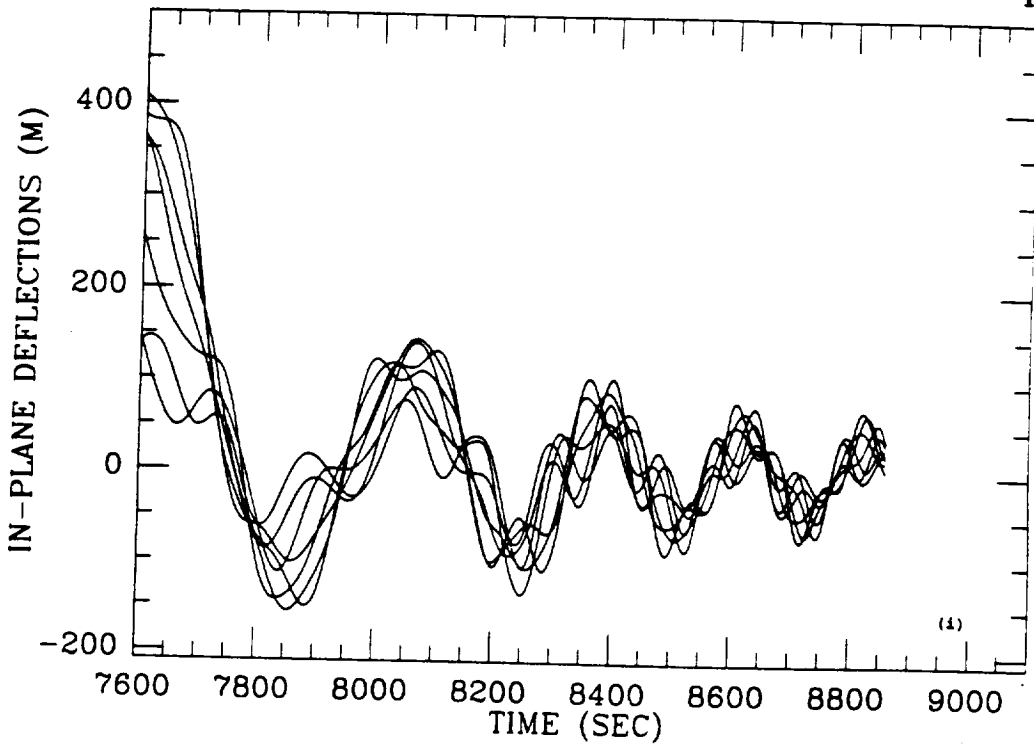
Figures 4(c) and 4(d).



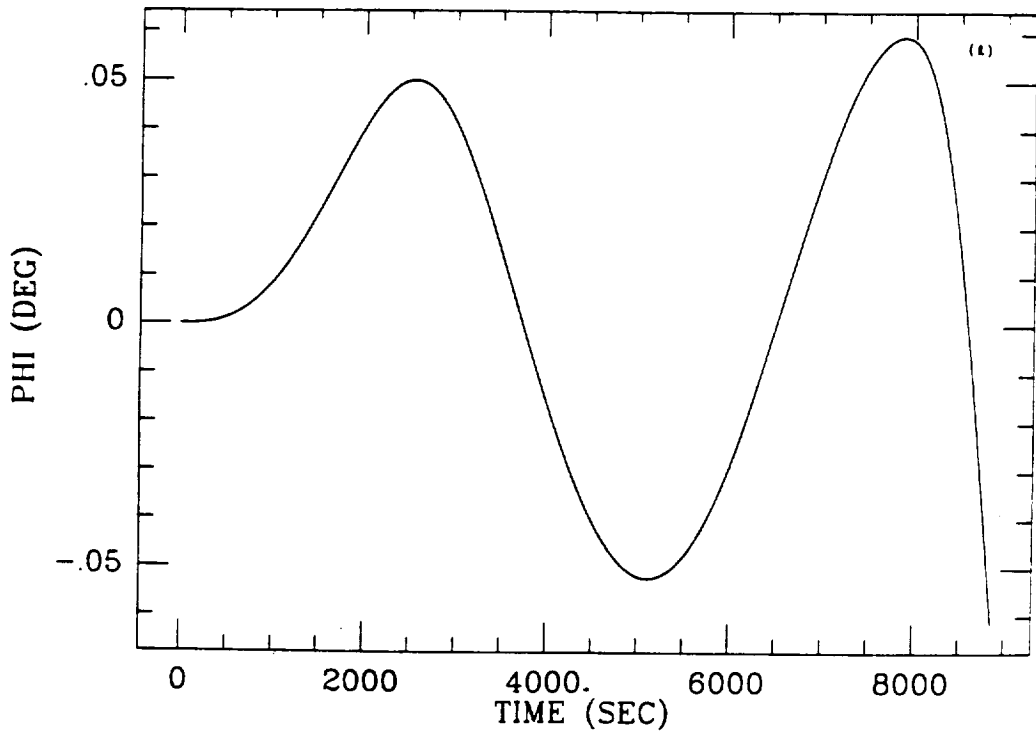
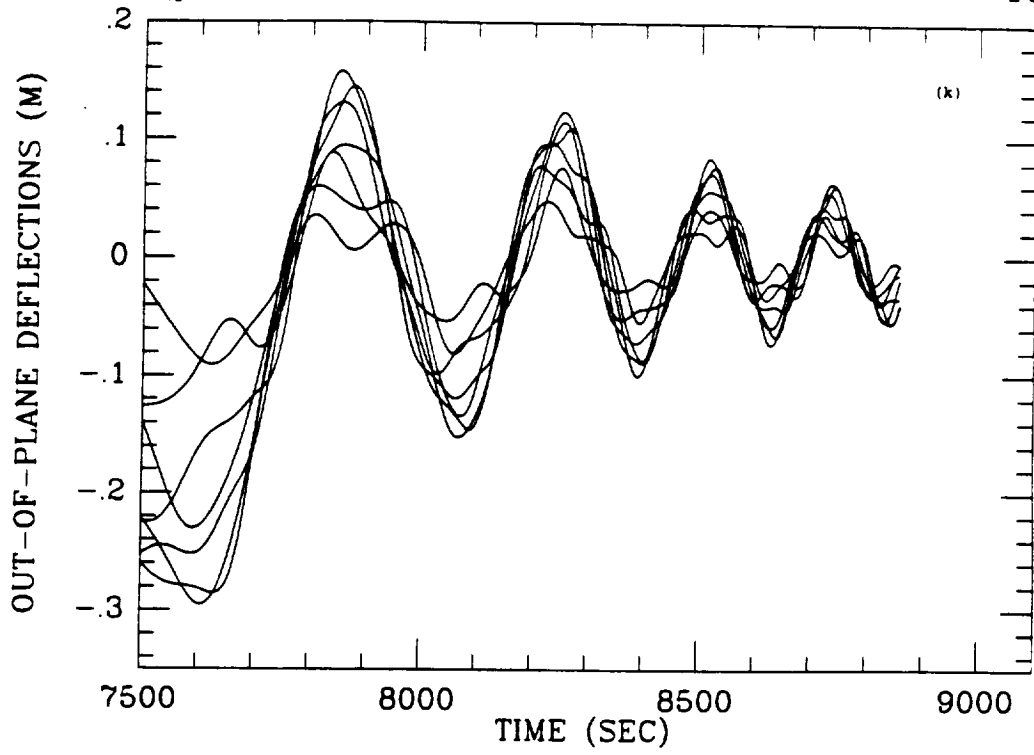
Figures 4(e) and 4(f).



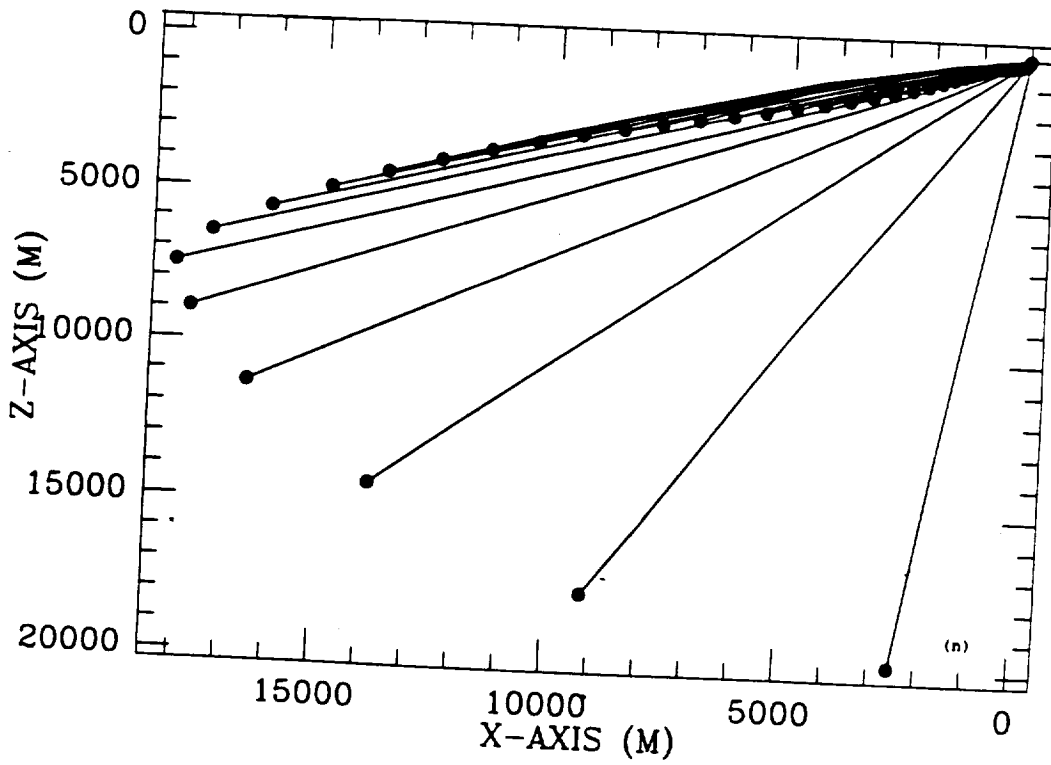
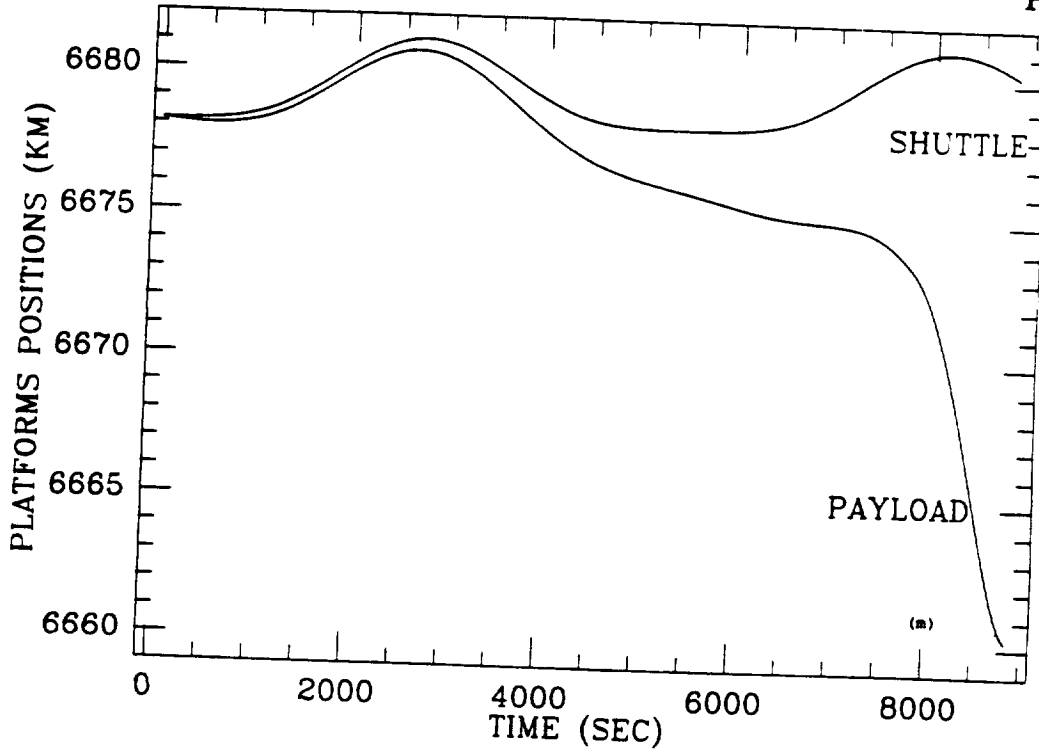
Figures 4(g) and 4(h).



Figures 4(i) and 4(j).



Figures 4(k) and 4(l).



Figures 4(m) and 4(n).

stretched and the deployed tether lengths during the final part of deployment. The deployment stops around 8100 sec and the stretched length reaches its steady-state value. Figure 4(d) depicts the payout velocity $\dot{\ell}$. The break reduces the value of $\dot{\ell}$ from 6.8 m/s to 0.6 m/s. The discontinuity at the end of the deployment, which is shown enlarged in Figure 4(e), is caused by the deployed tether length reaching its final value of 20 km as shown in Figure 4(c). Figure 4(f) shows the controlled tension. The three phases of deployment are easily recognizable from the plot. The oscillations in the final part are due to undamped longitudinal oscillations excited by the non zero value of the payout velocity at the end of the deployment. Figure 4(g) depicts the controlled tension and the tension at the payload during the final phase of deployment. Both tensions exhibit the same behavior with a slight difference in their magnitudes due to the tether mass. Figure 4(h) shows the in-plane deflections ϵ_l 's for all the inner lumps. Their values are zeros before the lump is released. Their indexes are referred to the indexes of the associated lumps as shown in Figure 3. All the deflections have a longer frequency at the beginning of the deployment and a shorter frequency at the end owing to the increasing magnitude of the tether tension during deployment. It is worth noticing that the "strengthen" phase provides an effective reduction of the tether "bowing". The residual lateral oscillations, however, cannot be damped unless an adequate tether control is adopted. The peak value of the bowing is 1350 m which is associated to the deflection of lump no. 4. At the end of deployment the deflections have a magnitude around 60 m as shown in the

enlarged plot of Figure 4(i). Figures 4(j), 4(k), and 4(l) depict the out-of-plane deflections, the enlarged view of their final values, and the out-of-plane libration angle φ . The out-of-plane dynamics is mainly excited by the J_2 -term (i.e. Earth oblateness). The out-of-plane deflections are below 1 m during the entire deployment and less than 20 cm at the end of the maneuver. Even though the out-of-plane angle φ tends to increase during deployment its magnitude is quite small. Figure 4(m) shows the radius vectors of the mother satellite and the payloads measured with respect to an Earth centered reference frame. The mother satellite radius shows an eccentricity e equal to 2×10^{-4} , ($e = \Delta h / 2R_p$, R_p = perigee radius = 6678 km) caused by the J_2 gravity term. The payload radius show the same behavior at the beginning of the deployment since it is almost free-flying during that phase. Figure 4(n) shows snapshots of the in-plane motion of the system. The snapshots are drawn every 200 sec. The payload is represented by the black dot. The flight direction is toward the left of the plot and the Earth is below. This plot shows some relevant features of the deployment dynamics, such as the near-horizontal deployment at the beginning of the maneuver, the initial tether bowing, and the large final libration.

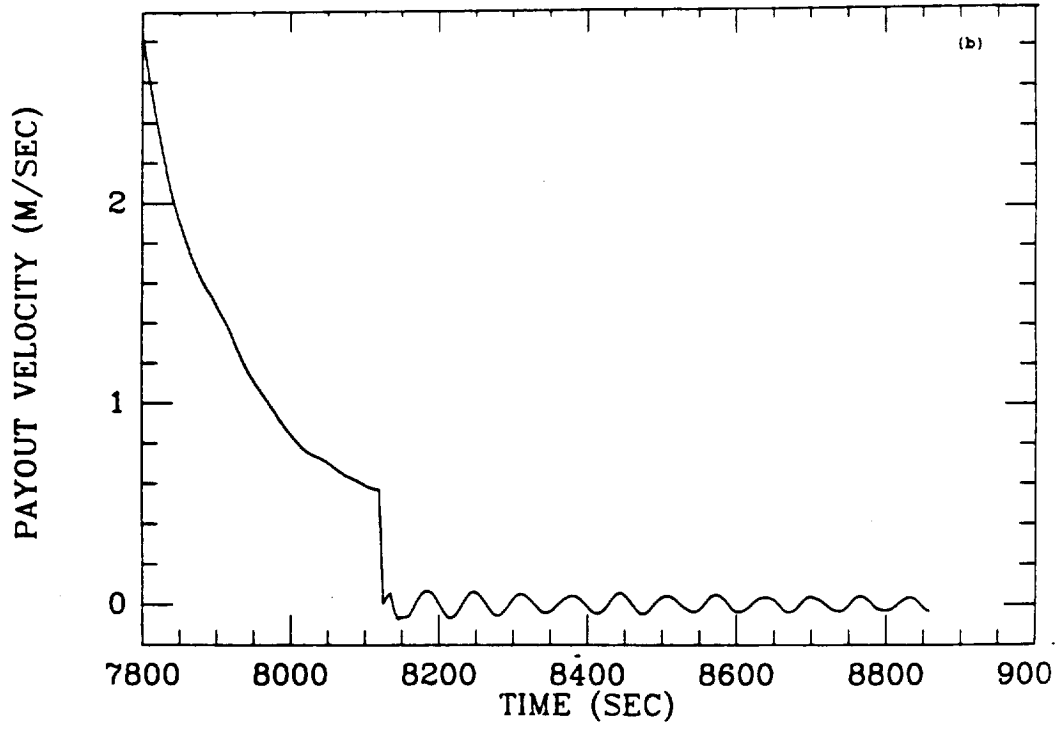
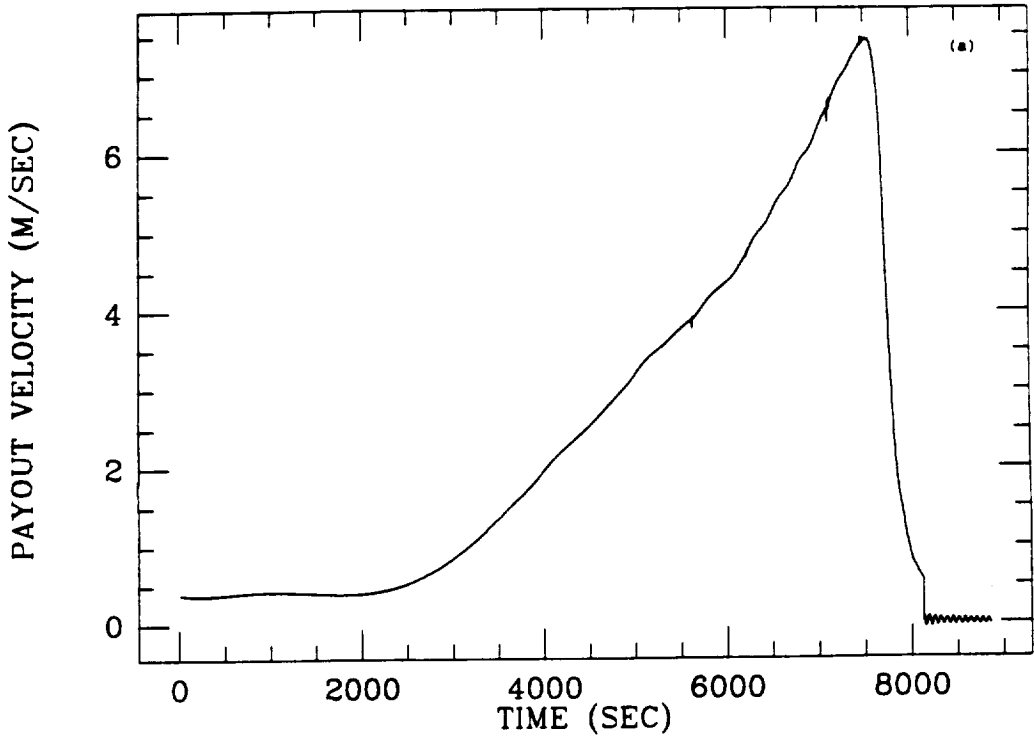
2.5.2 With Radar Targets

In order to detect the shape of the tether during *SEDS's* deployment maneuver, ANCO is proposing to add three radar targets, each with a mass of 100 gr, to the tether as the tether is reeled out of the spool. As already mentioned previously, the three radar targets are attached to the 5, 10, and 15 km points along the tether. The targets are expected to have a velocity mismatch, both along and orthogonal (in-plane) to the tether, of about $\pm 10\%$ of the deployment velocity. An issue of primary importance to this project is how the attachment of the radar targets affects *SEDS's* dynamics and in particular the shape of the tether. We run several simulations to address these issue and the results from one of them are shown in detail in this section. The model adopted for simulation run 3, presented here, is like the model adopted for the baseline simulation run of the previous section, namely 9 lumps. During deployment the three radar targets are attached to lumps 3, 5, and 7 respectively (see Figure 3). The velocity mismatch of the three radar targets is $+10\%$ of the payout velocity. Specifically, when each radar target is added to the tether lump, the initial velocity of the radar target plus tether lump is abruptly modified in the simulation model so that the initial linear momentum of the tether lump plus target is $+10\%$ of the initial linear momentum of the tether lump without the target. We will elaborate more on the discretization adopted in the next section. The results of this simulation run are shown in th next set of figures. Each figure of the set should be compared to the corresponding figures of the baseline simulation run shown in the previous section.

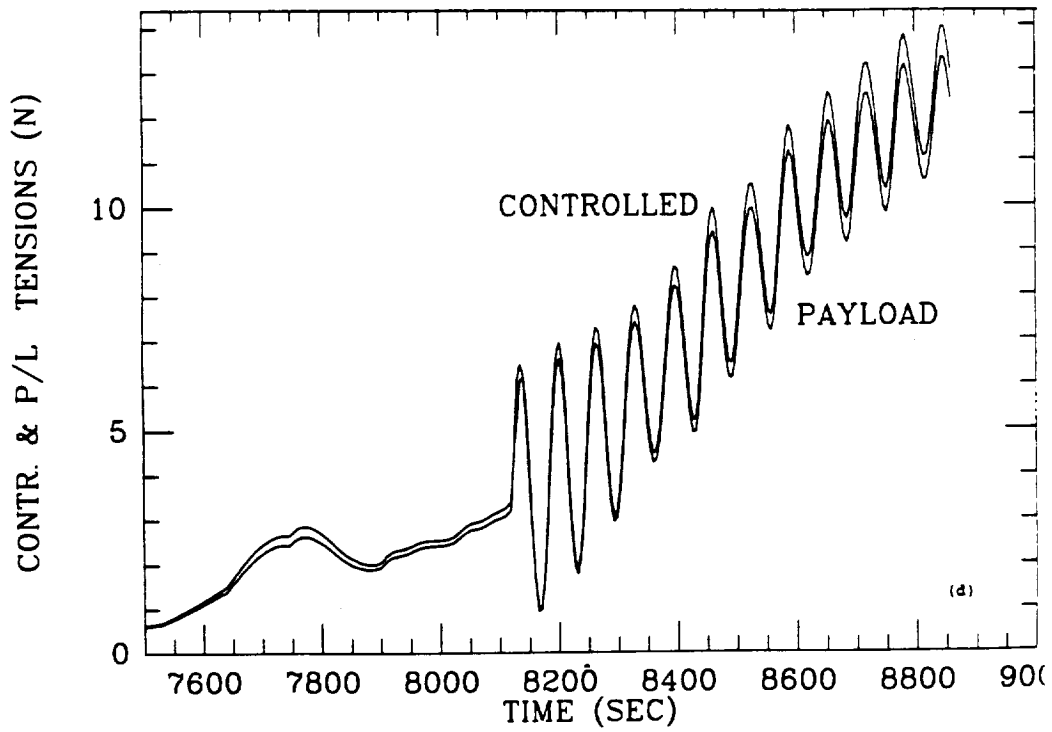
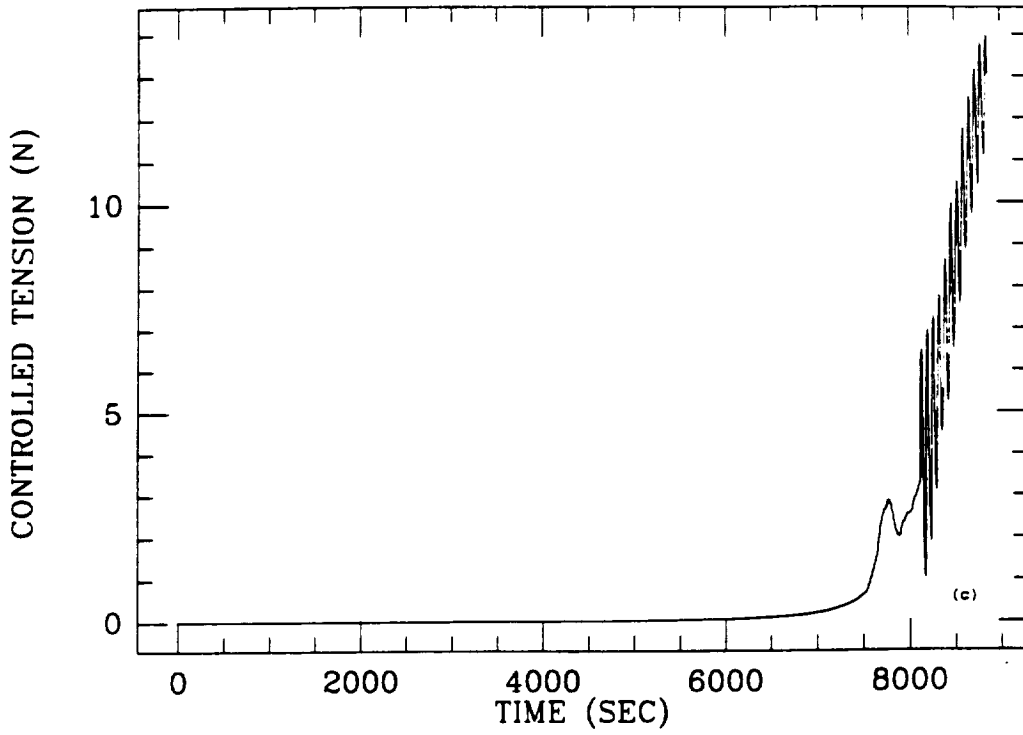
Most of the figures are self explanatory. We want to point out, however, some of the relevant features of the deployment dynamics with the radar targets. The tether payout velocity [see Figures 5(a), and 5(b) for the enlargement of the final phase] is almost unaffected by the addition of the radar reflections. The mass of the reflectors is too small to influence significantly the longitudinal dynamics of the "stiff" tether. Similar conclusions hold for the tether tension shown in Figure 5(c) and its enlargement during the final phase in Figure 5(d).

More appreciable but still small differences appear in the tether shape of which the deflections ϵ_I 's and ϵ_O 's provide the most visible representation. After accurately comparing Figure 5(e) with Figure 4(h) we can conclude that the maximum departure of the tether in-plane bowing from the baseline case (no radar targets) is less than 10% of the baseline bowing. Specifically the maximum differential bowings at the radar targets are as follows: 80m over 1350 m for target 1 (the one closer to the payload), 85 m over 1060 m for target 2, and 40 m over 400 m for target 3.

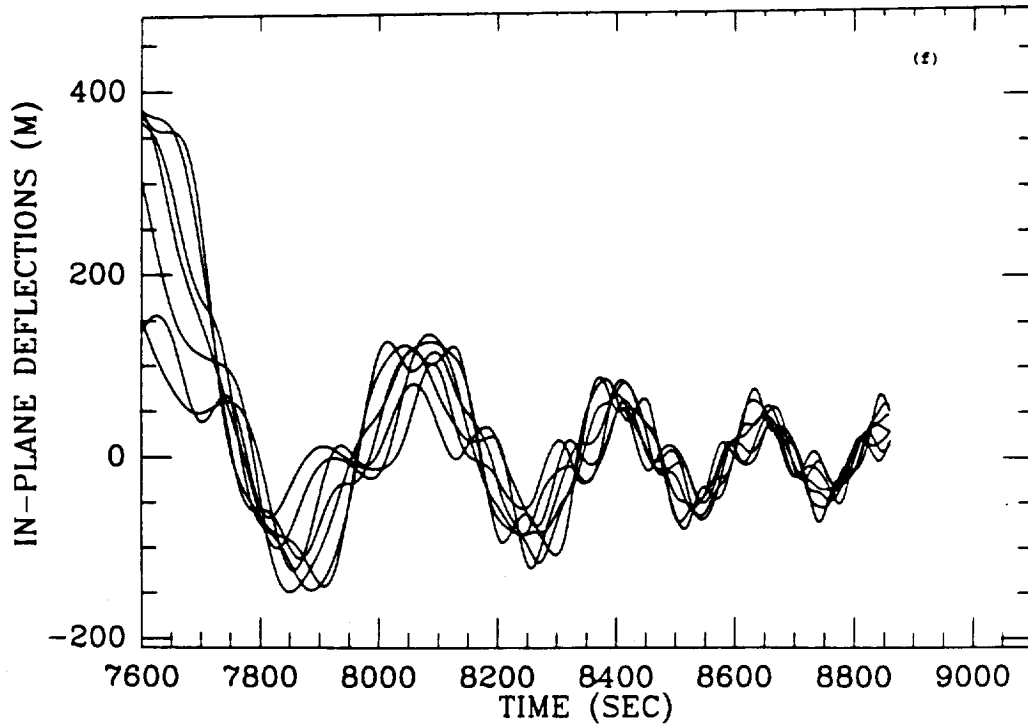
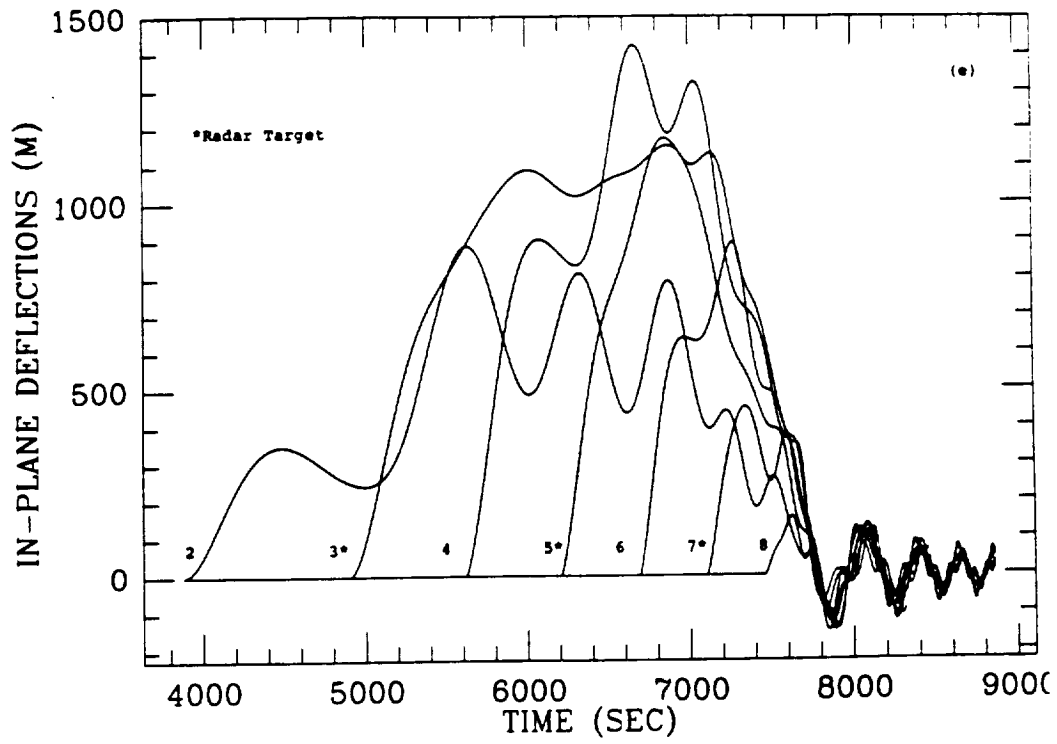
The out-of-plane bowing is also slightly affected by the attachment of the radar targets. This is probably caused by coupling between different *DOF*'s because there is no out-of-plane initial velocity mismatch in this simulation. The out-of-plane deflections however are small enough to be most probably below the ranging accuracy of the Shuttle's radar. Finally Figure 5(i) shows a snapshot side-view of the entire deployment. The black dot in the figure is the payload and the



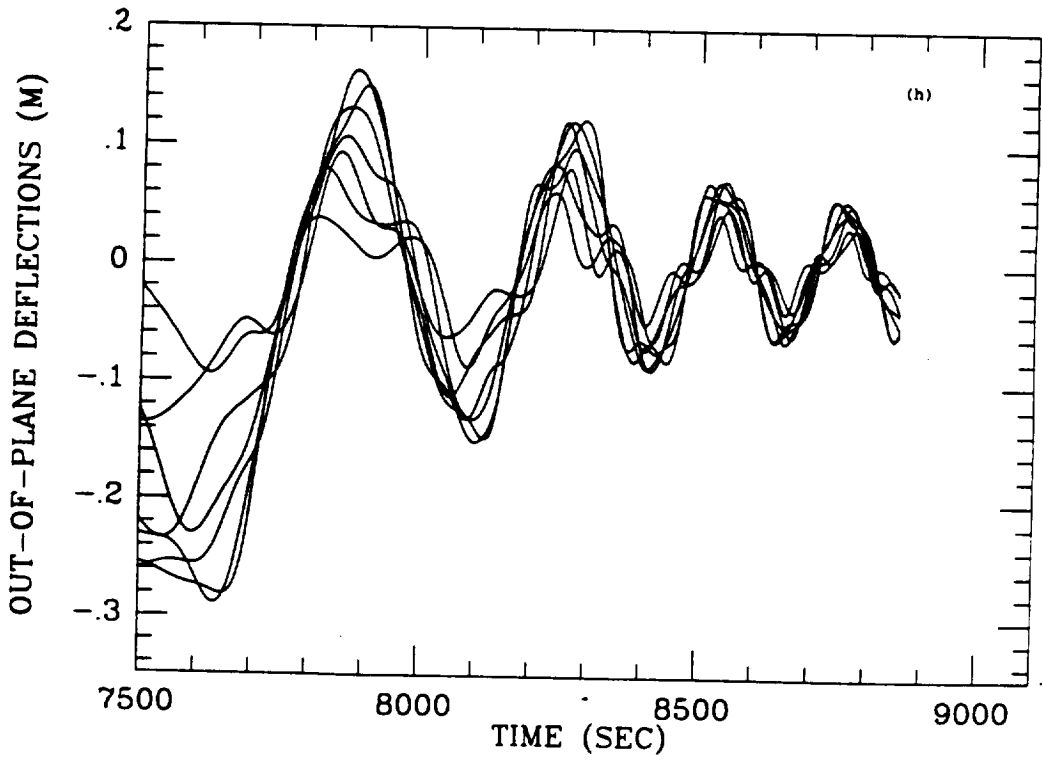
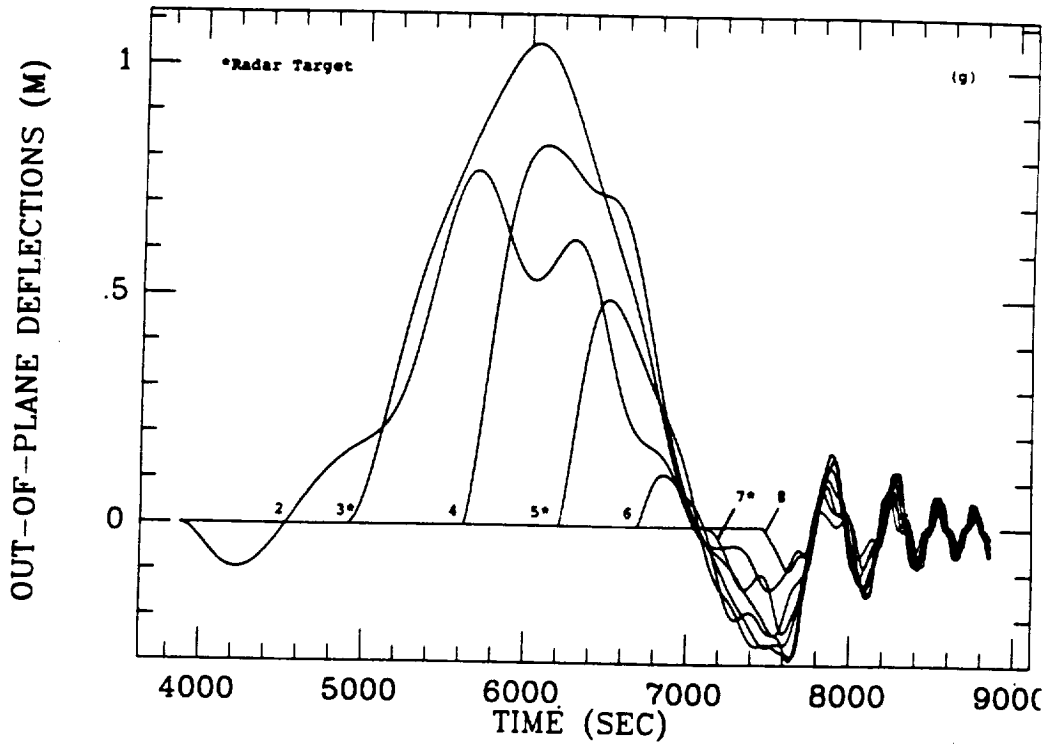
Figures 5(a) and 5(b).



Figures 5(c) and 5(d).



Figures 5(e) and 5(f).



Figures 5(g) and 5(h).

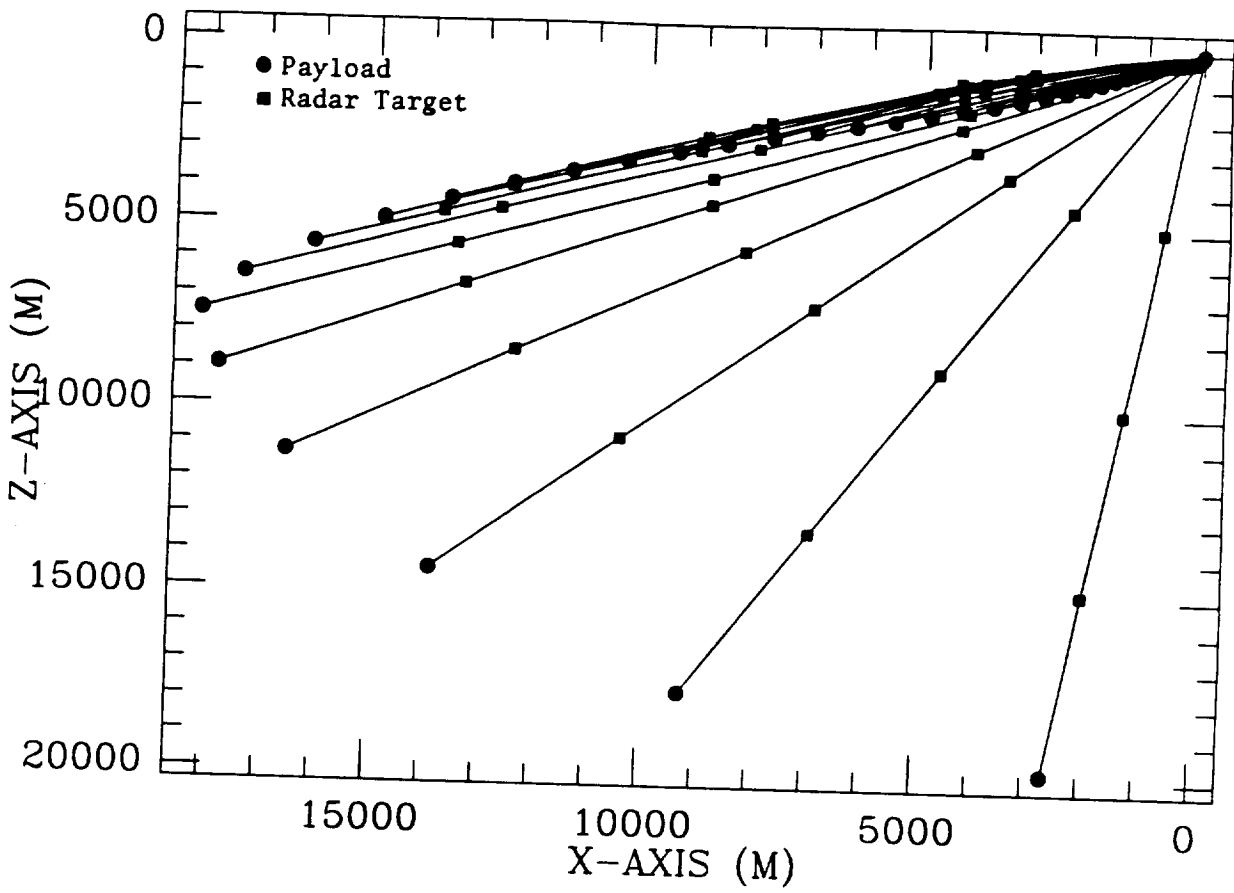


Figure 5(i).

black squares are the radar targets. The snapshots are taken every 200 sec. The qualitative behavior of the deployment maneuver with radar targets is just like the baseline maneuver depicted in Figure 4(n).

Other simulation runs with -10% initial velocity mismatch have confirmed the conclusions reported above. In particular the departure of the in-plane bowing from the baseline case is always within the 10% band.

These results lead us to conclude that the tracking of the three radar targets will provide a quite accurate measurement of the tether shape. We have to take into account, of course, that the tracking of three radar reflectors will provide information on the first three modal shapes of the tether and not on the higher harmonics. Even if we did not carry a quantitative analysis of the harmonic content of the tether shape we can however say that the first few modes are dominant in the tether in-plane dynamics.

ORIGINAL PAGE IS
OF POOR QUALITY

2.6 Tether Discretization And Accuracy

The 9-lump model adopted for the analysis described in the previous section of this report is the result of a compromise between CPU time consumption and resolution. Two legitimate questions are: (1) Is the resolution of the 9-lump model accurate enough for the purpose of our investigation? (2) Does the strategy adopted of attaching radar targets to tether lumps provide results which are accurate enough?

This sections is devoted to answering the two questions above. To this end we run several partial simulations with higher resolutions than the 9-lump model and also by adopting a different strategy for the attachment of the radar targets to the tether. According to the new strategy each radar target is attached to the tether in between two adjacent tether lumps instead than to the lump itself. This strategy has however the drawback that a lighter lump mass, a shorter tether length (hence higher frequencies), and the discontinuity of the initial velocity vector force the integrator to use extremely small steps following the attachment of the radar target. On several occasions the integrator become unstable at the attachment of the second radar target. All these problems may be solved by filtering the longitudinal tether dynamics (which however implies a loss of accuracy in the description of the system motion) and also by using more stable integrators (unfortunately the more stable integrators are usually the slowest!). Both these solutions, however, require an effort that is far beyond the scope and the funding

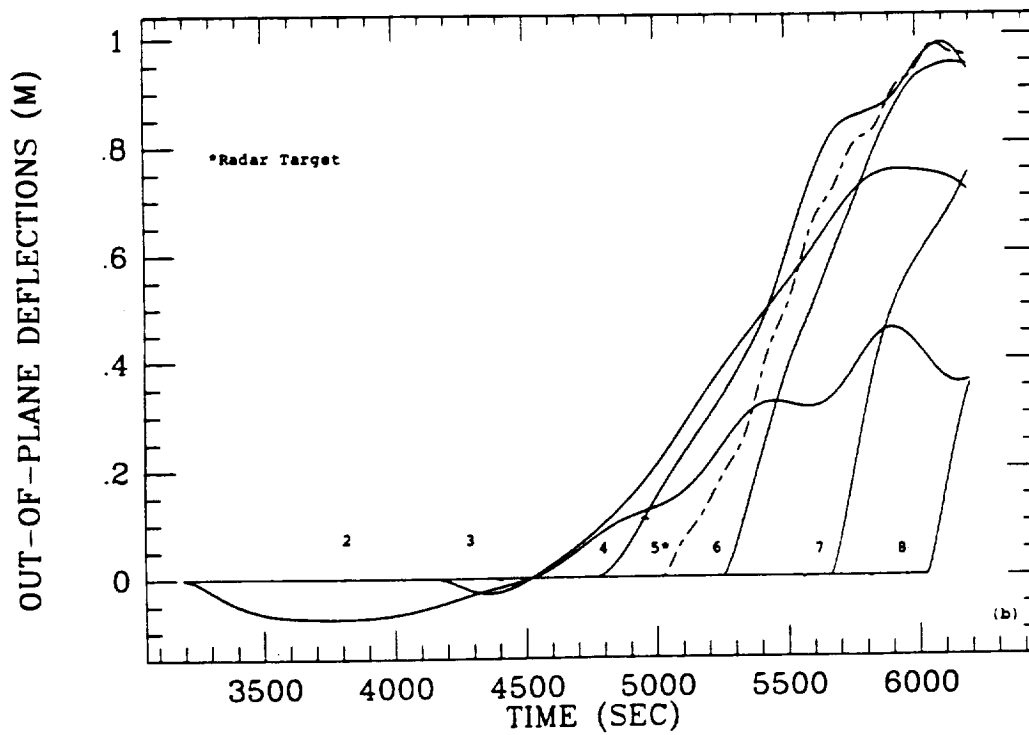
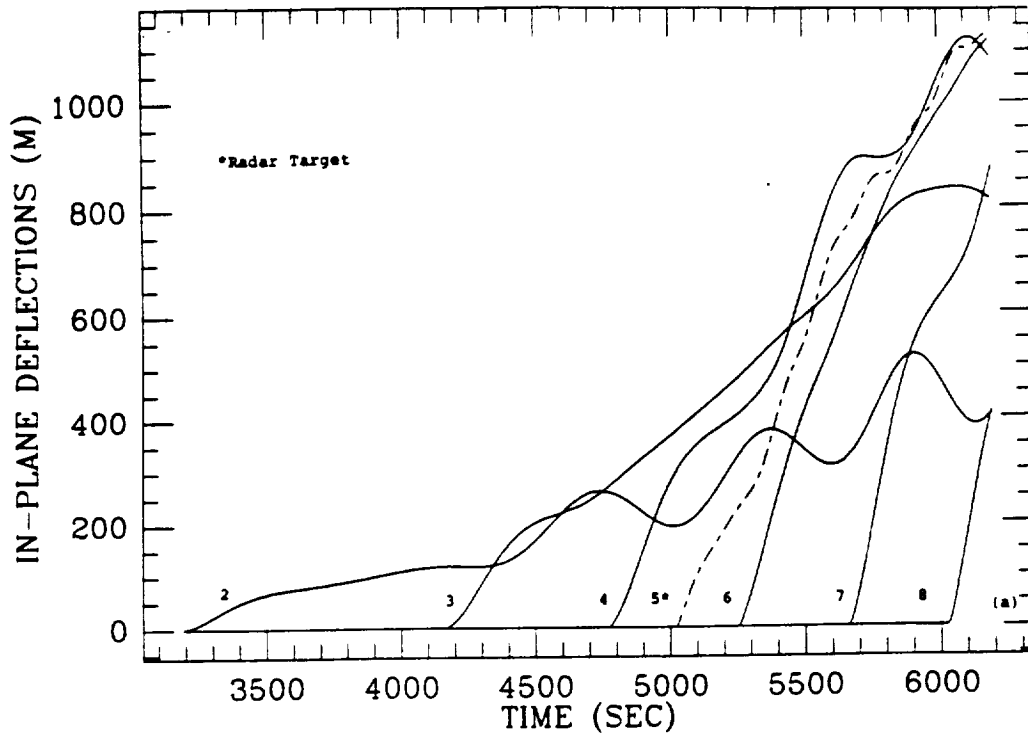
of the present contract.

We show in this section the results of a simulation (simulation run 4) which adopts the new strategy of radar reflector's attachment to the tether, +10% velocity mismatch, and which adopts a 17-lump model. The simulation run took 30 hrs. of CPU time on a MicroVAX to cover 75% (less than 2 hrs.) of deployment before the integrator became unstable at the attachment of the second radar target. The results of simulation 4 answer the two questions asked above.

Figure 6(a) shows the in-plane bowing of the tether between the ejection of the 2nd lump and the 8th lump. The radar target is lump 5 (see Figure 3) which occupies the position at 5 km from the payload, formerly occupied by lump 3 of simulation 3 (9-lump model). Lumps 2, 3, 4, 6, 7 and 8 do not occupy any position formerly taken by the lumps of the 9-lump model. The comparison between the 9-lump and the 17-lump model, therefore, must be based upon the overall tether bowing (i.e. the envelope of the relevant figures). Moreover we can compare the tether bowing at the first radar target: lump 5 in simulation 4 and lump 3 in simulation 3. The conclusion is that when we consider the first radar target and we take into account the slightly different time of ejection of the target (the different discretization model slightly affects the duration of deployment) the results of the two models are close. From Figure 6(a) we can also notice that the first target (lump 5) has a bowing which is almost midway between lumps 4 and 6. This means that the segment of tether between lumps 4 and 6

(the target is in the middle of that tether segment) is almost straight. The new strategy of attaching radar target, therefore, does not uncover any local significant deflection of the tether segment to which the target is attached. Consequently the new strategy does not improve the resolution with respect to the old strategy but, on the other hand, it worsen enormously the CPU time consumption of the computer code. Figure 6(b) shows the out-of-plane tether bowing. We can notice, again, that the magnitudes of the results are very close to the 9-lump model [see Figure 5(g)]. Finally Figure 6(c) shows the snapshot side-view of the first 6400 sec of deployment with the 17-lump model.

The conclusion to this section is that the 9-lump model is accurate enough for the purpose of this investigation. The strategy of adding radar targets to tether lumps also provides a correct representation of the actual dynamics.



Figures 6(a) and 6(b).

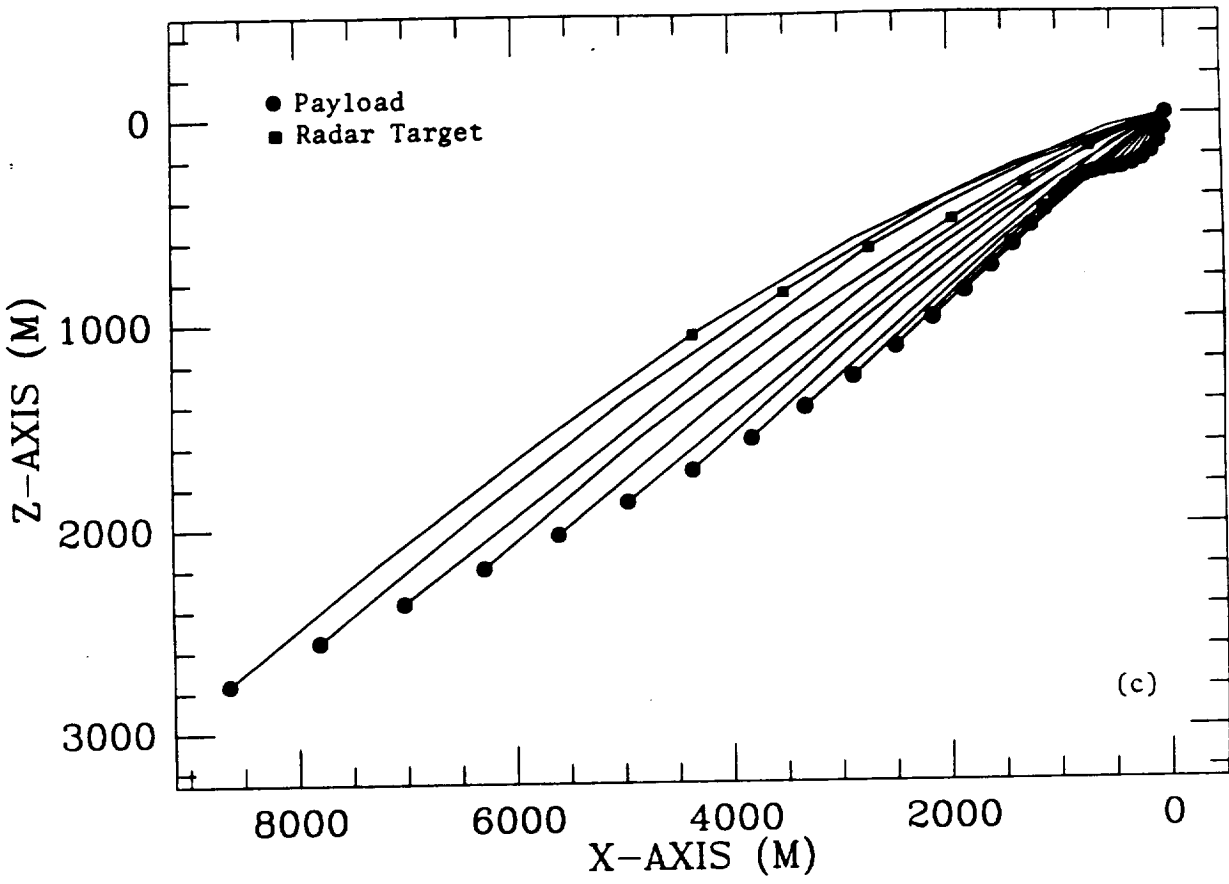


Figure 6(c).

2.7 Conclusions And Recommendations

The attachment of three radar reflectors at the 5, 10, and 15 km points of SEDS's tether during deployment does not impact appreciably the longitudinal dynamics of the system. Control variables such as tether tension, length, and payout velocity are almost unaffected by the attachment of the radar reflectors. The major effect of the reflectors is upon the in-plane shape of the tether. The departure of the in-plane bowing from the baseline case is, however, less than 10% of the baseline local tether bowing. These results are consistent with radar targets of 100 grams and with a longitudinal and transverse (in-plane) differential velocity components at attachment of $\pm 10\%$ of the predicted deployment velocity. These conclusions were obtained with a 9-lump model of the system and verified, for 75% of the deployment duration, with a 17-lump model.

The accurate tracking of the three radar targets from the Shuttle will provide, therefore, a quite accurate measurement of the tether shape.